AD-A132 575 A COMPACT SATCOM ANTENNA FOR X- AND Q-BAND(U) OHIO STATE UNIV COLUMBUS ELECTROSCIENCE LAB S J LIN ET AL. APR 82 ESL-713302-1 N00173-80-C-0367 1/2

UNCLASSIFIED F/G 9/5 NL

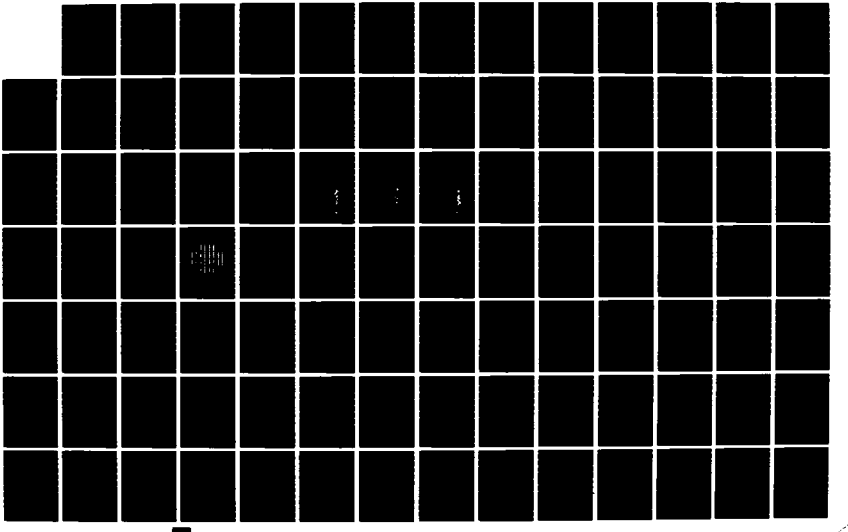

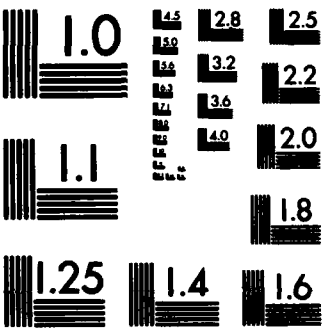

MICROCOPY RESOLUTION TEST CHART
NATIONAL BUREAU OF STANDARDS-1963-A

A COMPACT SATCOM ANTENNA FOR X- AND Q-BAND

S.J. Lin
L. Henderson
K. Miller
B.A. Munk

Final Report 713302-1

Contract N00173-80-C-0367

Department of the Navy
Naval Research Laboratory
Washington, D.C. 20375

50272-101

REPORT DOCUMENTATION PAGE	1. REPORT NO.	2.	3. Recipient's Accession No. AD-A132 575
4. Title and Subtitle: A COMPACT SATCOM ANTENNA FOR X- AND Q-BAND			5. Report Date: April, 1982
			6.
7. Author(s): S.J. Lin, L. Henderson, K. Miller, and B.A. Munk ESL			8. Performing Organization Rept. No. 713302-1
9. Performing Organization Name and Address: The Ohio State University, ElectroScience Laboratory, 1320 Kinnear Road, Columbus, Ohio 43212			10. Project/Task/Work Unit No.
			11. Contract(C) or Grant(G) No. (C) N00173-80-C-0367 (G)
12. Sponsoring Organization Name and Address: Department of the Navy, Naval Research Laboratory, Washington, D.C. 20375			13. Type of Report & Period Covered: Final Report
			14.

15. Supplementary Notes

AD-A132 251

16. Abstract (Limit: 200 words)

This report describes the development of a Satcom antenna for X- (7.25-7.75 GHz) and Q-band (43-46 GHz). The Q-band antenna is comprised of a dichroic parabolic dish of tripoles making it reflective in Q-band and transparent in X-band. The X-band antenna is made of 24 dipoles in front of a ground plane with the entire X-band array mounted directly behind the Q-band dish. Thus, two bands are covered with the same aperture making the combined antenna very compact.

In addition, planar surfaces we developed are transparent in K-band (19-21 GHz) and reflective in Q-band (43-46 GHz).

Accession For	
NTIS GRA&I	☑
DTIC TAB	☐
Unannounced	☐
Justification	
By	
Distribution/	
Availability Codes	
Dist	Avail and/or Special
A	

17. Document Analysis a. Descriptors

Satcom Antenna
Periodic Surface
Frequency Sensitive Surface
Arrays
Dichroic Surface
Monoplanar Surface
Biplanar Surface

b. Identifiers/Open-Ended Terms

c. COSATI Field/Group

18. Availability Statement: Approved for Public RElease; Distribution Unlimited

19. Security Class (This Report): Unclassified

21. No. of Pages

Security Class (This Page): Unclassified

22. Price

TABLE OF CONTENTS

LIST OF TABLES

LIST OF FIGURES

FIGURE PAGE

FIGURE

INTRODUCTION

The antenna described in this report is intended to serve as part of a communication link between a satellite and a vessel on earth. Due to its small size (diameter of ~5 1/2" and ~3 deep) the antenna can actually be mounted on or in a periscope. At the time this contract was started, there appeared to be a great interest in antennas operating in Q- and X-band, more specifically 43-46 GHz and 7.25-7.75 GHz. However, during the contract, the interest shifted from X- to K-band while the emphasis on Q-band remained. In consultation with our contract monitor, Mr. Stephen Nichols, then from the Naval Research Laboratory and now with Naval Electronics Systems Command, it was decided to finish the work on the X-band array and then, time permitting, develop a computer program which could handle an arbitrary number of arrays of tripoles sandwiched between dielectric slabs. This computer program would serve as our design tool in developing a Frequency Sensitive Surface (FSS) being reflective at Q-band and transparent in K-band. We are happy to report that we not only have finished the combined X- and Q-band antenna, but also the new computer program as well, including a flat panel design for the Q- and K-band. It would be a relatively minor task to make an actual dish for these new frequency ranges.

The concept of this antenna is due to Messrs. Russell Brown and Stephen Nichols and it is illustrated in Figure 1. It is comprised of an X-band dipole array mounted in back of a parabolic dish operating at 43-46 GHz. This parabolic dish is made of a Frequency Sensitive Surface (FSS) designed to be a good reflector at 43-46 GHz and virtually

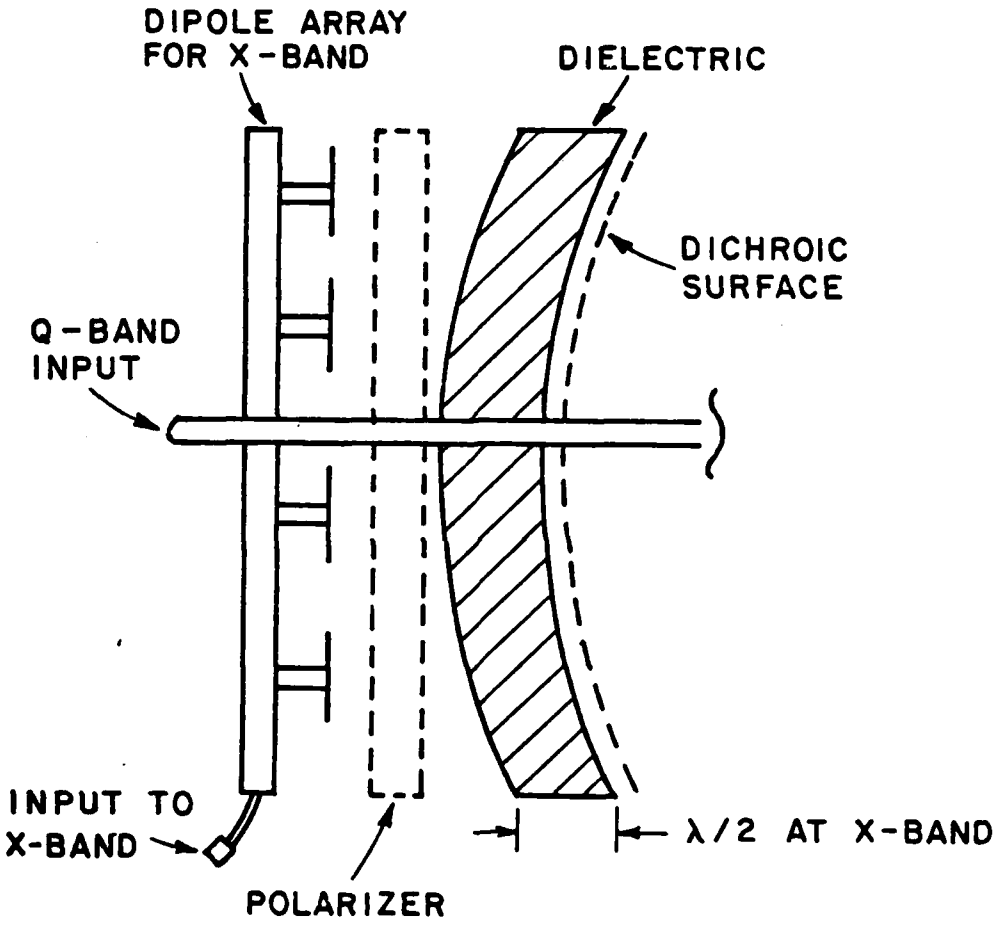

Figure 1. The entire antenna assembly comprised of the frequency sensitive dish and a dipole array for X-band.

transparent at the X-band frequencies (7.25-7.75 GHz). Further, a polarizer is inserted between the X-band array and the parabola. This polarizer transforms the linear polarized field from the X-band array into circular polarization.

This report is divided into two sections. In section I we show the layout and design of the frequency sensitive surface attached to the parabolic surface made of polyethylene. Also shown is the radiation pattern obtained in Q-band under various circumstances. In section II we describe the development of the X-band array, in particular, the layout of the feeding structure, impedance and radiation pattern, showing the effect of the dichroic dish as well as the polarizer mounted in front of the array.

SECTION I

Q-BAND DICHROIC DISH

1. LAYOUT OF DISH

The layout of the parabolic surface is shown in Figure 2. It is comprised of small tripoles arranged in a triangular grid as shown. When exposed to an incident wave, such a surface will act as a good reflector if the length of a tripole leg is approximately one quarter wavelength long. At frequencies below and above, some transmission and some reflection will take place. Some difficulty arises because of the double curvature of the parabolic dish. This problem is solved by cutting the FSS up into small triangles as shown in Figure 2. However, in order for these triangles to fit properly, they are made up of isosceles triangles with a top angle somewhat smaller than 60 degrees

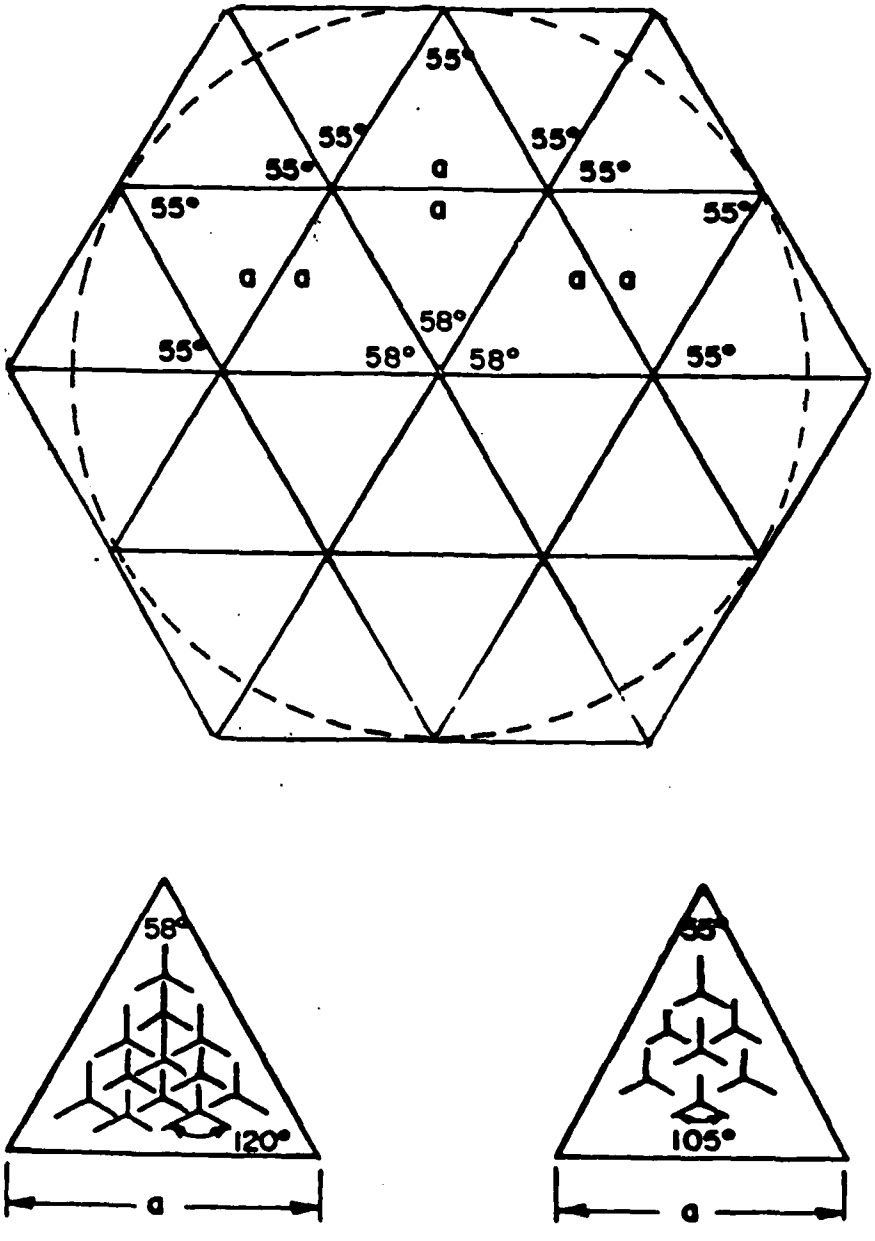

Figure 2. Top: The parabolic surface seen from the front.

Bottom: The 58° and 55° patches used at the center and rim portion of the dish, respectively.

depending on how far away from the vertex they will be mounted. Two types of triangles are used in the present design: namely, a top angle of 58 degrees for the one closest to the vertex and 55 degrees for the one closest to the rim. In order not to cut any elements along the circumference of the patches, the array grids have been changed such that they coincide exactly with the triangular shape of the patches. A closer investigation reveals that if the array angle is changed we must also change the leg angle between the tripoles somewhat. Otherwise, cross polarization and loss will result. This is why the leg angle for the 55° top angle is 105° instead of the usual 120°. However, for the 58° top angle, the required change in leg angle is so small that we have retained 120°.

The various triangular patches were glued onto a parabolic dish made of polyethylene. High density polyethylene was chosen because of its excellent machineability, good strength, low dielectric constant (ε_r = 2.3), and low loss properties. The only drawback to polyethylene is the difficulty encountered in attaching the patches. Like many plastics, polyethylene has a very high surface tension and as a result the glue sits on the surface and does not form a good bond. This problem can be solved by roughing the surface with fine sand paper and then using a high voltage electric discharge or an oxidizing flame to break up the surface tension. We used the oxidizing flame technique which merely requires that the surface of the dish be passed through the oxidizing flame of a bunsen burner once or twice. Care must be taken when performing this operation since overheating the surface will cause

it to become lossy and even deform. The microwave circuit board material is teflon based and also presents the same difficulty, however a commercially available chemical surface preparation (Tetra Etch made by W.L. Gore) was used to facilitate gluing. Once these steps have been performed, many readily available adhesives will form a good bond. For our experimental models, we used a spray on contact cement (3M #77).

2. CONSTRUCTION OF THE DISH

In order to minimize the transmission loss at X-band, the thickness of the dielectric dish is approximately half wave. In fact, it is made slightly thinner in order to compensate for the slight effect of the FSS at X-band frequencies. The front (parabolic) surface of the dish was cut on a lathe as a sequence of 5 radii which approximated the desired parabola with a maximum error of .005 inches. In order to keep the plastic assembly from acting like a concave dielectric lens to the X-band array, the back of the dish was also cut in an approximate parabolic shape formed by three cones as seen in Figure 3. This approximate shape was adequate since the back of the plastic dish is "seen" only by the X-band frequencies.

3. THE TRIPOLE SURFACES

The layout of the tripole arrays is shown in Figure 4 with the dimensions given in Table 1.

TABLE 1

DIMENSIONS FOR THE FREQUENCY SENSITIVE SURFACES

	SURFACE 1 (in center)	SURFACE 2 (at the rims)
T	0.025 mm	0.025 mm
W	0.2 mm	0.2 mm
L	1.2 mm	1.3 mm
α	120°	105°
Dx	1.5 mm	1.7 mm
Dz	2.2 mm	2.4 mm

Computed curves for the surface with α = 120° (using a computer program described in the next section) showing the reflection and transmission properties as a function of frequency for various angles of incidence of the FSS and a dielectric slab (the dish) are shown in Figures (5-10). Observe that we have a broad range from 40 to 50 GHz where the reflection coefficient is practically unity and similarly, we observe a transmission loss of up to 0.1 dB around 7.5 GHz. The nulls seen every 7 GHz are due to the dielectric resonances of the dish.

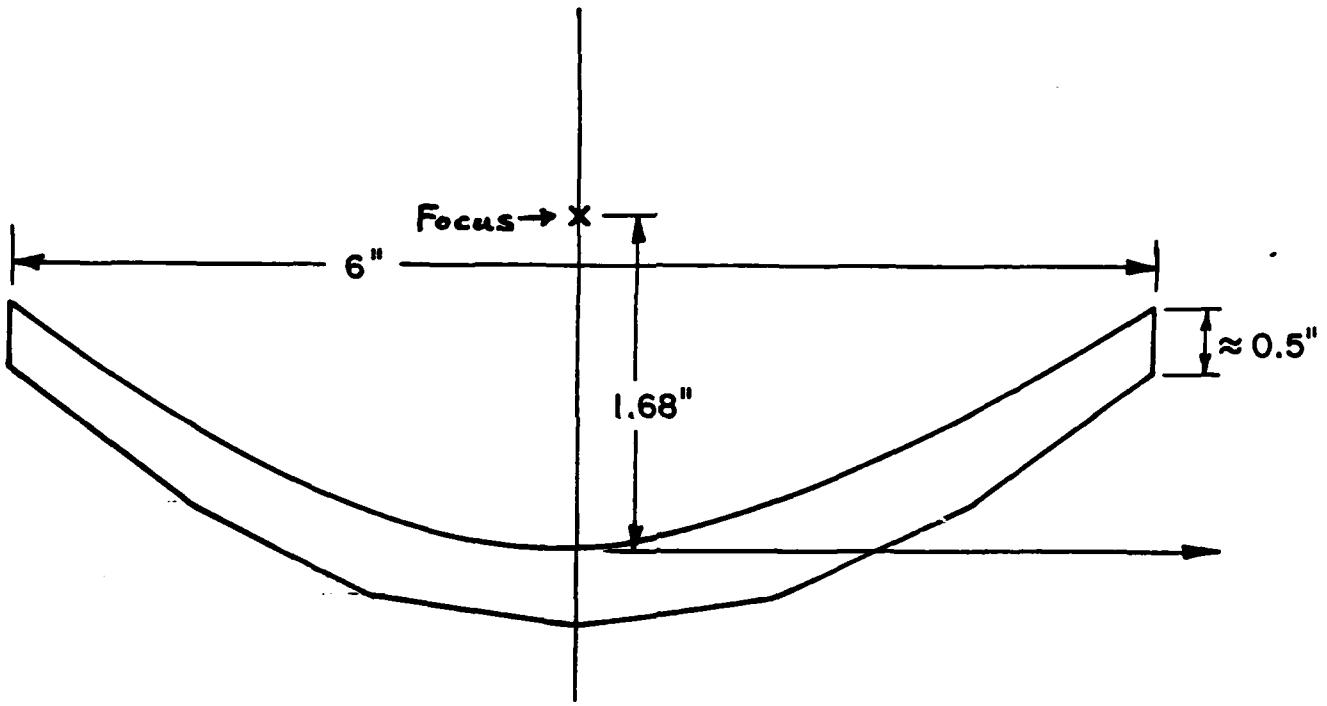

Figure 3. Cross section of the dielectric dish made with an accuracy of 0.005" at the front and with the back as shown (being seen only at X-band).

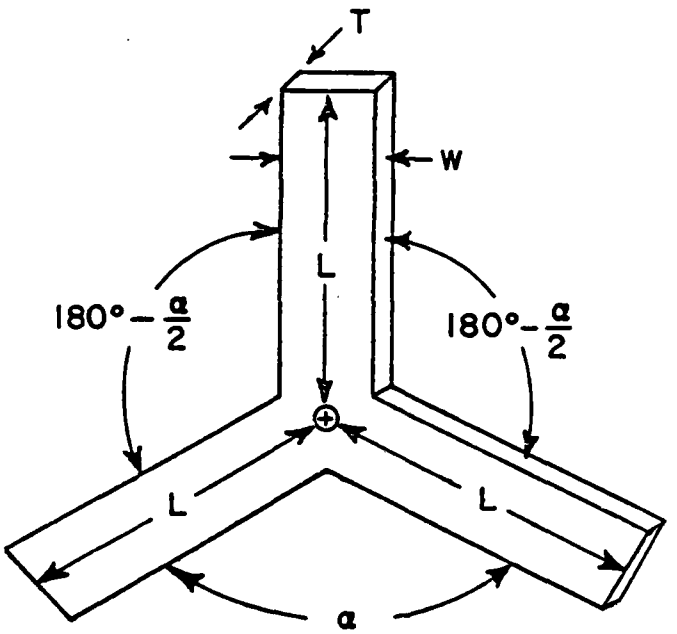

Figure 4a. A single three-legged unloaded element.

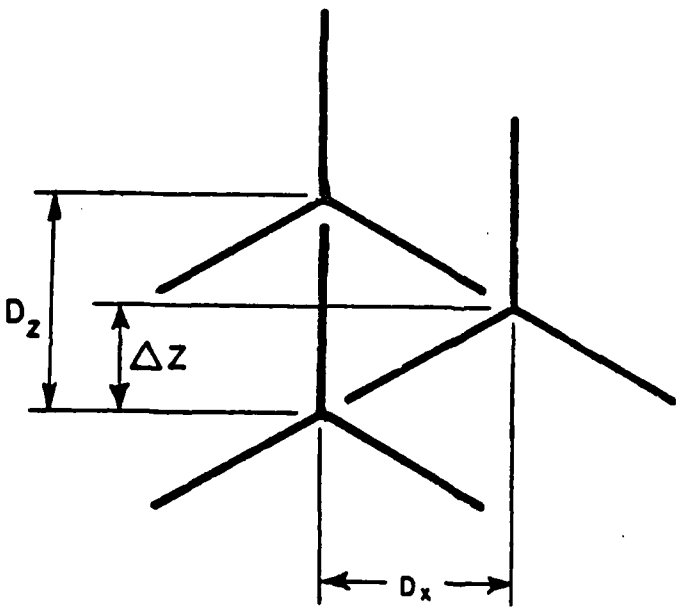

Figure 4b. The array used for the three-legged element shown in Figure 2.

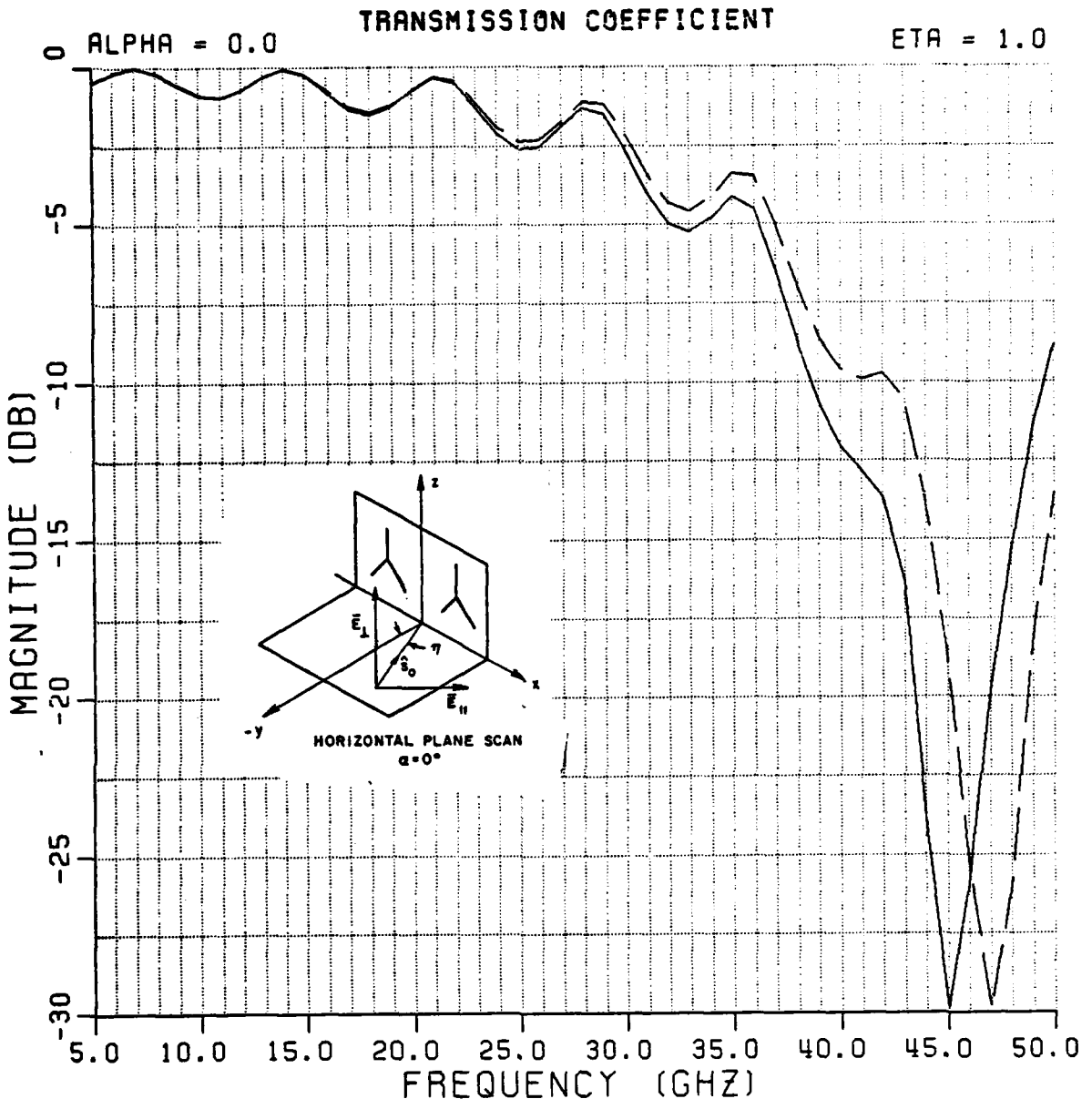

Figure 5. Computed transmission coefficient of the array of 3-legged elements and the dielectric dish. Angle of incidence 1°.

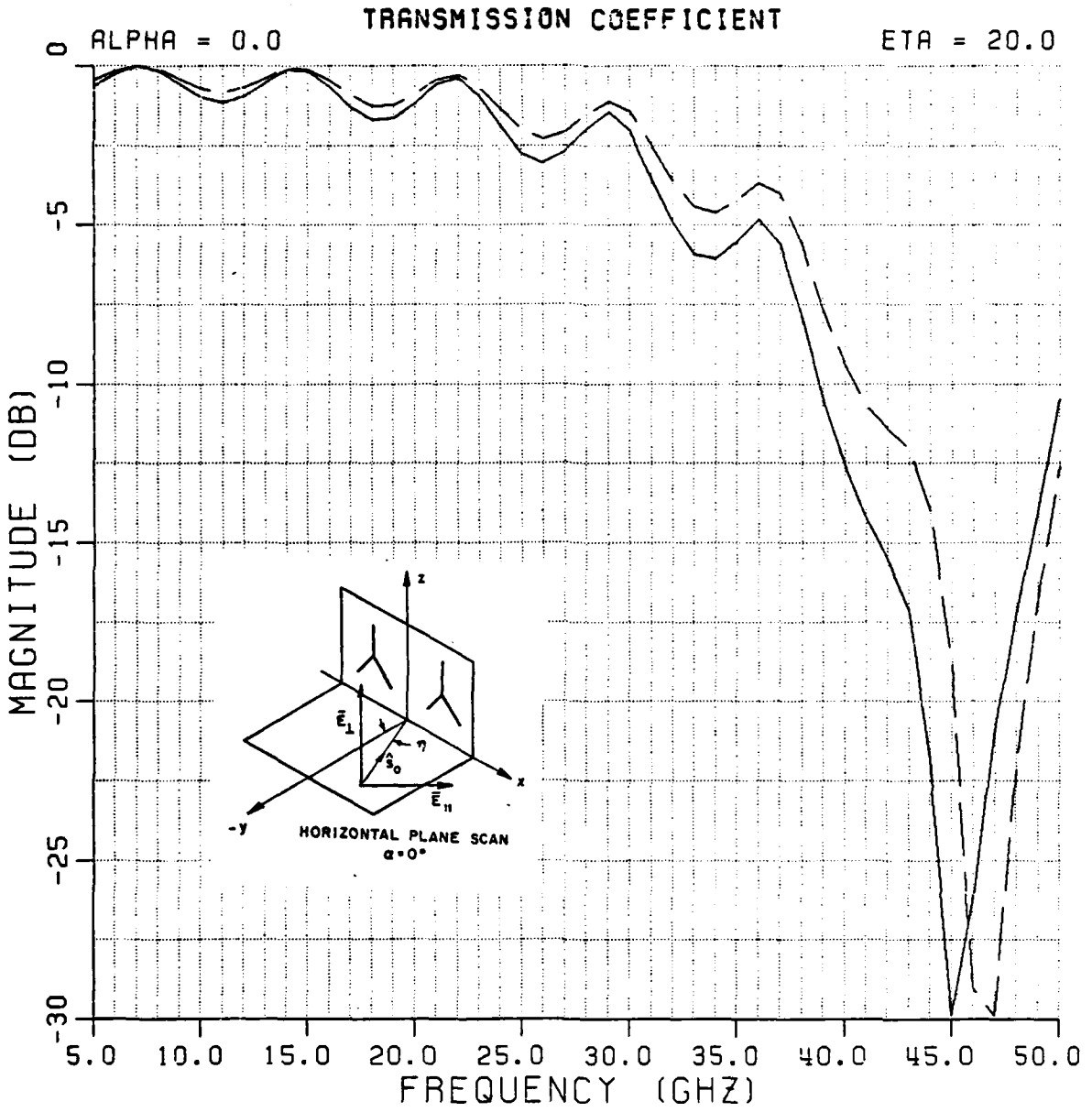

Figure 6. Computed transmission coefficient of the array of 3-legged elements and the dielectric dish. Angle of incidence 20°.

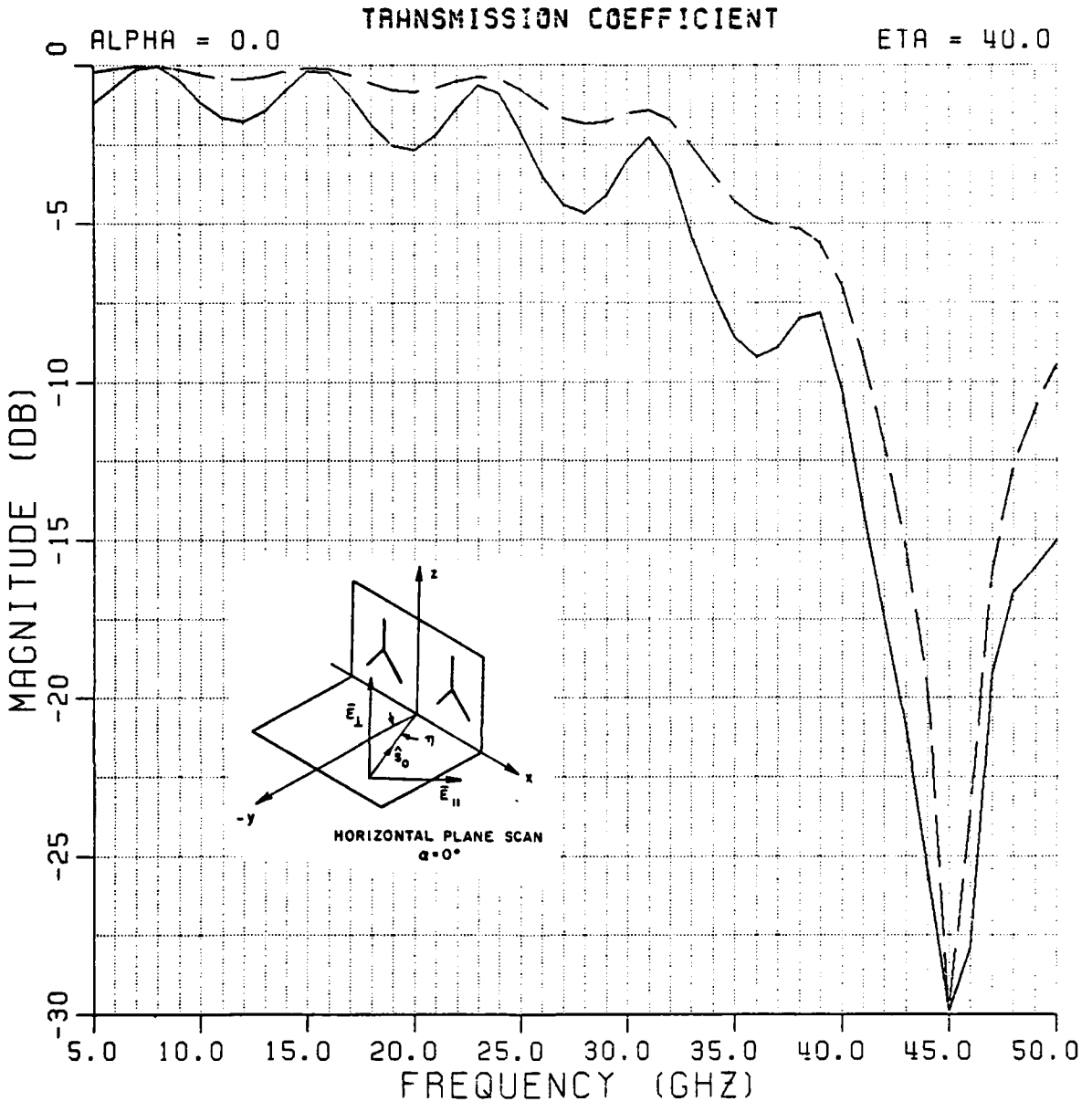

Figure 7. Computed transmission coefficient of the array of 3-legged elements and the dielectric dish. Angle of incidence 40°.

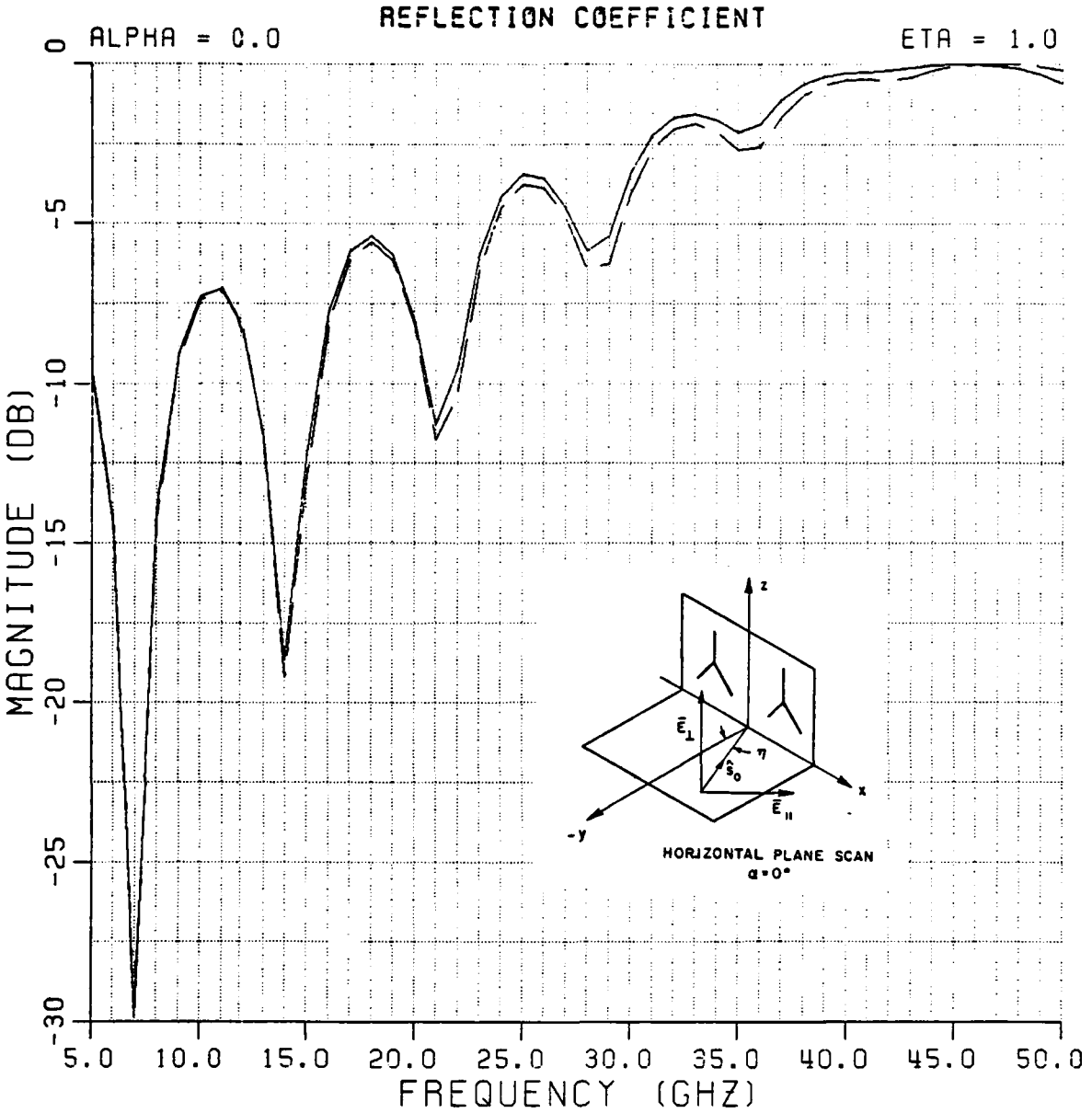

Figure 8. The computed reflection coefficient of the array of tripoles and the dielectric dish. Angle of incidence 1°.

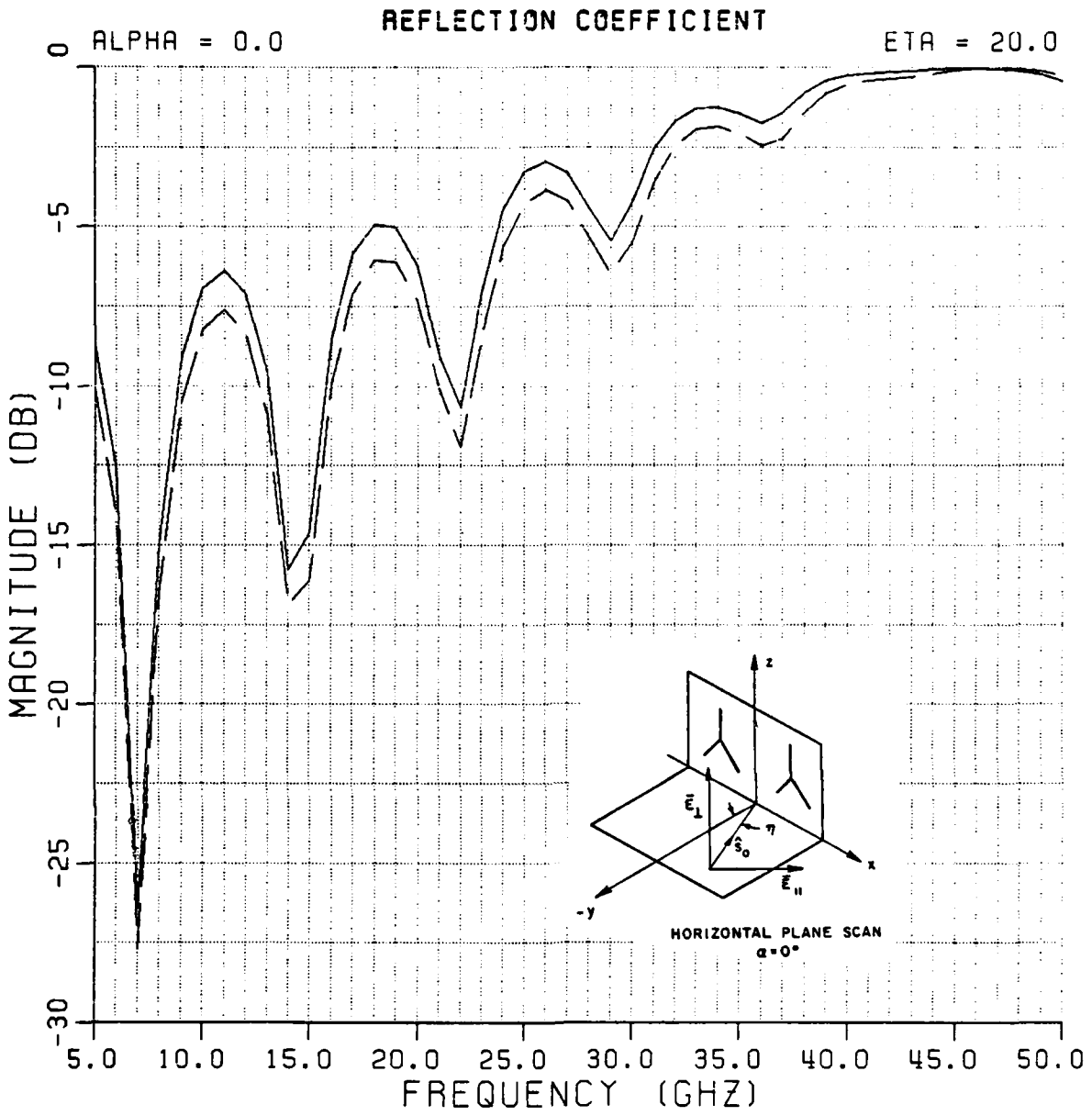

Figure 9. The computed reflection coefficient of the array of tripoles and the dielectric dish. Angle of incidence 20°.

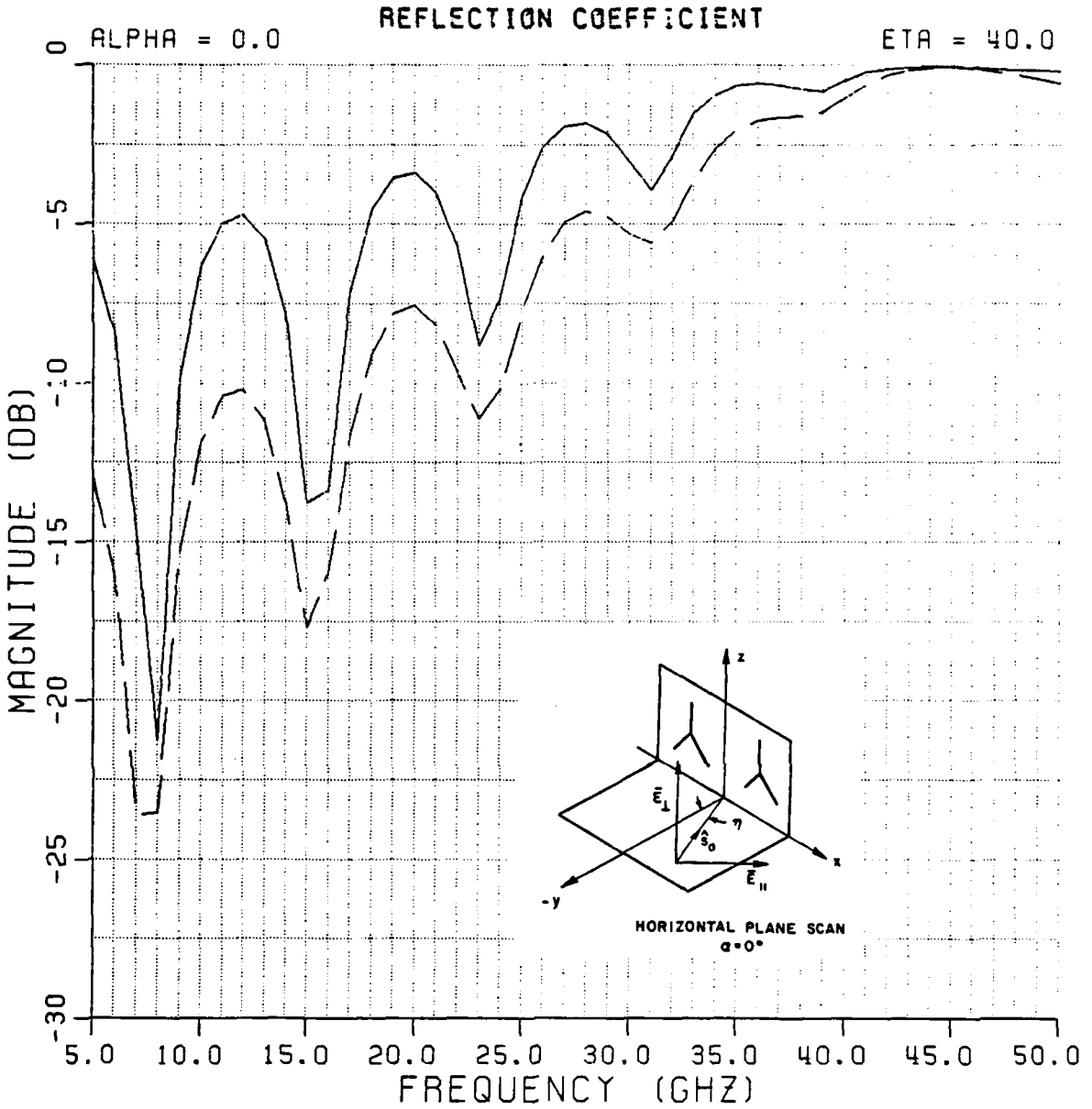

Figure 10. The computed reflection coefficient of the array of tripoles and the dielectric dish. Angle of incidence 40°.

4. MEASURED PATTERNS OF THE Q-BAND DISH

We further show in Figures 11-16 the E and H plane radiation patterns throughout the band. It is observed that the radiation level in the back direction is always at least 30 dB below the main beam. This is very much the same as obtained by a solid dish with the same feed, in fact all the patterns are very much the same through the entire Q-band.

5. 20/45 GHz SYSTEM

A secondary objective of this contract was to design a periodic surface which would perform much like the first surface except the pass (transmission) band would be 19-21 GHz rather than 7.25-7.75 GHz. To facilitate the analysis of this surface a computer program was written which would analyze an arbitrary number of generalized three legged dipole arrays. These arrays can be imbedded in a general, stratified, dielectric media with or without loss. A users manual for this program is documented in a separate report. The reduced separation between the pass band and the stop band posed a new problem since the unloaded three-legged element is by nature a broad band device. The bandwidth can be reduced somewhat by spacing the elements farther apart but this adversely affects the performance at high incidence angles causing resonance shifts and grating lobes to appear. The bandwidth can also be reduced by reducing the effective wire radius but this is not enoug'. The solution is to use two layers of elements and then cause the interactions between the two layers to generate the desired response.

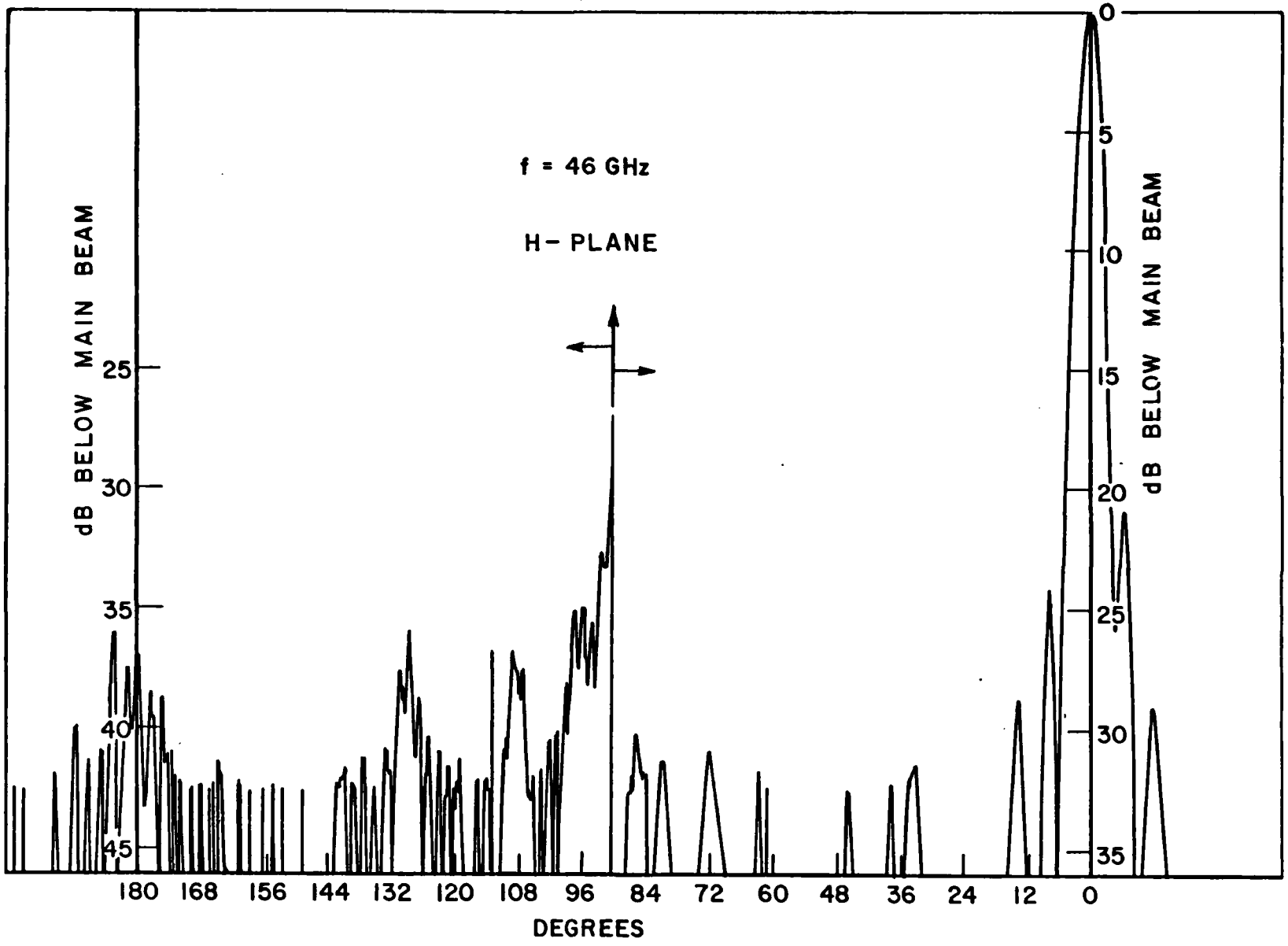

Figure 11. H plane pattern of the dish without the X-band array. Power was increased 10 dB at 90° to show detail in the back lobes.

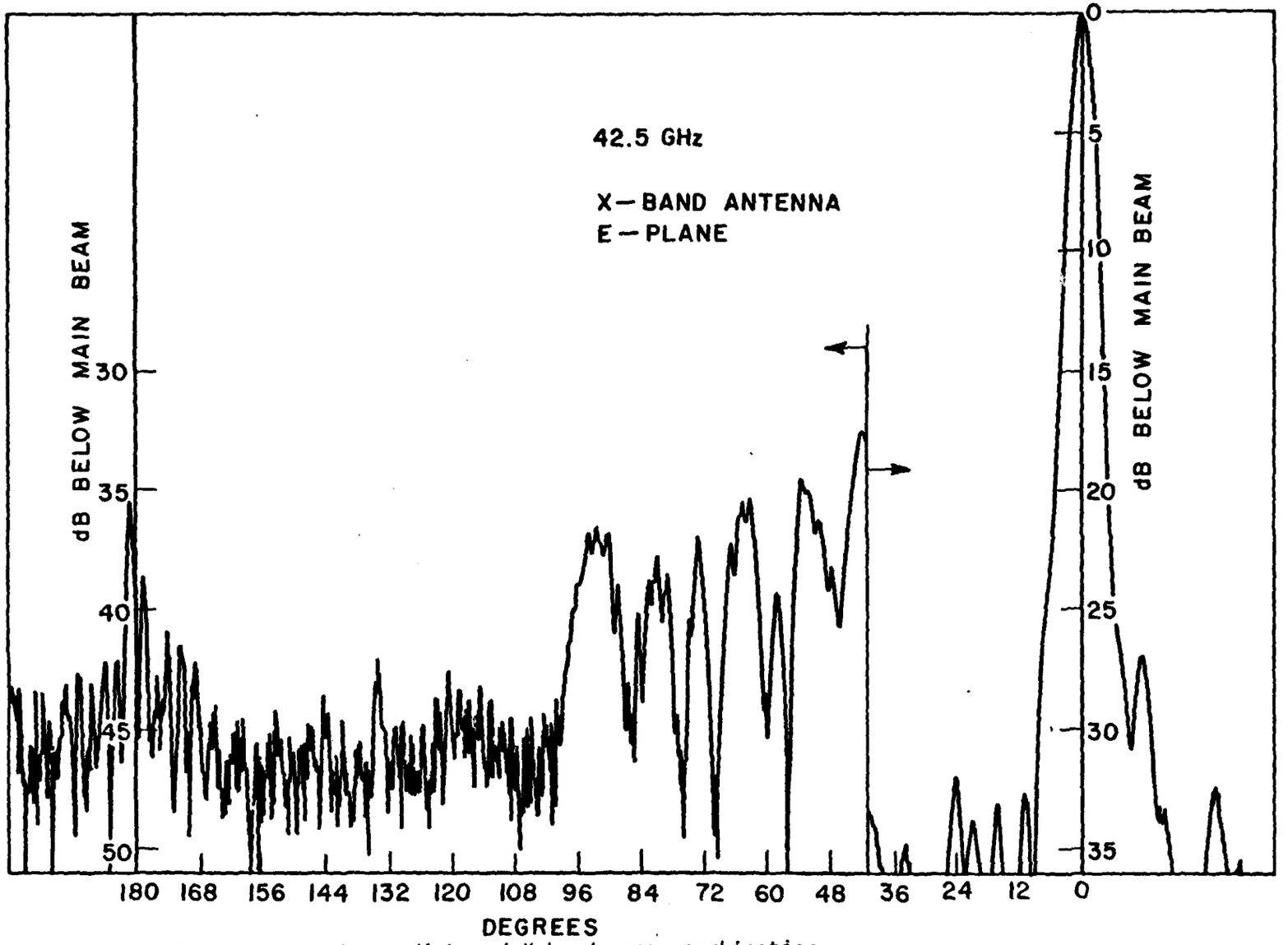

Figure 12. E plan pattern of the dish and X-band array combination. Power was increased 15 dB to show detail in the back and side lobes.

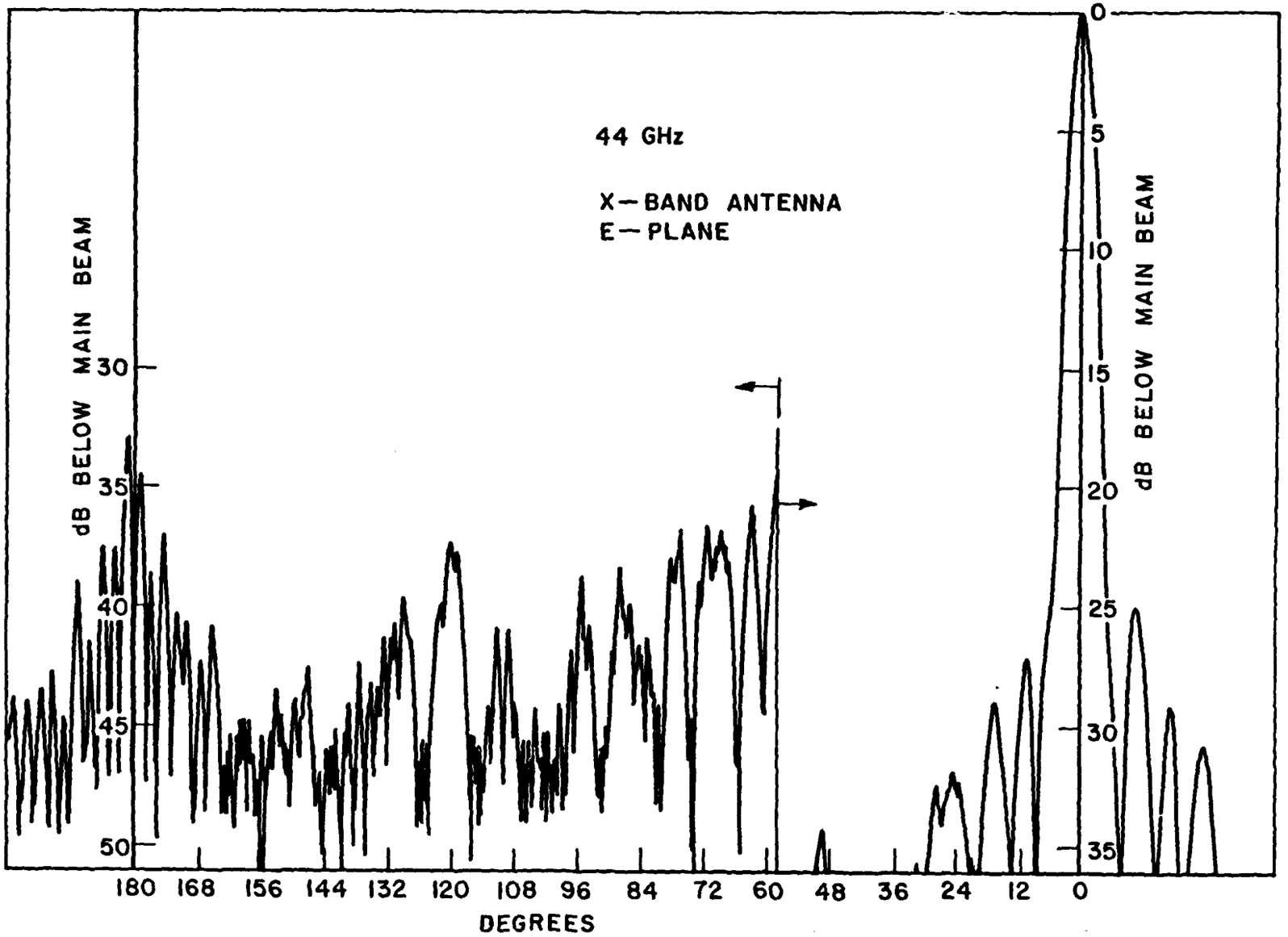

Figure 13. E plane pattern of the dish and X-band array combination. Power was increased 15 dB to show detail in back and side lobes.

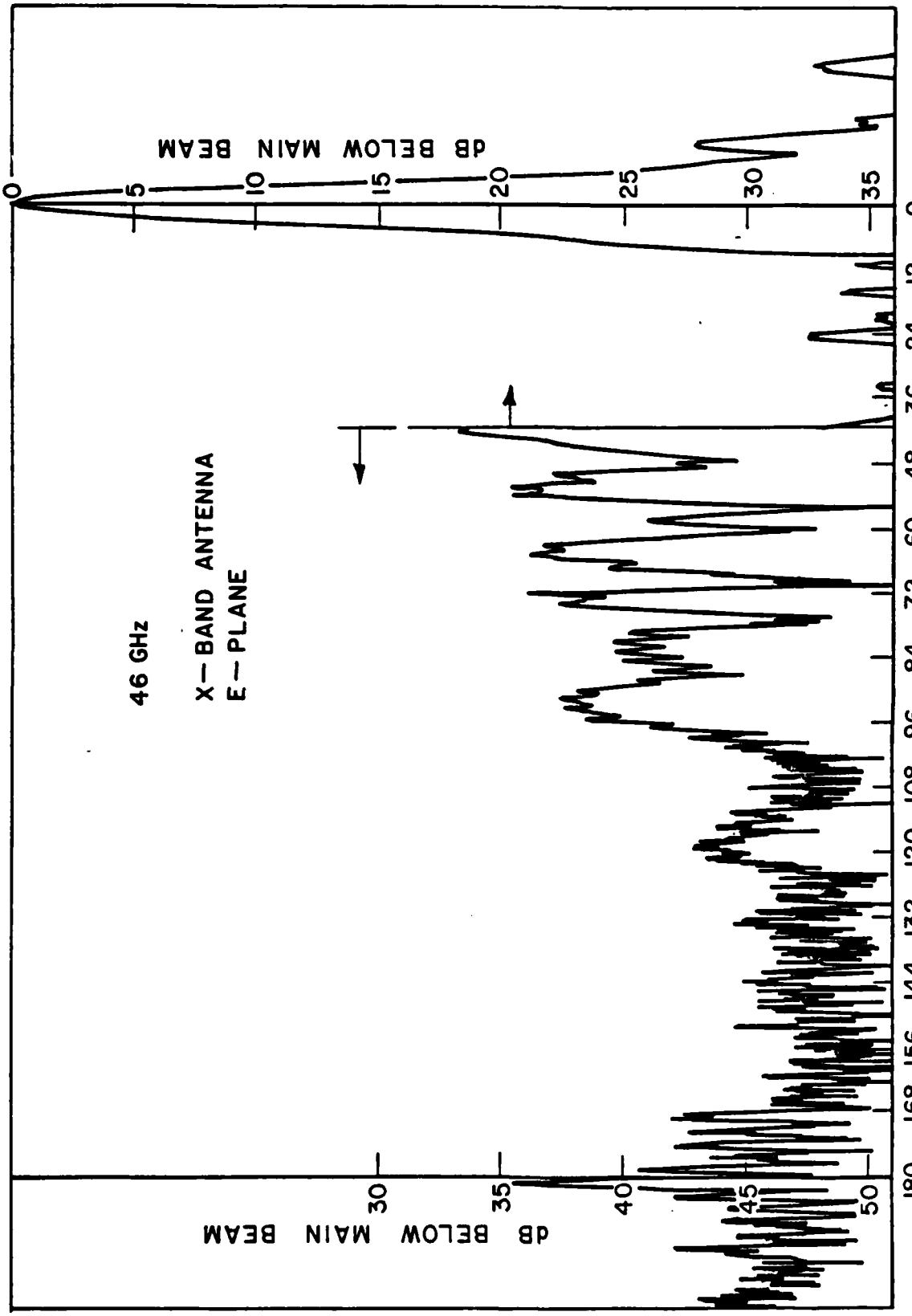

Figure 14. E plane pattern of the dish and X-band array combination. Power was increased 15 dB at 40° to show detail in the back and side lobes.

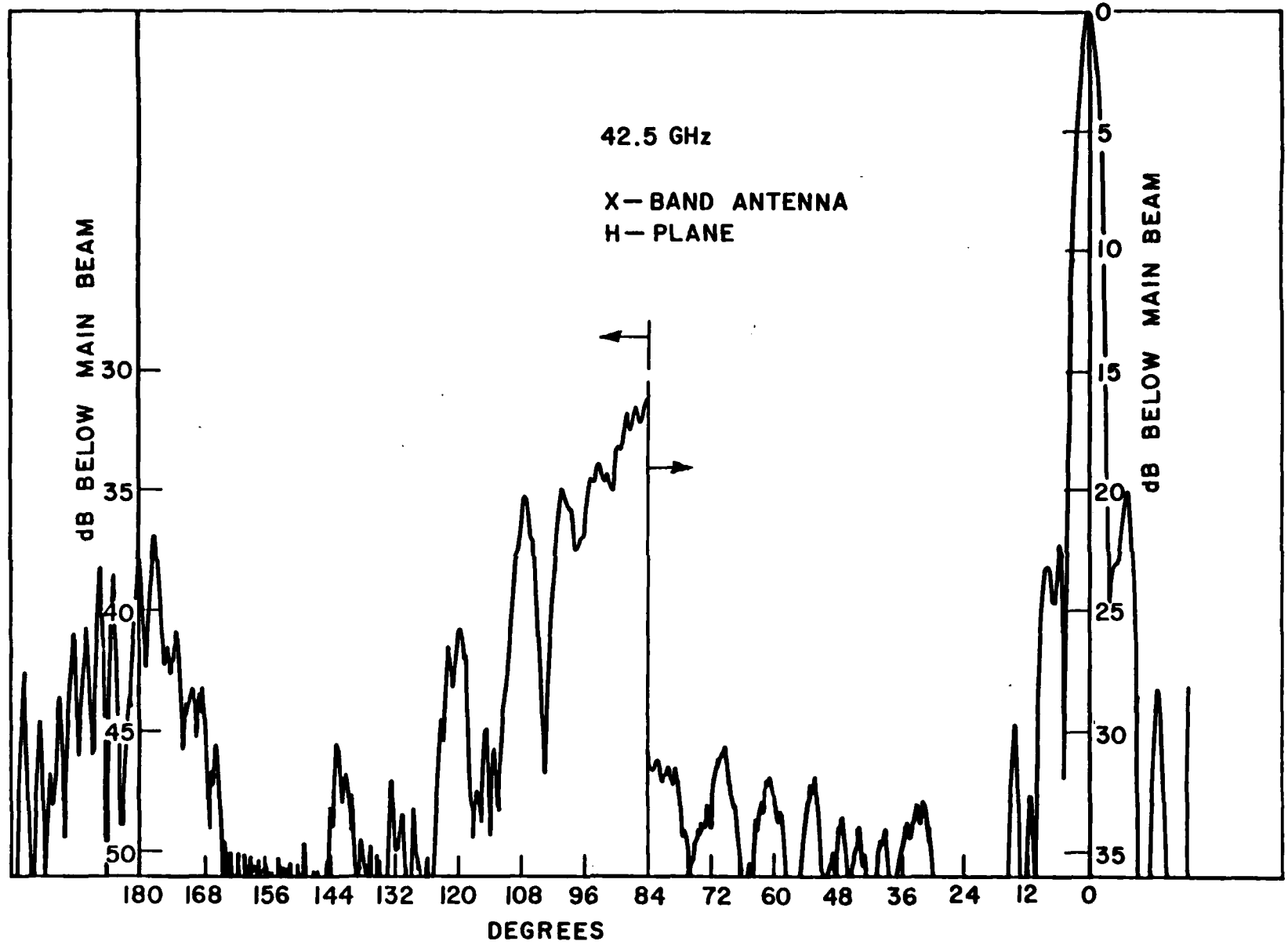

Figure 15. H plane pattern of the dish and X-band array combination. Power was increased 15 dB at 84° to show detail in the back and side lobes.

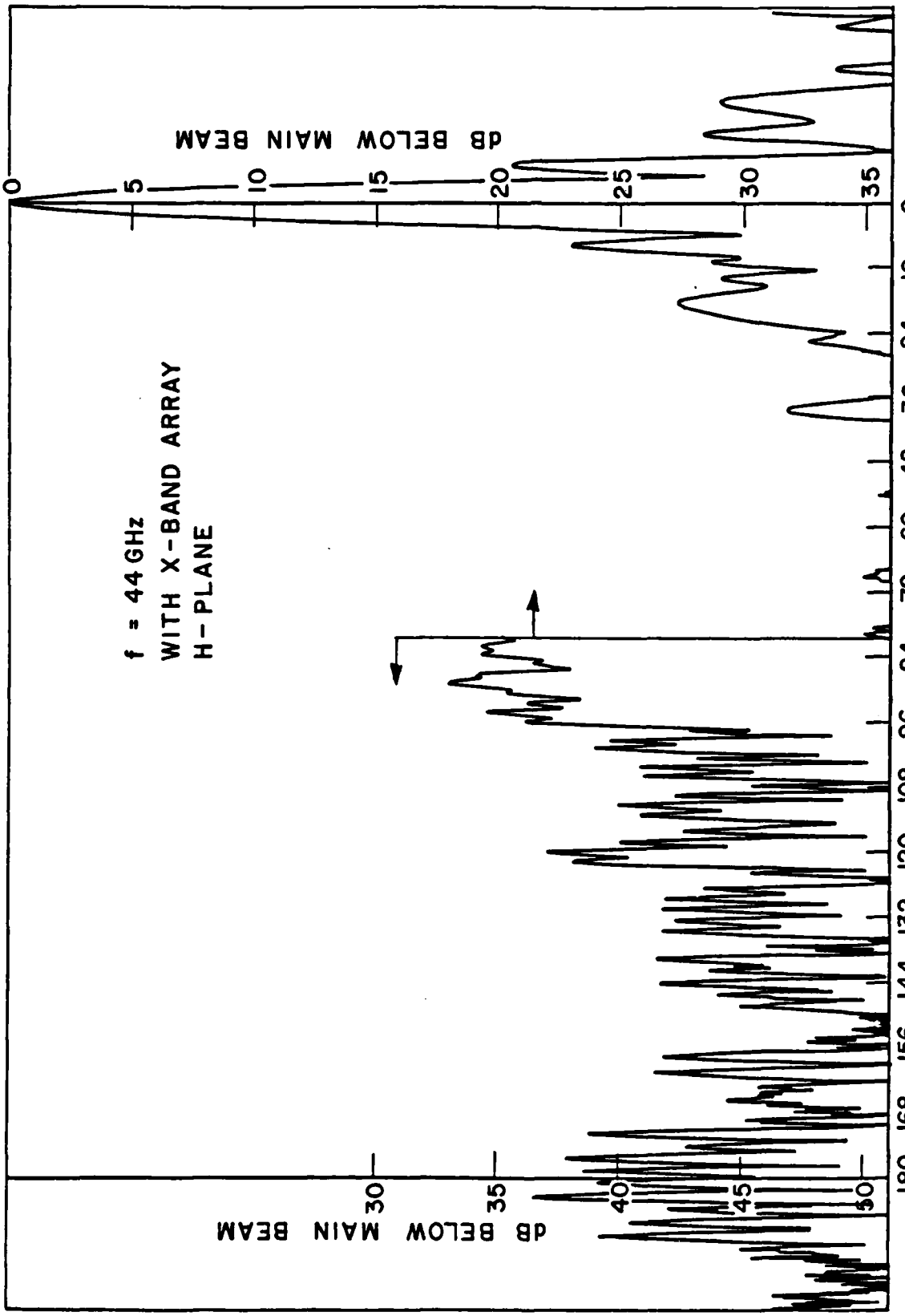

Figure 16. H plane pattern of dish and X-band array combination. Power was increased 15 dB at 80° to show detail in back lobes.

The two arrays are designed to resonate at 45 GHz and spaced such that at 21 GHz interference effects cause the reflected wave to be cancelled out, resulting in a transmission coefficient of unity (much like a quarter wave transformer). Such a system is shown in Figure 17 consisting of two arrays of tripoles separated by one dielectric slab of thickness d. Although it was preferable to have dielectric slabs also on the outside of the two arrays, it was ruled out in the present case for mechanical reasons when making the curved surface for a dish. The performance curves are shown in Figures 18-21. The dimensions are given in Table 2 with reference to Figure 4.

TABLE 2

DIMENSIONS FOR THE

20/45 GHz SYSTEM

L	=	.14	cm
W	=	.025	cm
T	=	.0025	cm
Dx	=	.15	cm
Dz	=	.173	cm
ε	=	2.2	
d	=	.22	cm

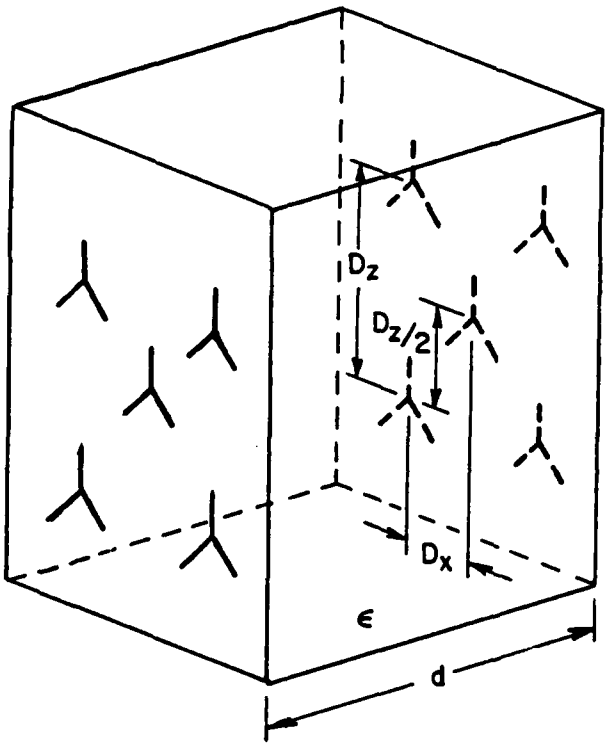

Figure 17. Construction of a biplanar surface comprised of two arrays of tripoles separated by one dielectric slab of thickness d.

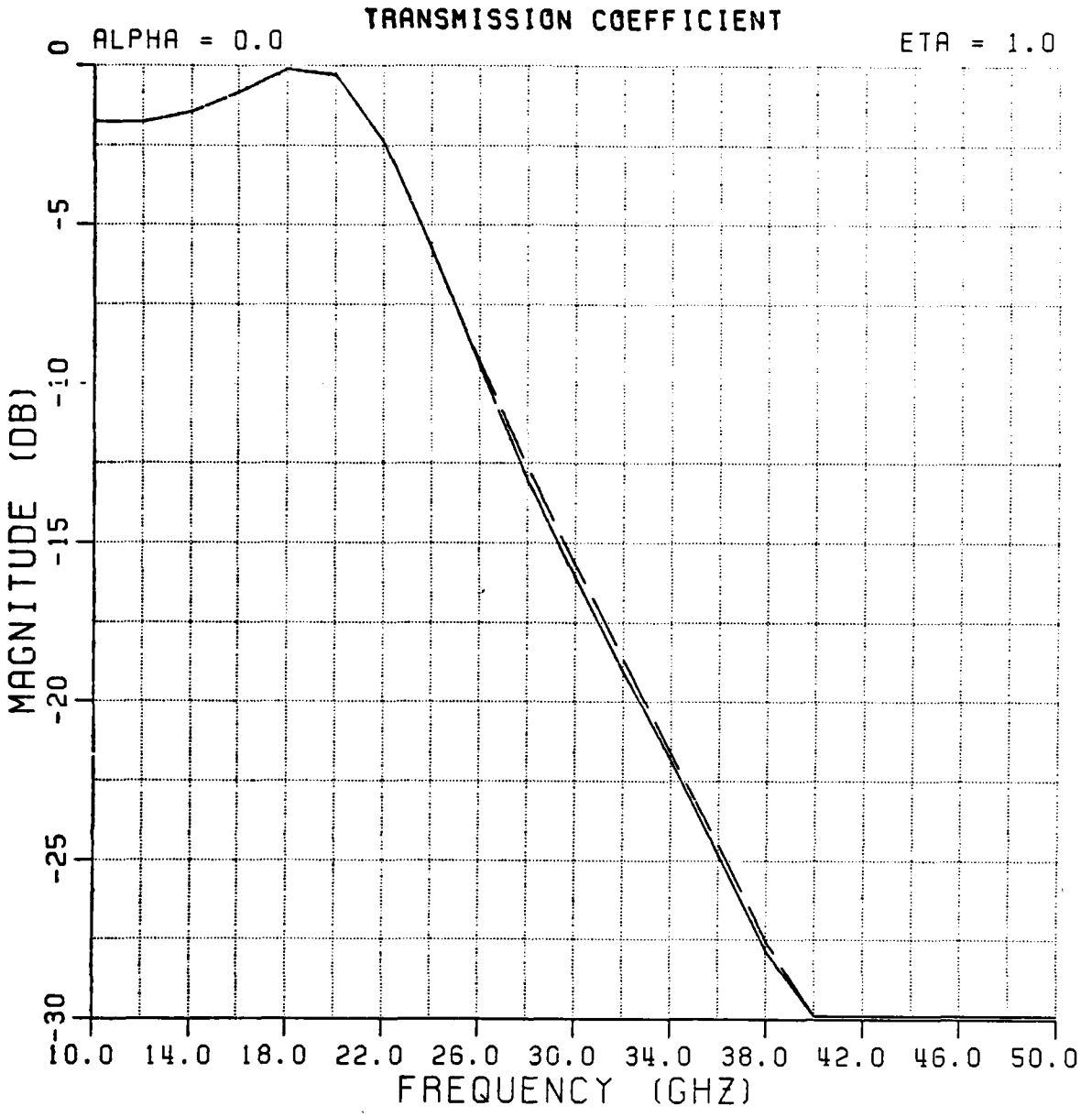

Figure 18. Transmission coefficient of the biplanar array (see Table 2 for dimensions). Angle of incidence 1°.

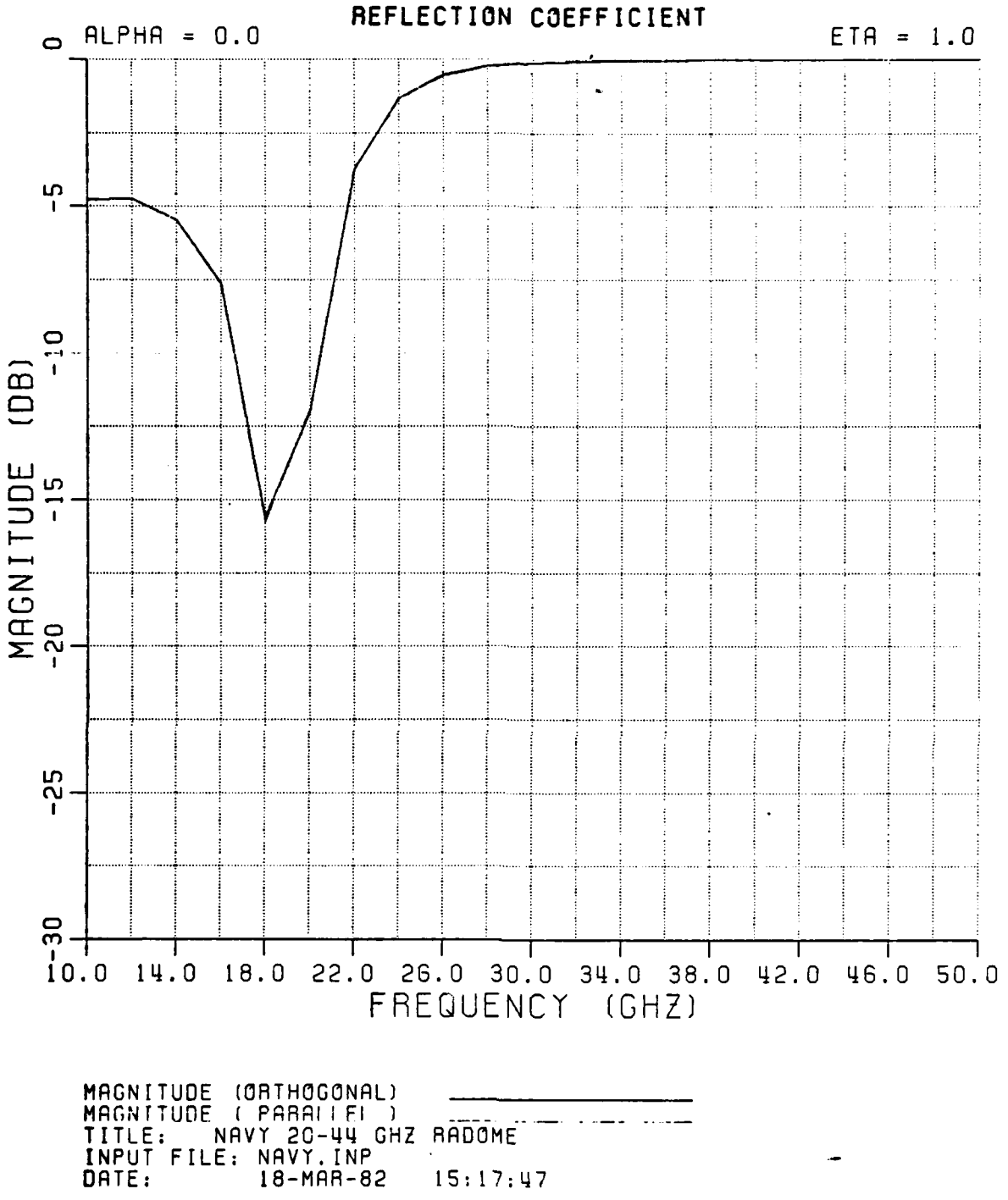

Figure 19. Reflection coefficient of the biplanar array (see Table 2 for dimensions). Angle of incidence 1°.

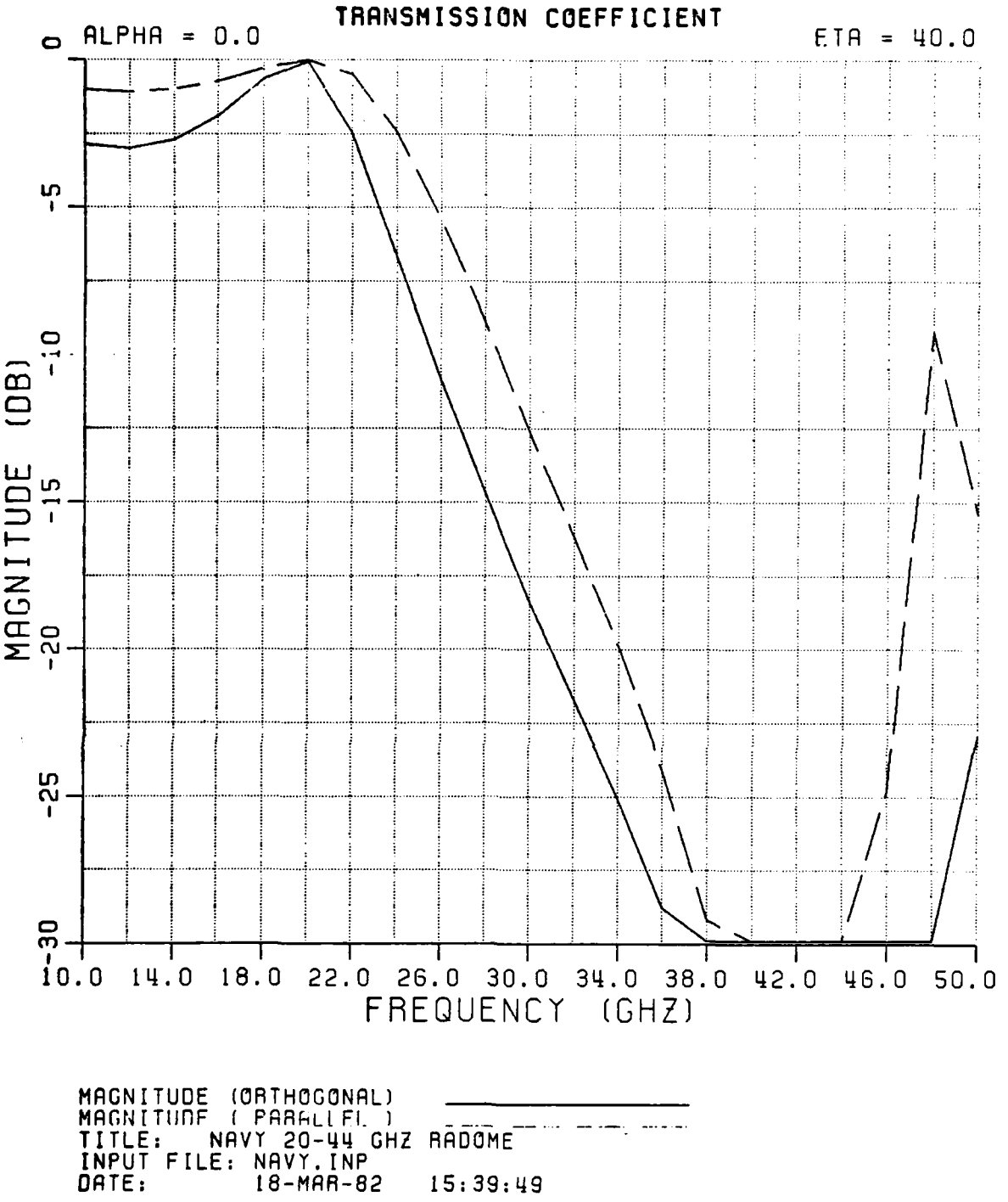

Figure 20. Transmission coefficient of the biplanar array (see Table 2 for dimensions). Angle of incidence 40°.

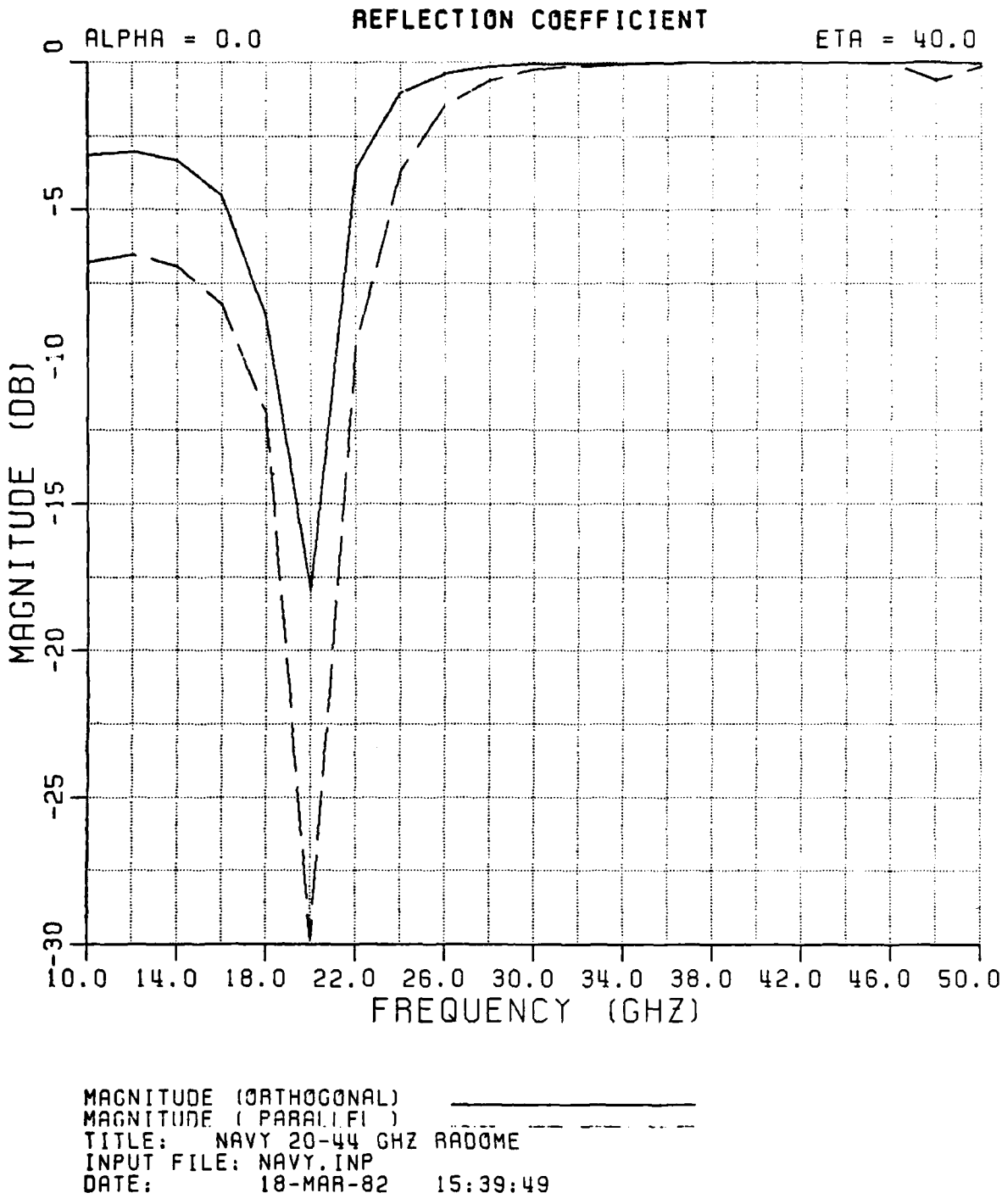

Figure 21. Transmission coefficient of the biplanar array (see Table 2 for dimensions). Angle of incidence 40°.

SECTION II

THE X-BAND ARRAY

1. LAYOUT

The X-band array, mounted behind the Q-Band dish, is comprised of 24 dipoles as shown in Figure 22. They are connected in pairs by balanced two-wire transmission lines. The entire array, including these balanced transmission lines, is etched on a circuit board of very low loss dielectric of thickness 1/32". It is mounted 6 mm (~0.16 λ) in front of a groundplane. This groundplane is actually made of two double-sided circuit boards mounted back to back as shown in Figure 23. The two outsides of these circuit boards are used for etching the balanced transmission lines which feed the dipole pairs. The balanced transmission lines run either in vertical or in horizontal directions. In order to avoid the problem of vertical and horizontal lines crossing each other, differently running lines are etched on opposite sides of the groundplane. Connection between these two sets of lines is established by drilling small holes in the circuit boards, etching out the copper around the holes in the groundplane and inserting small copper wires which are soldered to the etched transmission lines (see Figure 23). The general layout of the harness is seen in Figure 24. It is observed to be of the broad band type. The coaxial input is a Robert's balun where the balanced output is connected directly to the two-wire transmission lines.

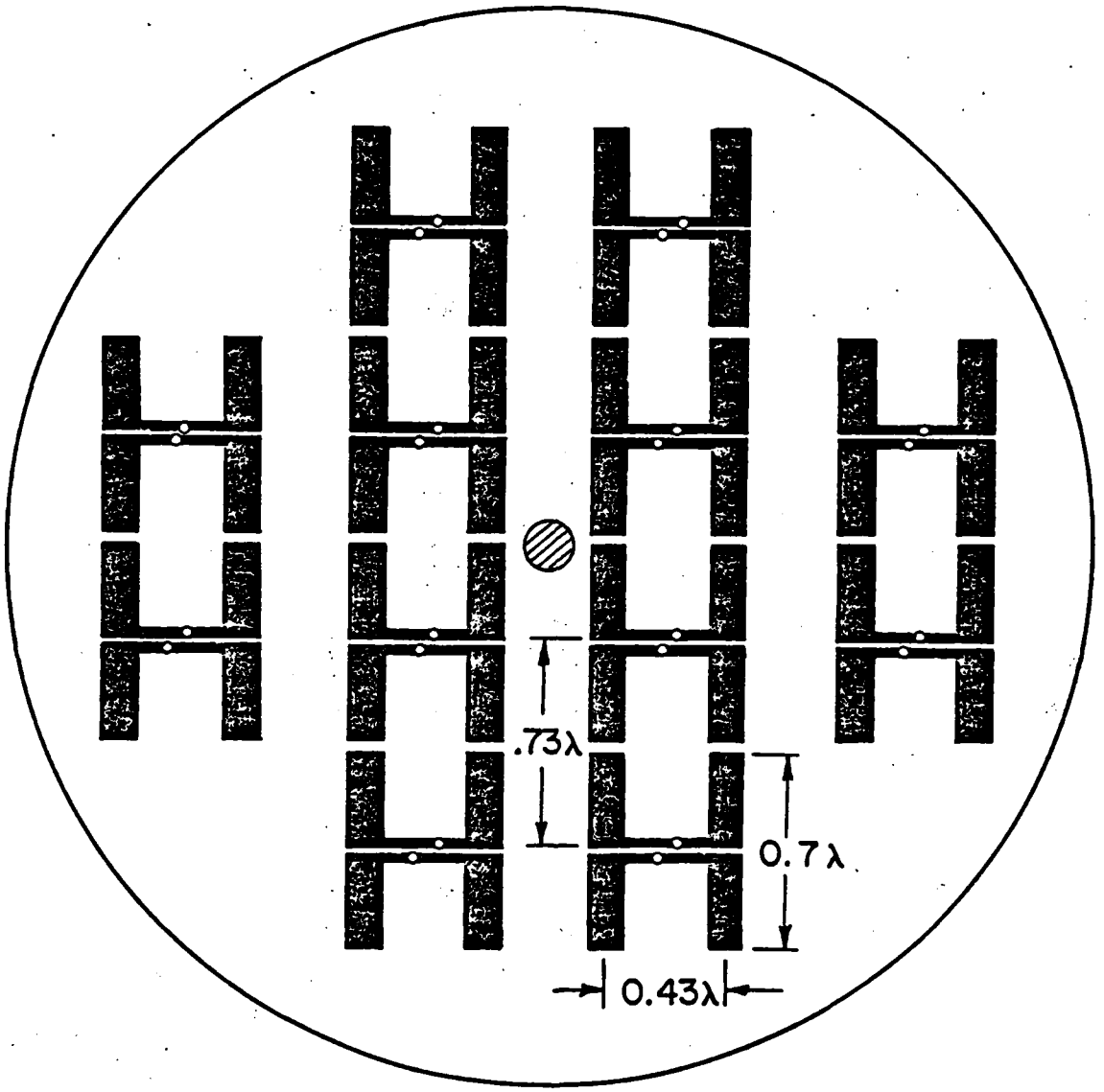

Figure 22. The layout of the X-band array showing the dipoles connected in pairs with balanced two-wire transmission lines. The entire configuration is etched on a circuit board.

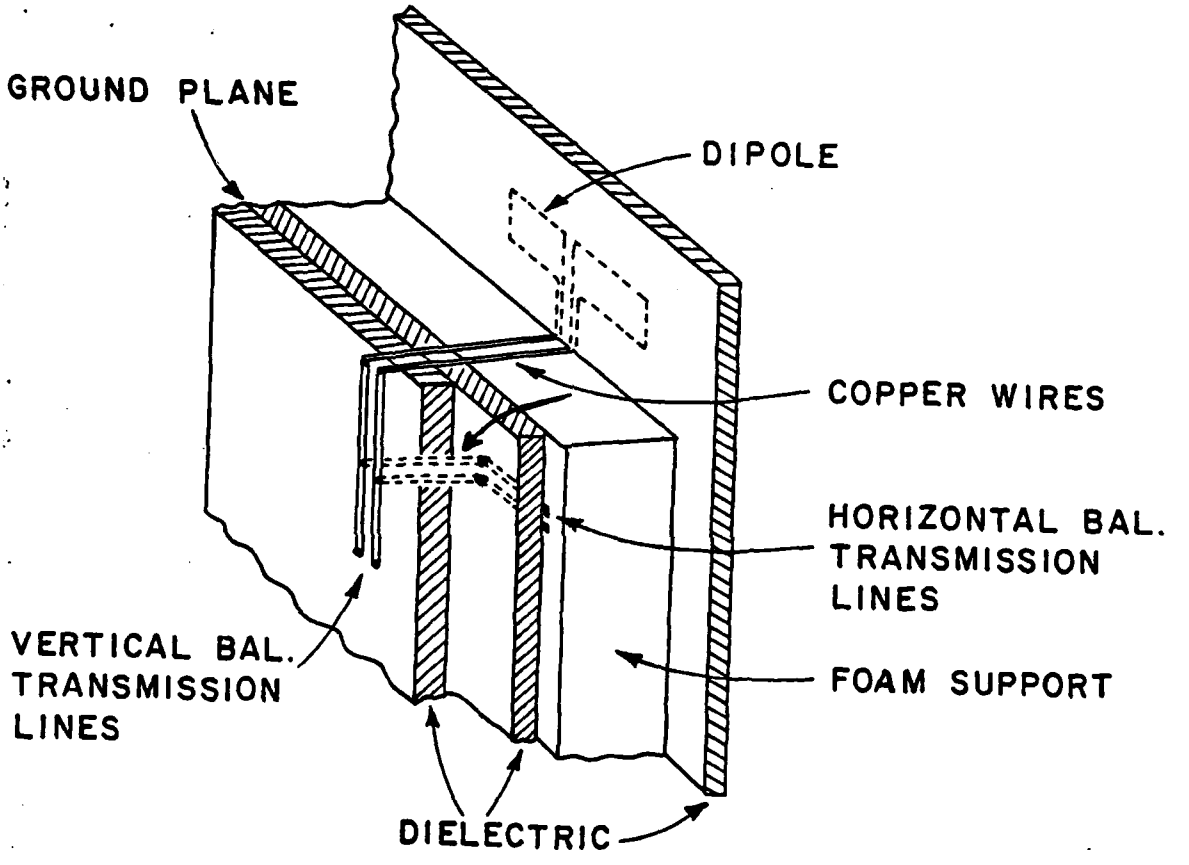

Figure 23. Sideview of the groundplane showing the vertical and horizontal balanced two-wire transmission lines on each side.

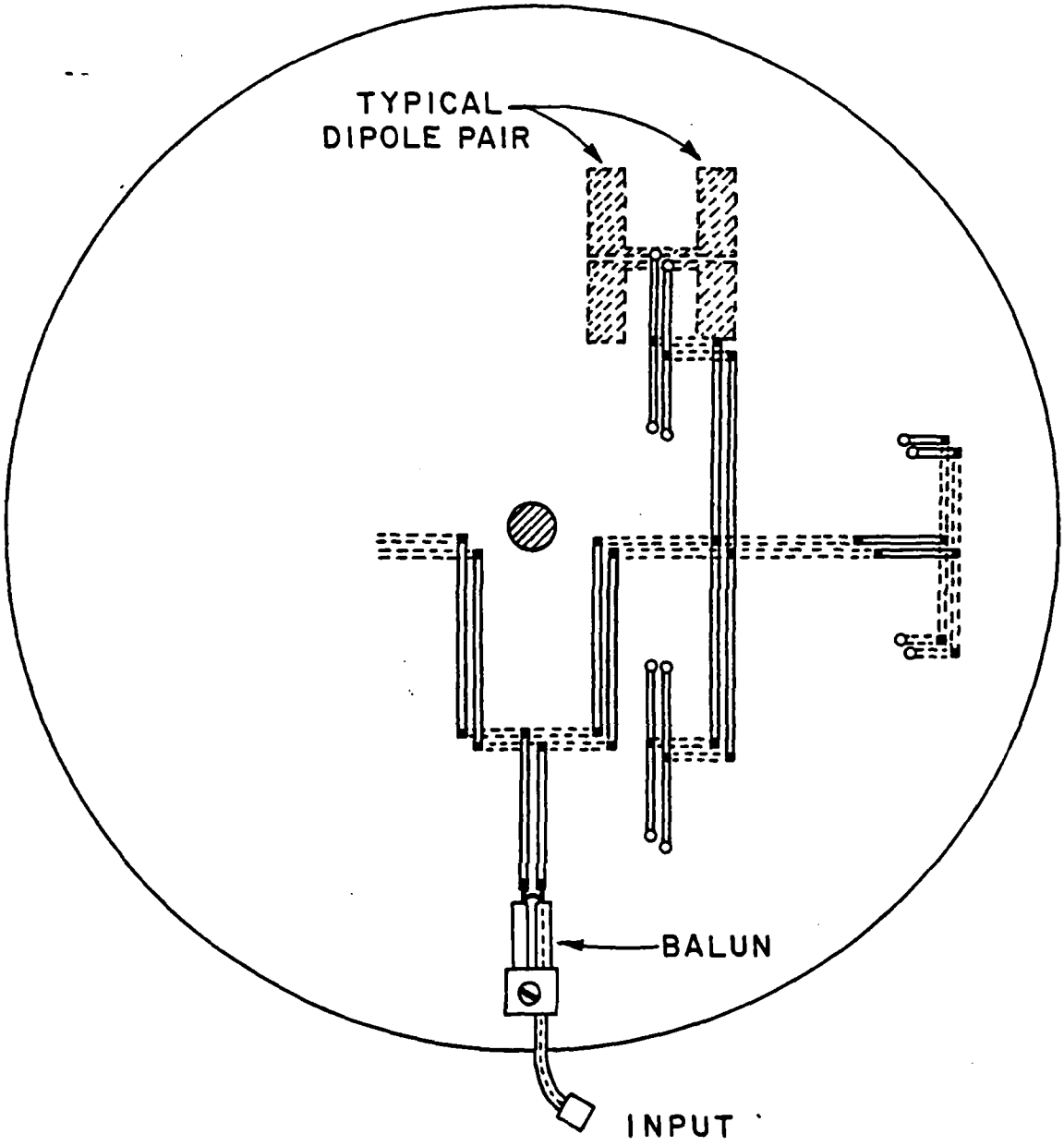

Figure 24. The layout of the broad band harness for the X-band array. It is etched on the printed circuit boards with the exception of the balun at the input.

2. RADIATION PATTERN VERSUS APERTURE ILLUMINATION

The desired X-band array is operating between 7.25 GHz and 7.75 GHz. The radiation pattern has the main beam pointing in the broadside direction and the sidelobes are down 18 dB or more.

It is well known that the broadside and low sidelobe radiation can be achieved by using an array with tapered current distribution and with every element fed in phase. With this idea in mind, the X-band array was designed and a successful array was obtained as shown in Figure 22.

The array is comprised of 24 dipoles etched on a circuit board and fed in phase by balanced transmission lines far from a common balun. The dipoles are connected in pairs and arranged as shown in Figure 22. The dipoles are fed with equal amplitude, and the aperture taper in the array is automatically obtained due to the "circular" shape of the aperture. The array has satisfactory to good radiation patterns over most of the operating band. The measured patterns will be shown later in subsection 5.

3. ROBERT'S BALUN AND FEEDING NETWORK

As mentioned earlier, the dipoles in the array need to be fed in phase with balanced currents of the same magnitude. To meet this end, a balanced current source is required and a feeding arrangement to make the balanced current equally divided and fed in phase to every dipole in the array is necessary.

In our design, the balanced current is supplied from a Robert's balun connected at the input of a feeding network which has 12 outputs at the center below every dipole pair (see Figure 24). The outputs are connected individually through a pair of small copper wires with circular cross sections, right up to the midpoints of the interconnecting two-wire transmission lines between every two dipoles (see Figure 23). In the network, the transmission lines are arranged to divide the currents evenly to the outputs; the distances between input and every output are adjusted to be electrically equal.

A. Robert's Balun

Due to the high frequency, the Robert's balun is necessarily small in size. It is made of a small 50-ohm flexible coaxial cable mounted and soldered in a copper frame as shown in Figure 25.

The copper frame is made of two tiny rigid copper pipes of different length. The two pipes are placed parallel with a spacing of 1 mm, and soldered together at one end with a 8 mm wide copper clamp as seen in Figure 25b. The copper clamp is used to mechanically maintain a uniform spacing between the two copper pipes and electrically provide a good short circuit approximately a quarter wavelength away from the open end. A small hole drilled in the frame is used for mounting purposes.

The cable is partially peeled without outerconductor. The peeled section, with dielectric and innerconductor only, fits tightly into the longer pipe. This protruding line is bent and its innerconductor soldered on to the shorter pipe. The outerconductor of the cable is

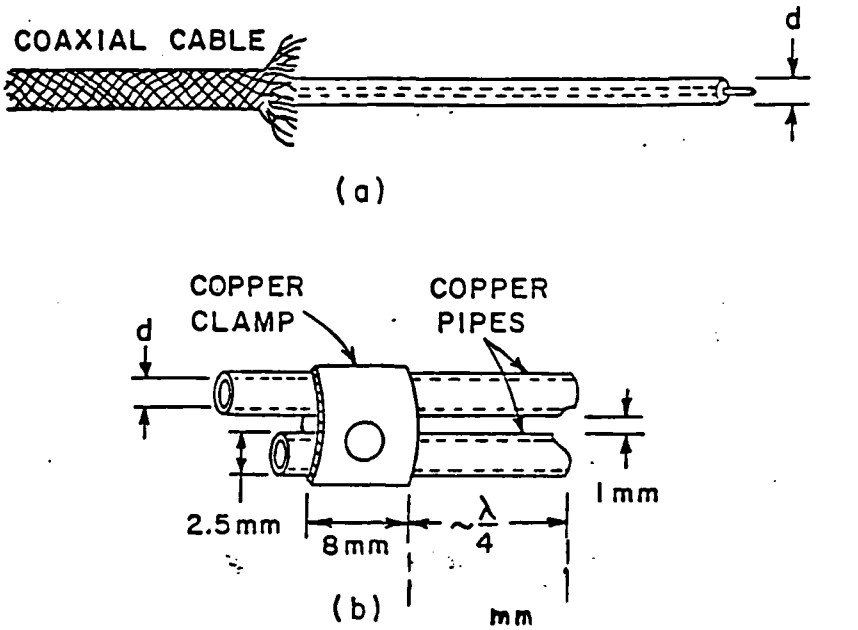

Figure 25. a. A small flexible 50-ohm coaxial cable with outer conductor partially peeled.

b. A copper frame made of two tiny copper pipes connected together at one end with a copper clamp.

c. The completed Robert's balun.

soldered on to the longer pipe. Two small copper wires soldered on the copper pipes at the open end serve as an output for the Robert's balun. With these two copper wires, the balun is connected to the input of the feeding network.

It has been shown by the experiment that the Robert's balun was working very well within the operating band; it supplied almost balanced currents to the feeding network at its output. But it was also found that there was a very weak radiation coming from the balun causing some spurious radiation in the radiation pattern of the X-band array. This problem was solved by a special arrangement to be shown later.

B. Feeding Network

Balanced currents are two oppositely going currents with equal magnitudes. In order to guide and transmit the balanced currents from one place to another, without losing their original properties along the transmission path, an appropriate transmission line is required.

The two-wire transmission line chosen here is made of two parallel copper wires on top of a dielectric substrate backed by a groundplane, as seen in Figure 26. This kind of transmission line is easy to make on a double-sided circuit board by etching a pair of parallel strip lines on one side of the circuit board. The copper on the other side is saved for groundplane. The characteristic impedance of the two-wire

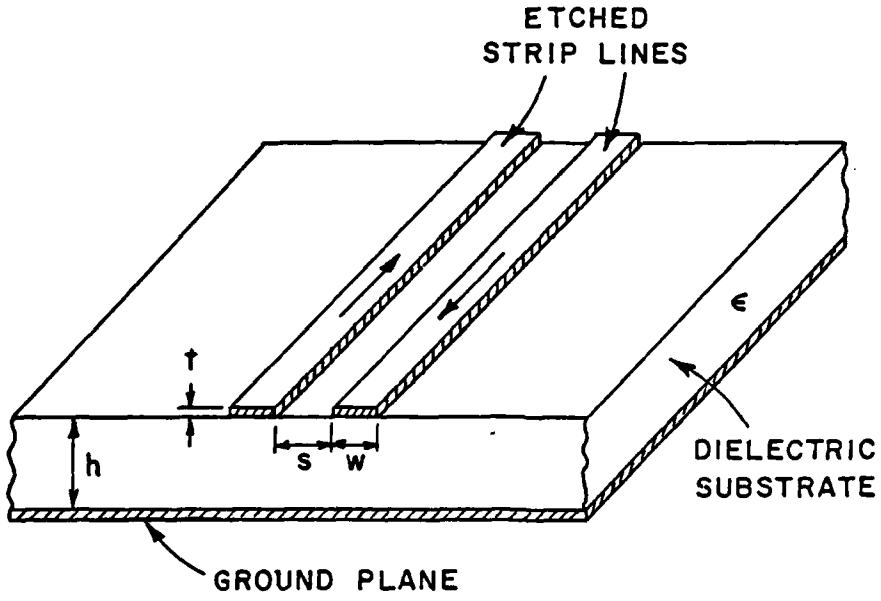

Figure 26. Typical configuration of a two-wire transmission line.

transmission line is a function of width (w) and thickness (t) of the strips, spacing (s) between the strips, and thickness (h) and dielectric constant (ε_r) of the substrate.

First, we layed out a complete wiring diagram showing the whole network structure which satisfied all the desired requirements. Next we developed a suitable interconnecting technique to accomplish all the connections appearing in the diagram. The results of this planning are shown next.

1. Wiring Diagram

In order to feed the dipoles pairs and make the dipoles currents the same in both magnitude and phase, the feeding network has to meet the following requirements:

1. It must have 12 outputs located right below and at midpoints of all dipole pairs,
2. the balanced current supplied by the balun at the input of the feeding network is evenly divided and transmitted through two-wire transmission lines to all dipoles,
3. the transmission paths from input to all outputs are equal in electrical length.

Following these guidelines, many wiring diagrams were drawn and compared. A simple example shown in Figure 27 was adopted. The term 'simple' means the network shown in the diagram is simple in structure and is possible to make without use of high level techniques or any expensive components.

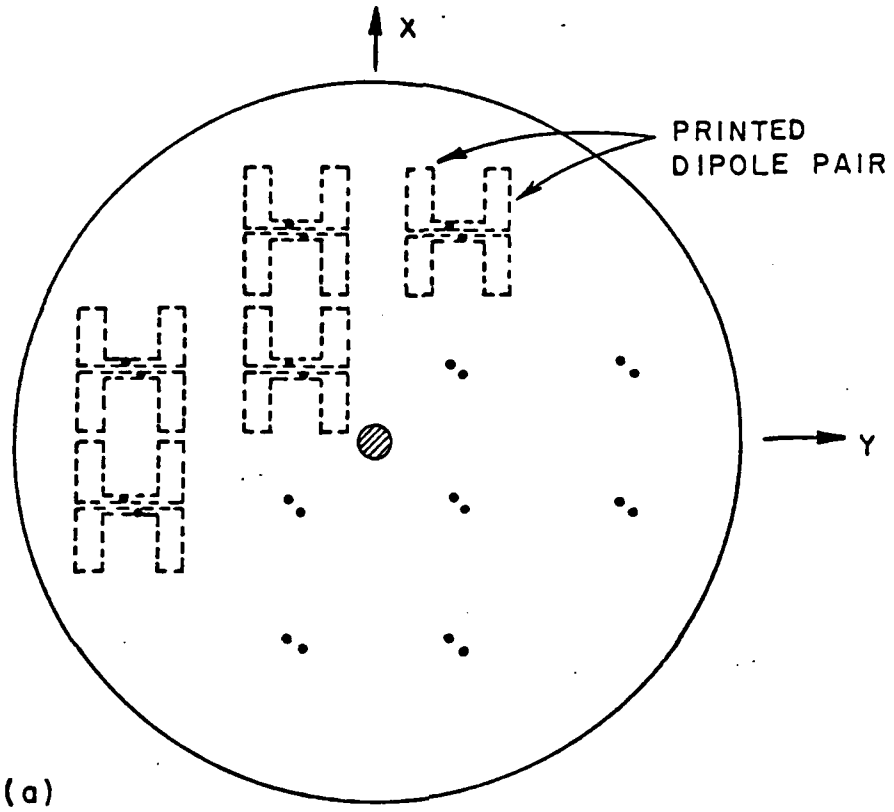

(a)

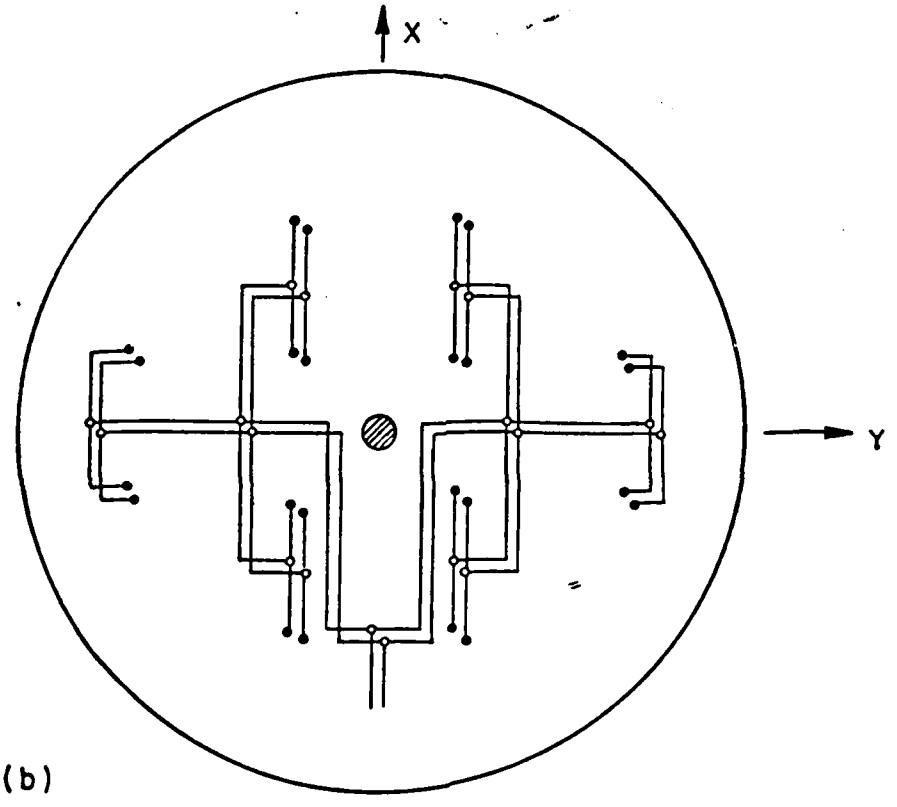

(b)

Figure 27. a. 12 dot pairs showing the locations of the outputs of the feeding network.
b. A simple wiring diagram satisfying the desired requirements for a feeding network.

As seen in Figure 27, the outputs indicated by solid dot-pairs are located around the midpoints of all dipole pairs. The small circles represent branching points from where the currents are evenly divided into two or three components. Further, the parallel lines connecting the dots and circles represent two-wire transmission lines. The total length of lines connecting the input to every output is approximately 12.6 cm long, corresponding to about 3.05 - 3.26 in wavelengths. A big circle at the center of the wiring diagram is a hole which is reserved for the Q-band feed of the parabolic dish antenna which is placed in front of the X-band array.

It is also seen in Figure 27 that all the lines in the wiring diagram are running either vertically or horizontally. Those differently oriented lines meet at the branching points and the turning points where the lines are joined and cross-over occur. To solve the problem of cross-over, the two-faced network distribution technique was developed. The details will be covered in the next subsection.

2. Network Realization

While the wiring diagram shown in Figure 27 is conceptually simple, we encountered difficulty in the wiring of the cross-over existing between the vertical and horizontal transmission lines. This problem had to be solved before we started to construct the feeding network.

In an ideal cross-over, orthogonal lines must not touch or interfere with each other, nor should the currents in the two lines be affected by the presence of the cross-over. In order to make the

cross-over as perfect as possible, several methods were tried and analyzed. Our final method was simply to place the differently running transmission lines on opposite faces of the groundplane. By doing this, the lines will never touch each other.

This kind of cross-over is made of two double-sided circuit boards mounted face to face as shown in Figure 28a. The orthogonal transmission lines are etched on the opposite faces of the combined circuit board and share a common groundplane, as shown in Figure 28b. With this arrangement, the transmission lines on both faces are automatically isolated and the problem of cross-over is solved. Connection between the lines on different faces is established by drilling small holes in the circuit board, etching out a little copper around the holes in the groundplane and inserting small copper wires which are soldered to the etched transmission lines (see Figure 28b).

By using the above method, the cross-over problem is readily solved. This method was applied to construct all the connections appearing in the wiring diagram shown in Figure 27. Five typical wirings are shown in Figure 29; the solid and dashed transmission lines are etched on the opposite faces of the combined circuit boards. They are interconnected at the places marked by the solid dots using the method shown in Figure 28b.

Two different layouts were obtained. They are shown in Figure 30 (LAYOUT I) and Figure 31 (LAYOUT II).

The feeding networks, LAYOUT I and LAYOUT II, were both working well in feeding the dipole array. However, LAYOUT I had a disadvantage,

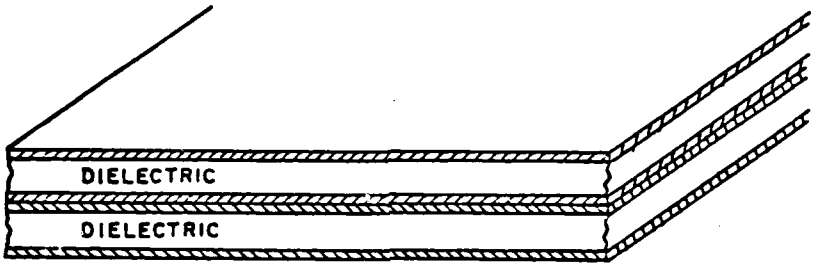

(a)

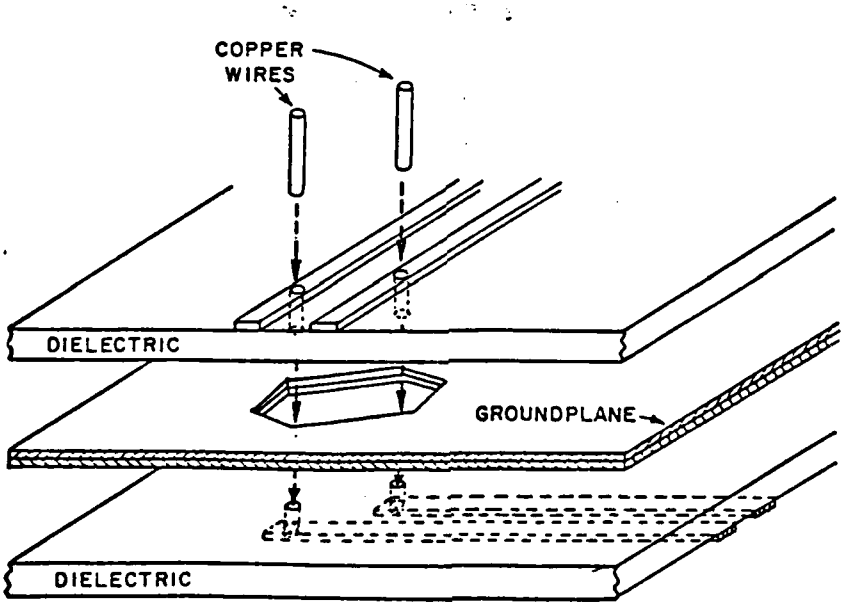

(b)

Figure 28. a. A combined circuit board.

b. The interconnection scheme used to connect the two-wire transmission lines etched on the opposite faces of a combined circuit board.

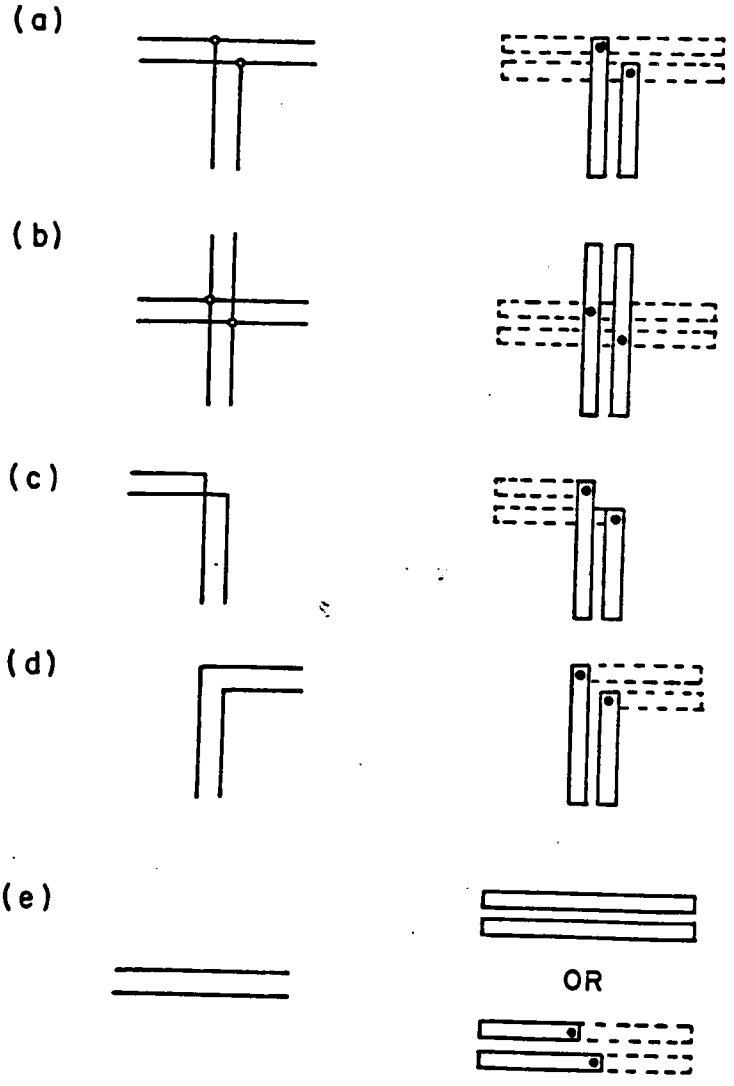

Figure 29. Five typical wirings and their circuit layouts.

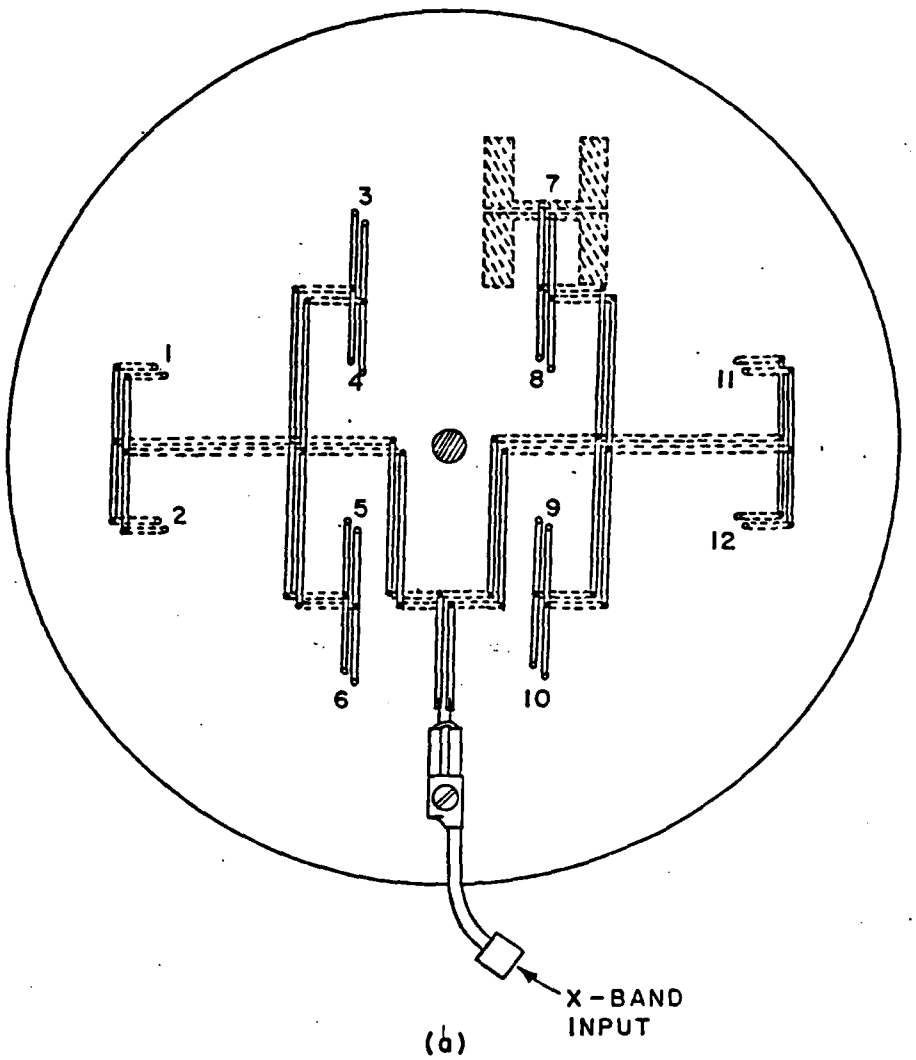

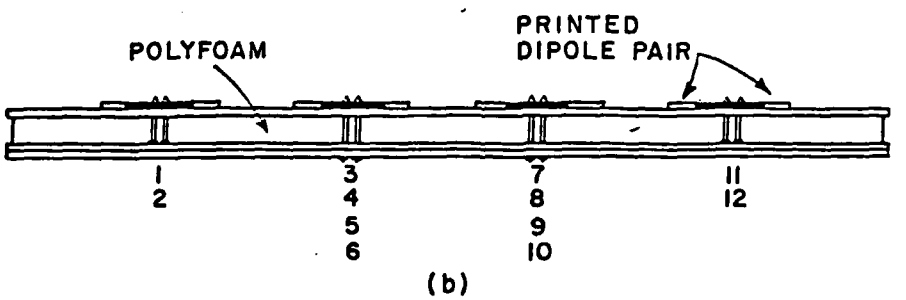

Figure 30. a. Feeding network LAYOUT I.

b. Schematic diagram showing the connections between dipole pairs and the outputs in the feeding network LAYOUT I.

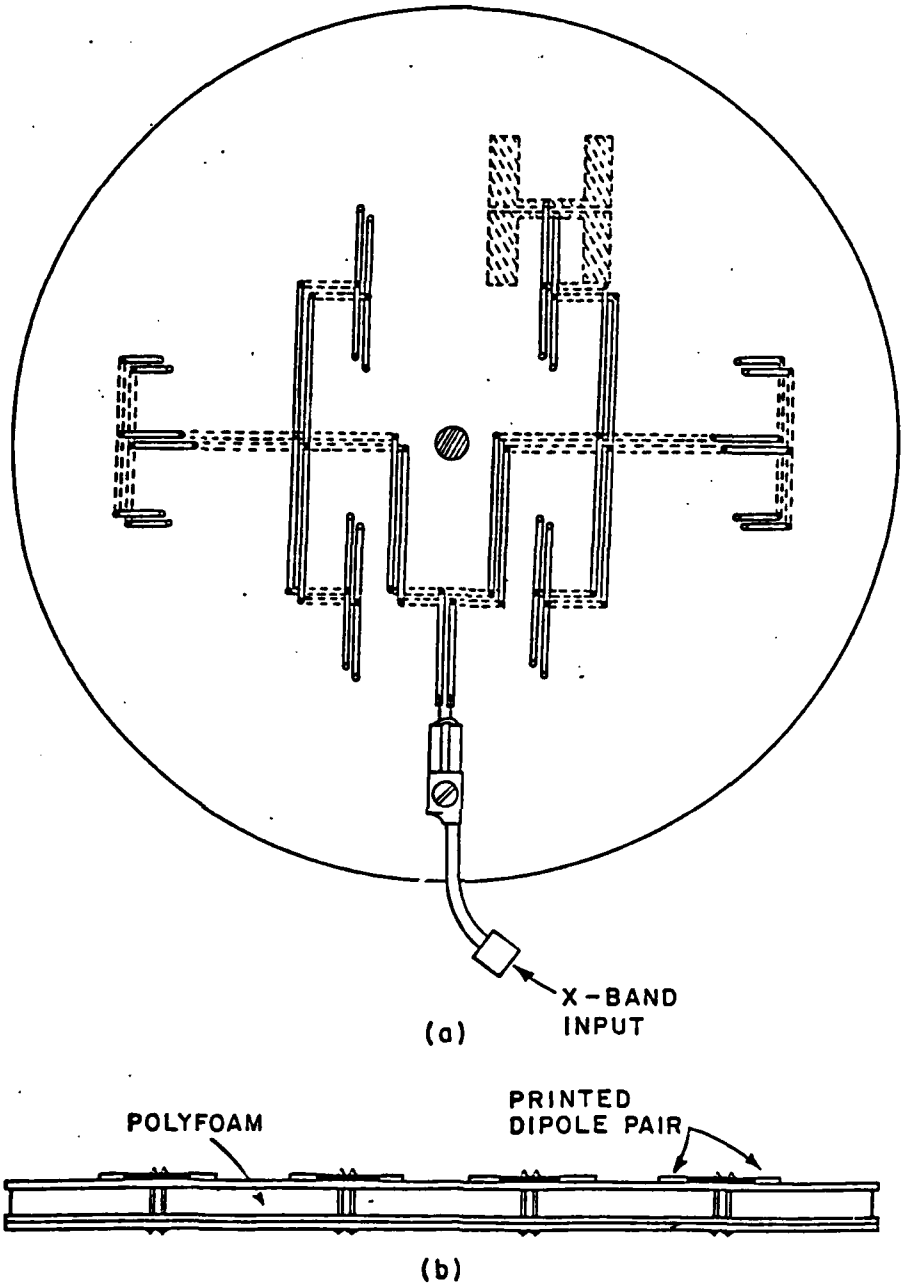

Figure 31. a. Feeding network LAYOUT II.

b. Schematic diagram showing the connections between dipole pairs and the outputs in the feeding network LAYOUT II.

namely difficult soldering position of the outputs (labeled by 1,2,11,12 in Figure 30a) on the left and right hand sides of the feeding network. In assembling the X-band array, these four outputs were on the top face of the combined circuit board and covered by the supporting foam while their output terminals were not accessible from the outside. This made soldering very difficult. Although this calamity can be overcome in the lab, the procedure is long and complicated. In the LAYOUT II, this problem does not exist; all the output terminals are on the bottom face of the combined circuit board. The connection and soldering work can be done from the outside with little effort. Figure 32 is a schematic diagram showing the details of the scheme which was used to connect the dipole pair and the output in the LAYOUT II.

The total length of the transmission lines in the feeding network is approximately 55 cm long. In order to avoid too much energy lost in the transmission path, a low loss 3M teflon/fiber circuit board with dielectric constant ε_r=2.5 and a thickness of 1/32 inch was used. The dissipation factor of the circuit board at X-band frequencies is less than 0.0015.

All the transmission lines shown in the feeding network were etched with the same pattern. The dimensions of the transmission lines are shown in Figure 33. With these dimensions, the characteristic impedance of the transmission line is ~ 70 ohms.

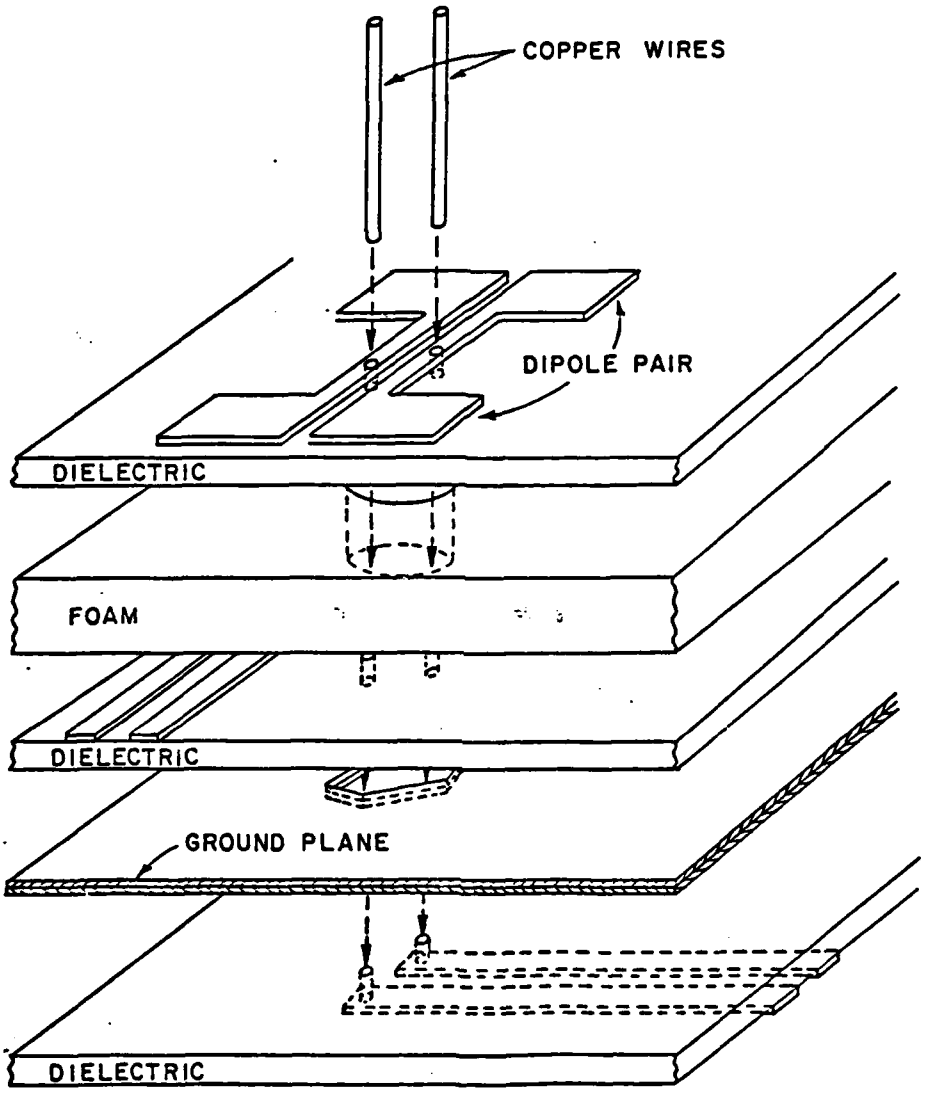

Figure 32. The details of the connection arrangements between dipole pair and the output in the feeding network LAYOUT II.

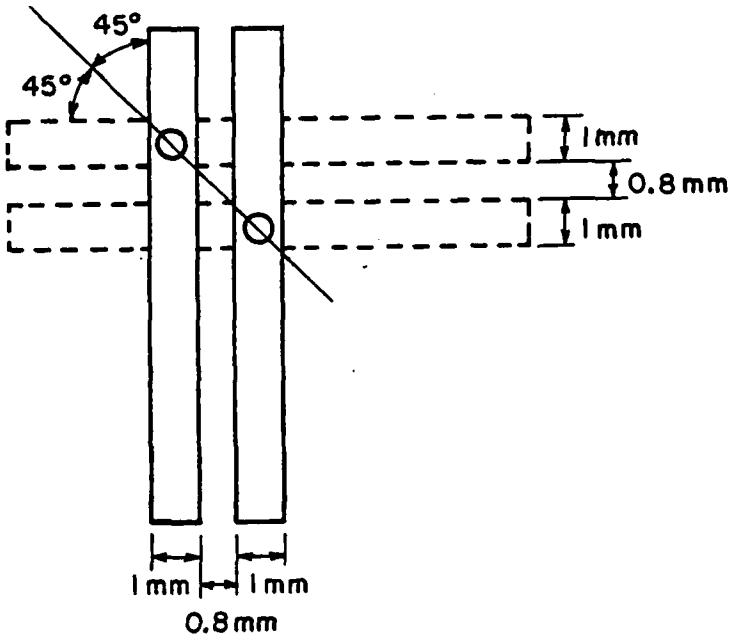

Figure 33. The dimensions of the transmission lines.

4. IMPEDANCE OF X-BAND ARRAY

The measured impedance of the X-band array before matching is seen in Figure 34. The reference plane is the balun at the transition to the balanced transmission line. The actual matching was somewhat complicated by the fact that we did not know the precise effect of the two wire lines connecting the vertical and horizontal lines. Consequently, the matching was somewhat experimental in nature rather than a precise calculation of the actual dipole impedance based on the measured impedance at the balun.

An improvement of the input impedance of the X-band array is obtained by the modified feeding network shown in Figure 35. The input impedance of the X-band array fed by this "modified" feeding network is shown in Figure 36. By properly adjusting the lengths of the five stub lines, the impedance curve was compressed to a smaller region somewhat away from the center of the Smith chart. The final centering was achieved by inserting a small dielectric slab between the two copper pipes of the balun and attaching a capacitive load on the two-wire transmission line (see Figure 37 for details). The matched input impedance is presented in Figure 38. This result is considered adequate although further improvement would be possible had time permitted.

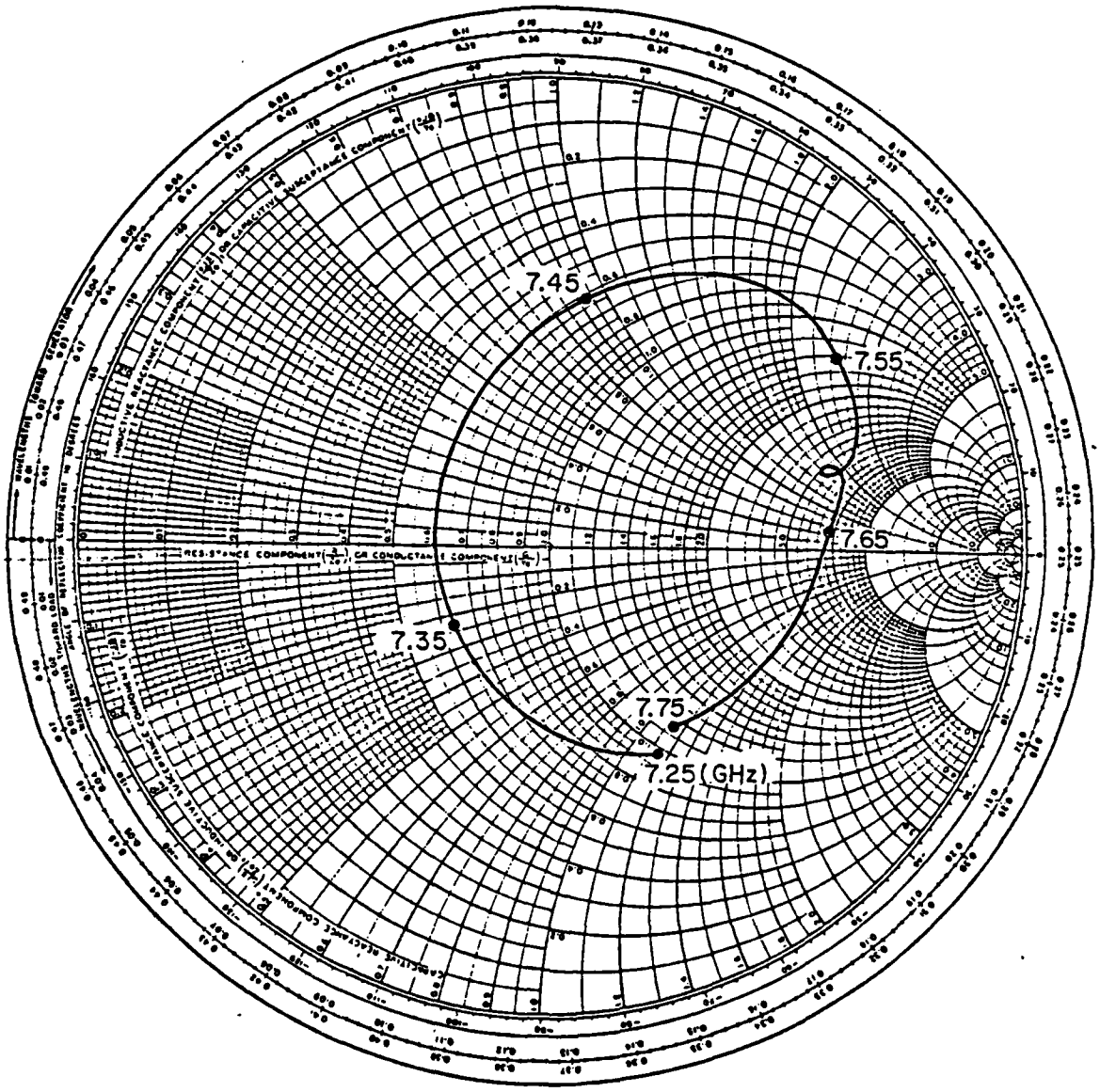

Figure 34. The input impedance of the X-band array before matching by feeding network shown in Figure 30. The impedance was measured at the balun where it connects to the two-wire transmission line.

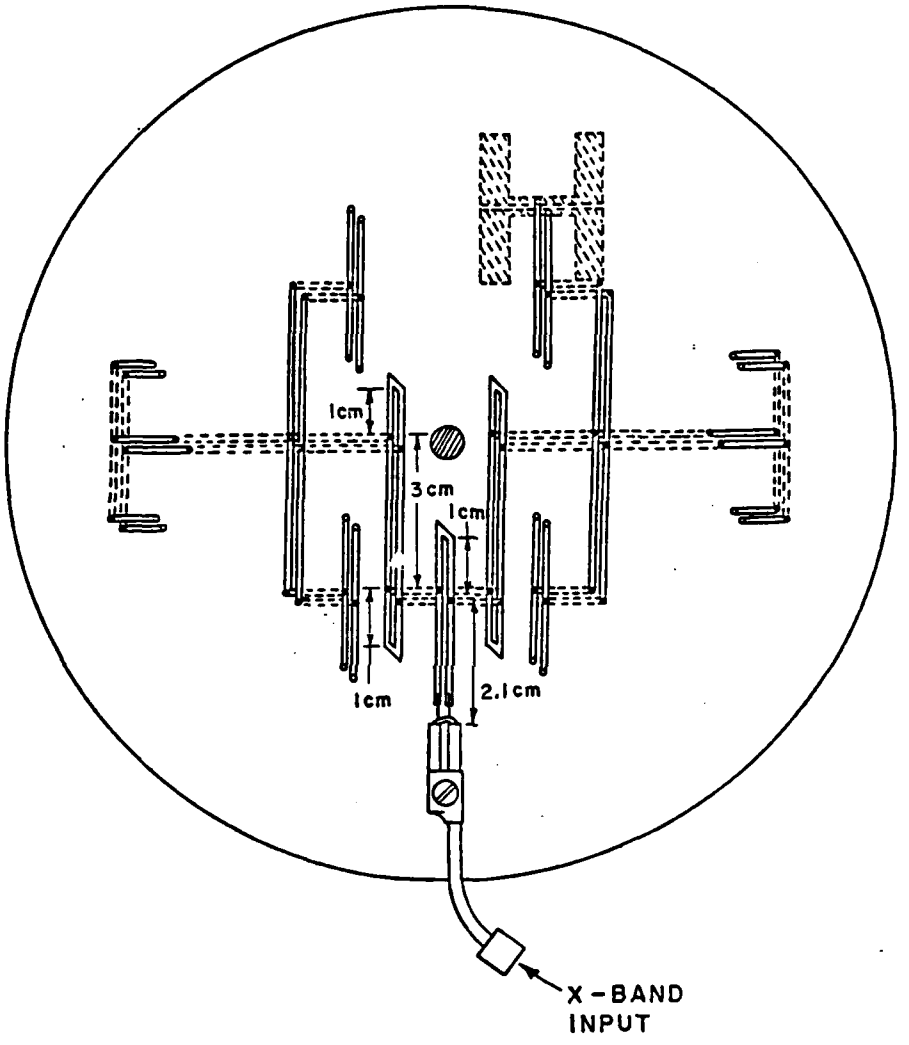

Figure 35. The modified feeding network containing five short stub lines used for tuning the input impedance.

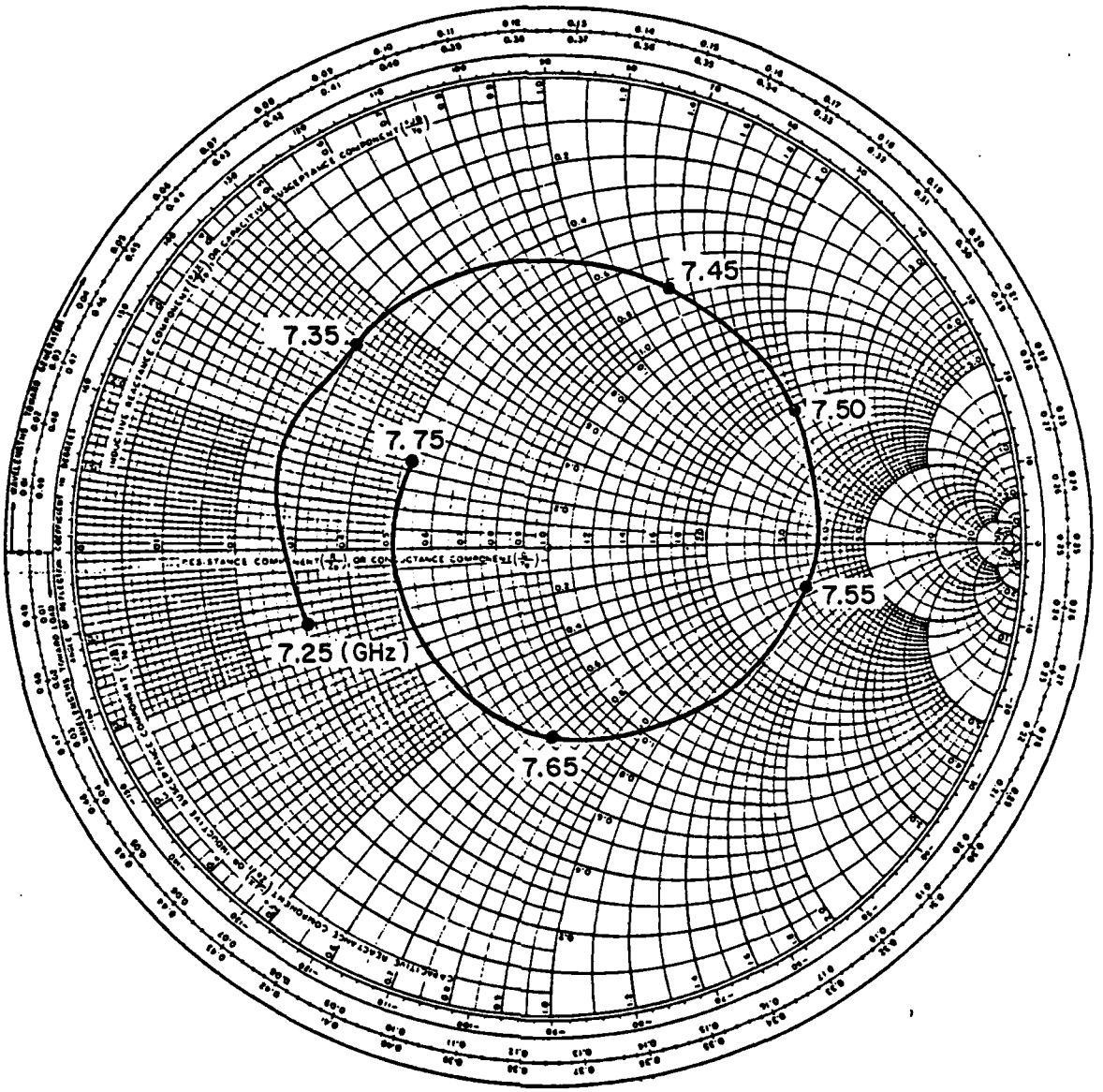

Figure 36. The input impedance of the partly matched X-band array fed by the "modified" feeding network (Figure 35). The impedance was measured at the balun where it connects to the two-wire transmission line.

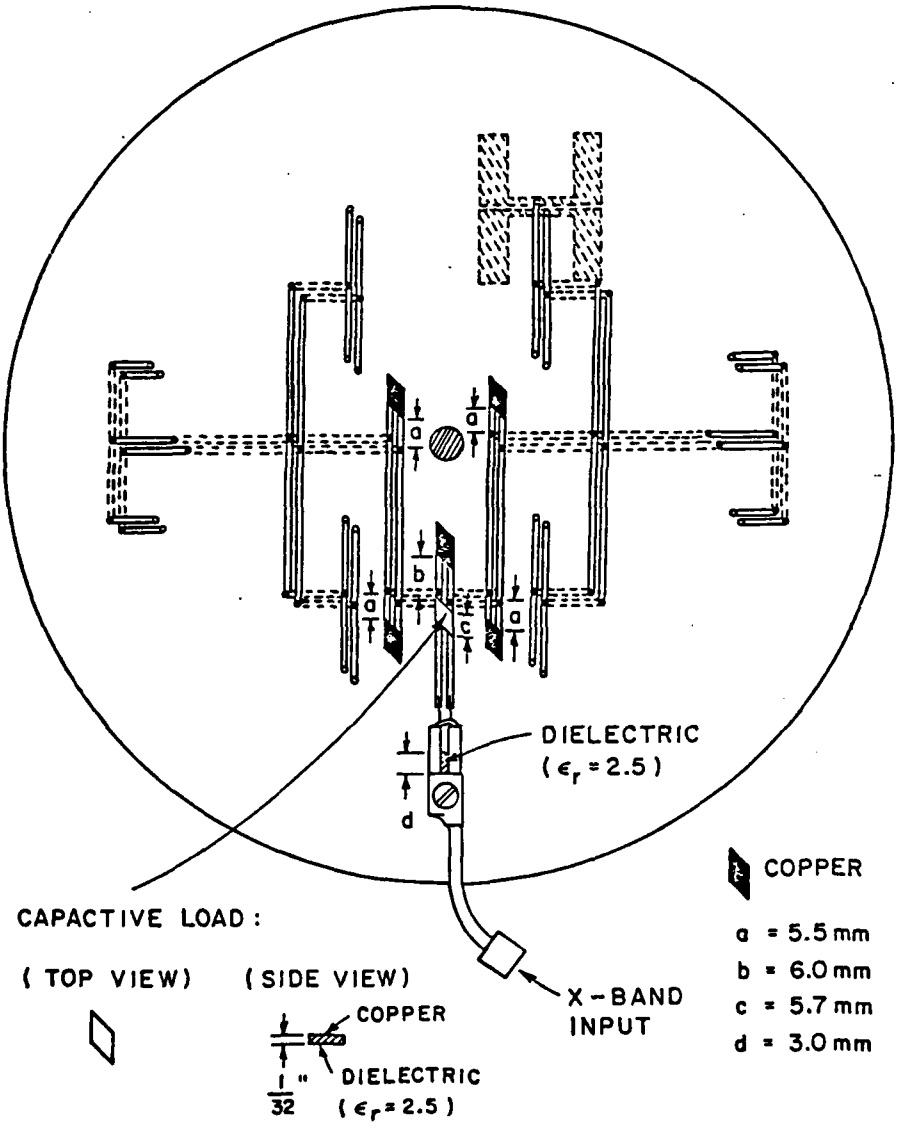

Figure 37. The matched feeding network.

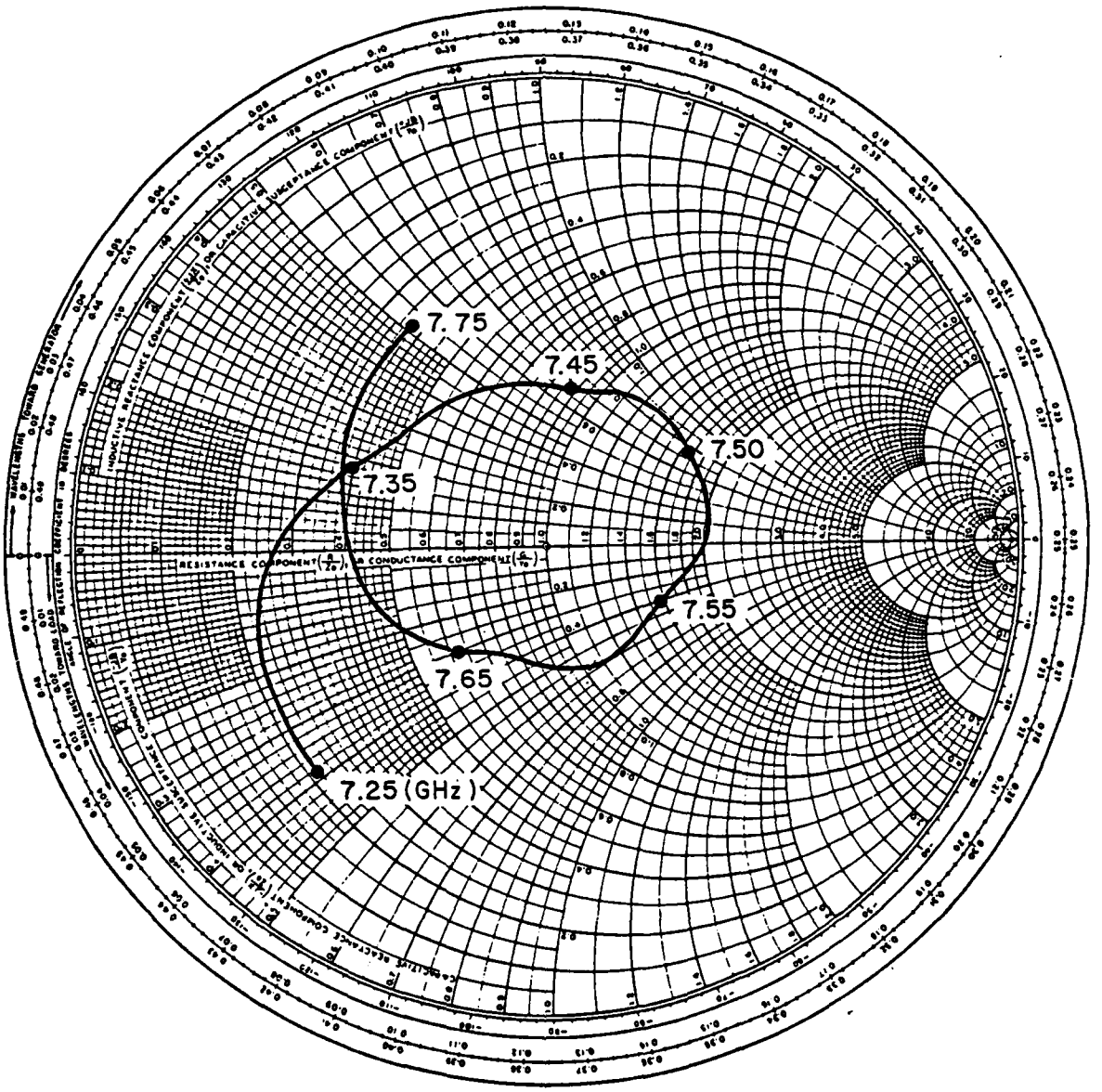

Figure 38. The matched input impedance of the final X-band array at the balun where it connects to the two-wire transmission line.

5. RADIATION PATTERN OF X-BAND ARRAY

The radiation patterns of the matched X-band array were measured in the principal planes as shown in Figure 39. First, the patterns were measured without shielding the balun as shown in Figures 40-46. It is apparent from the figures that the X-band array has satisfactory radiation patterns over most of the operating band, especially at the middle of the band. However, the backlobes and cross polarized pattern levels are somewhat high at the ends of the operating band.

The occurrence of the high backlobes was not too surprising. During the impedance measurements, we noticed that the Robert's balun was slightly radiating. Although this radiation compared with that from the dipole array was relatively weak, it caused some undesired radiation in the back direction at certain frequencies. Closely examining the radiation patterns of the X-band array, we noted that the strong cross polarized pattern was always accompanied by the radiation pattern with high back radiation. This gave us the hint that the radiation from the balun might also have some effect on the cross polarized patterns of the X-band array.

In order to eliminate the possible radiation from the balun, we decided to shield the balun with a copper plate as shown in Figure 47. The copper plate is the same size as the groundplane to which it is connected with three sections of copper foil. Inside this copper cavity is polyfoam which is used to maintain suitable spacing between the copper plate and the balun. In order not to affect the already matched input impedance of the X-band array, a polyfoam with a thickness of 6 mm was used.

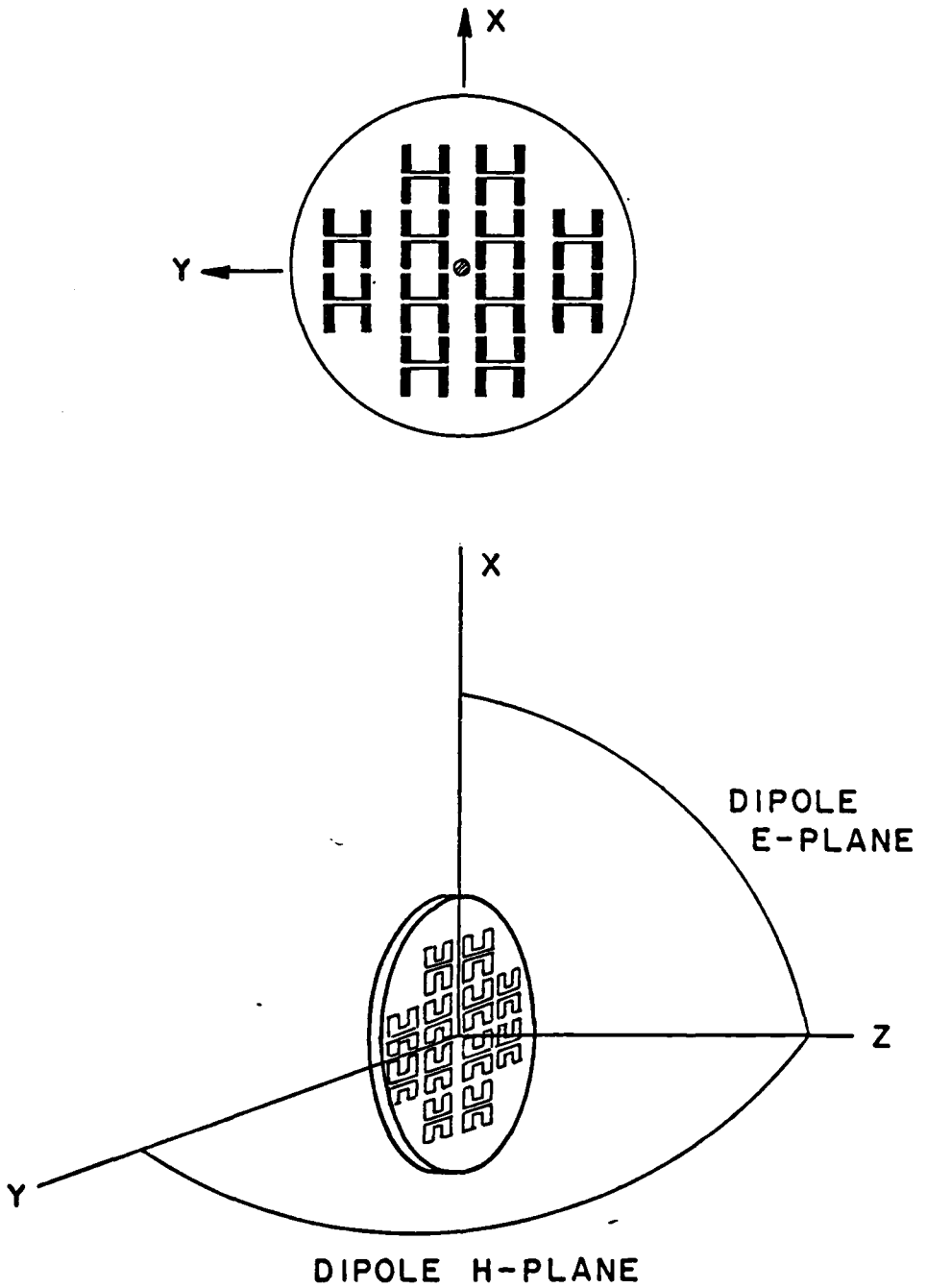

Figure 39. The definitions of "dipole H-plane" and "dipole E-plane". All the radiation patterns of the X-band array were measured at these two perpendicular cuts.

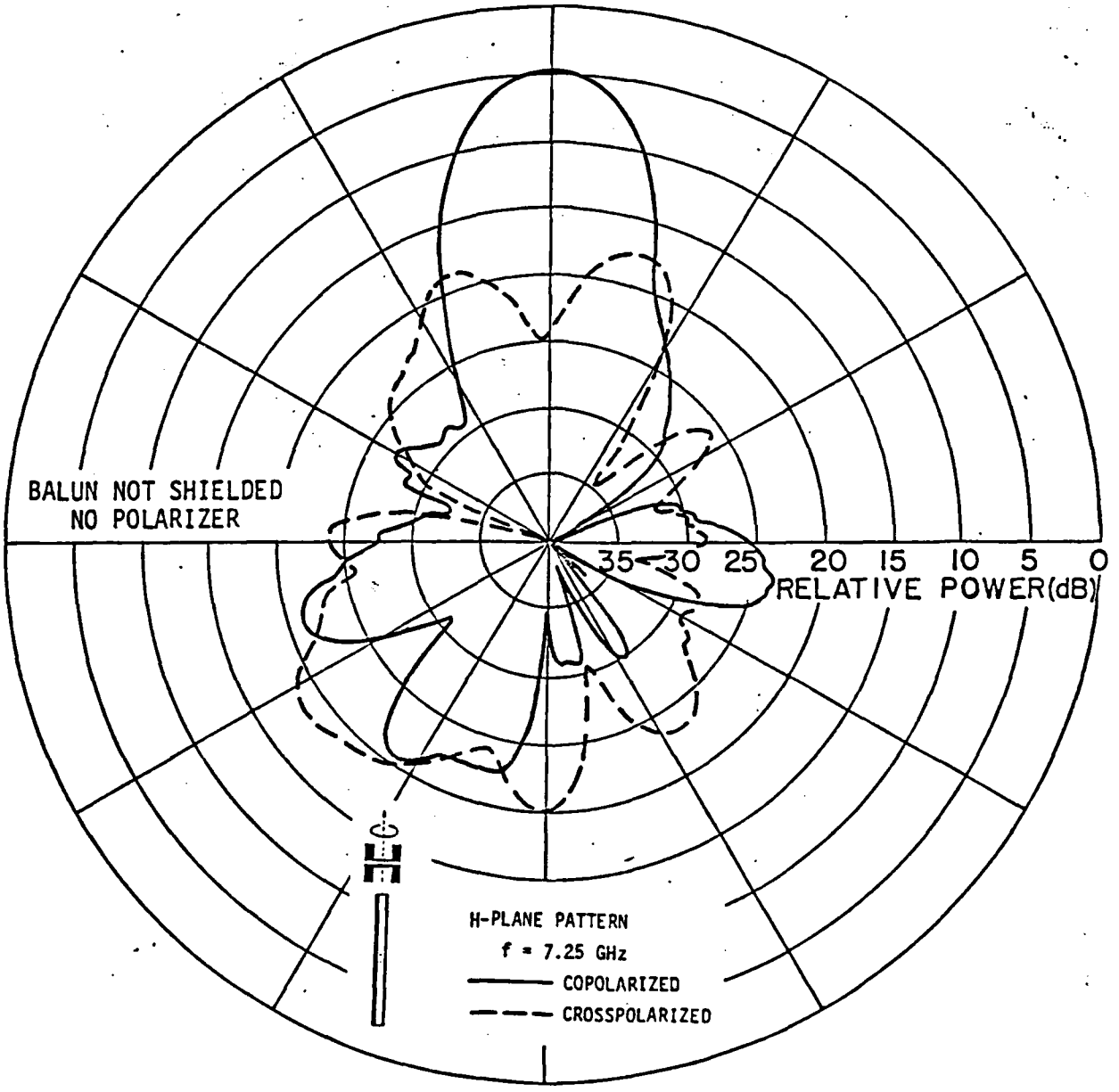

Figure 40. a. The radiation pattern of the X-band array without balun shielded. H-plane, f = 7.25 GHz.

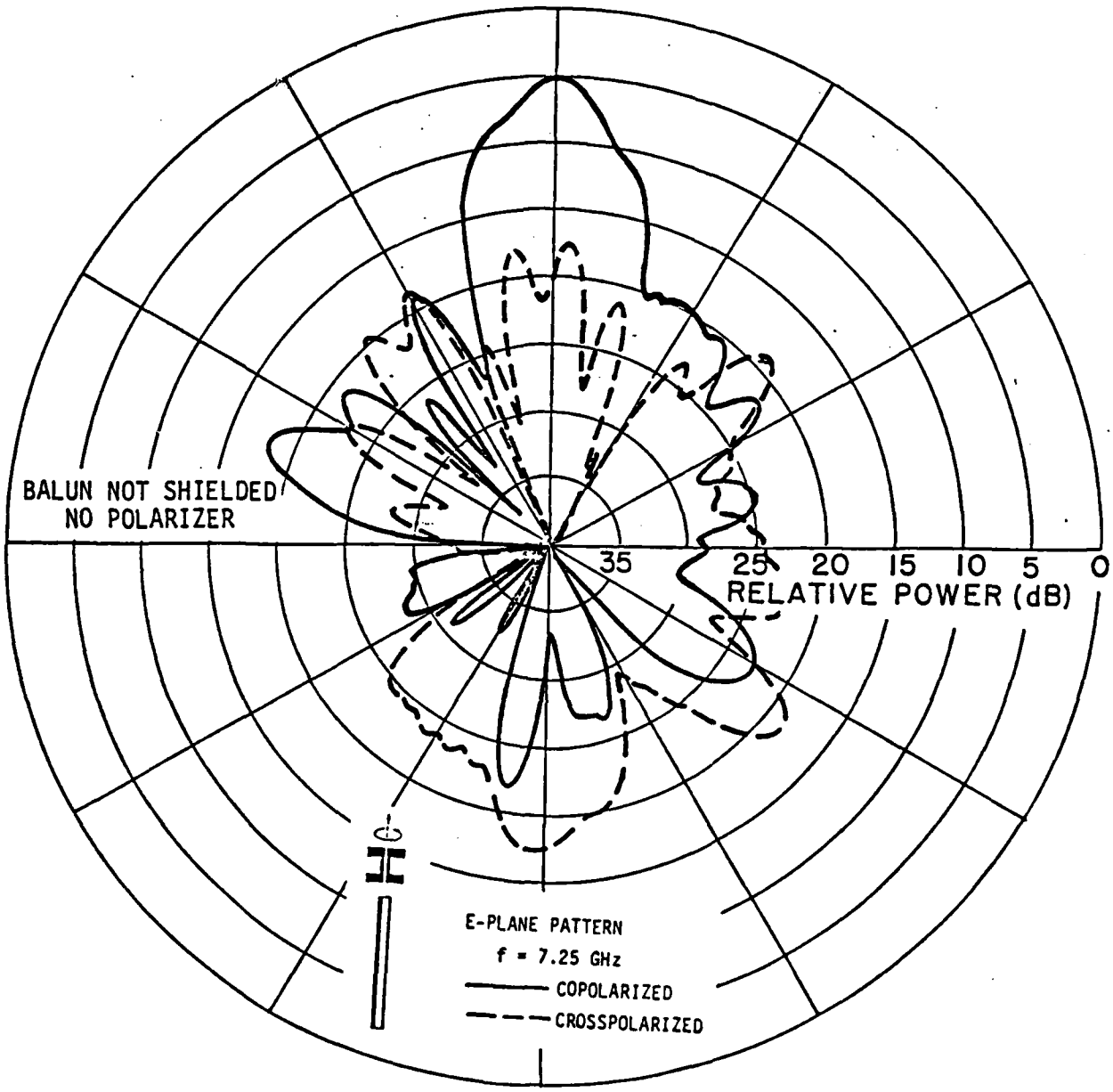

Figure 40. b. The radiation pattern of the X-band array without balun shielded. E-plane, f = 7.25 GHz.

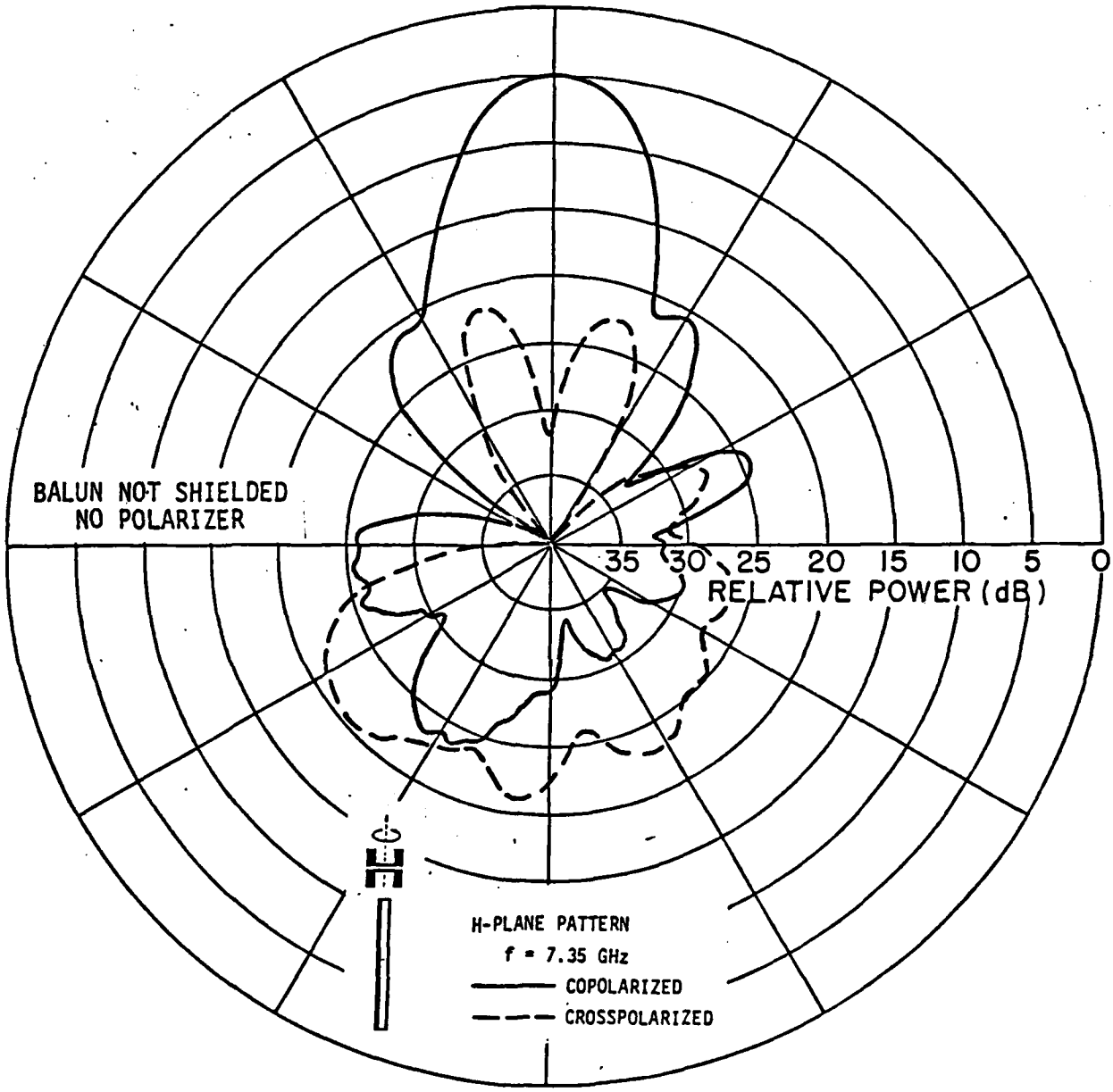

Figure 41. a. The radiation pattern of the X-band array without balun shielded. H-plane, f = 7.35 GHz.

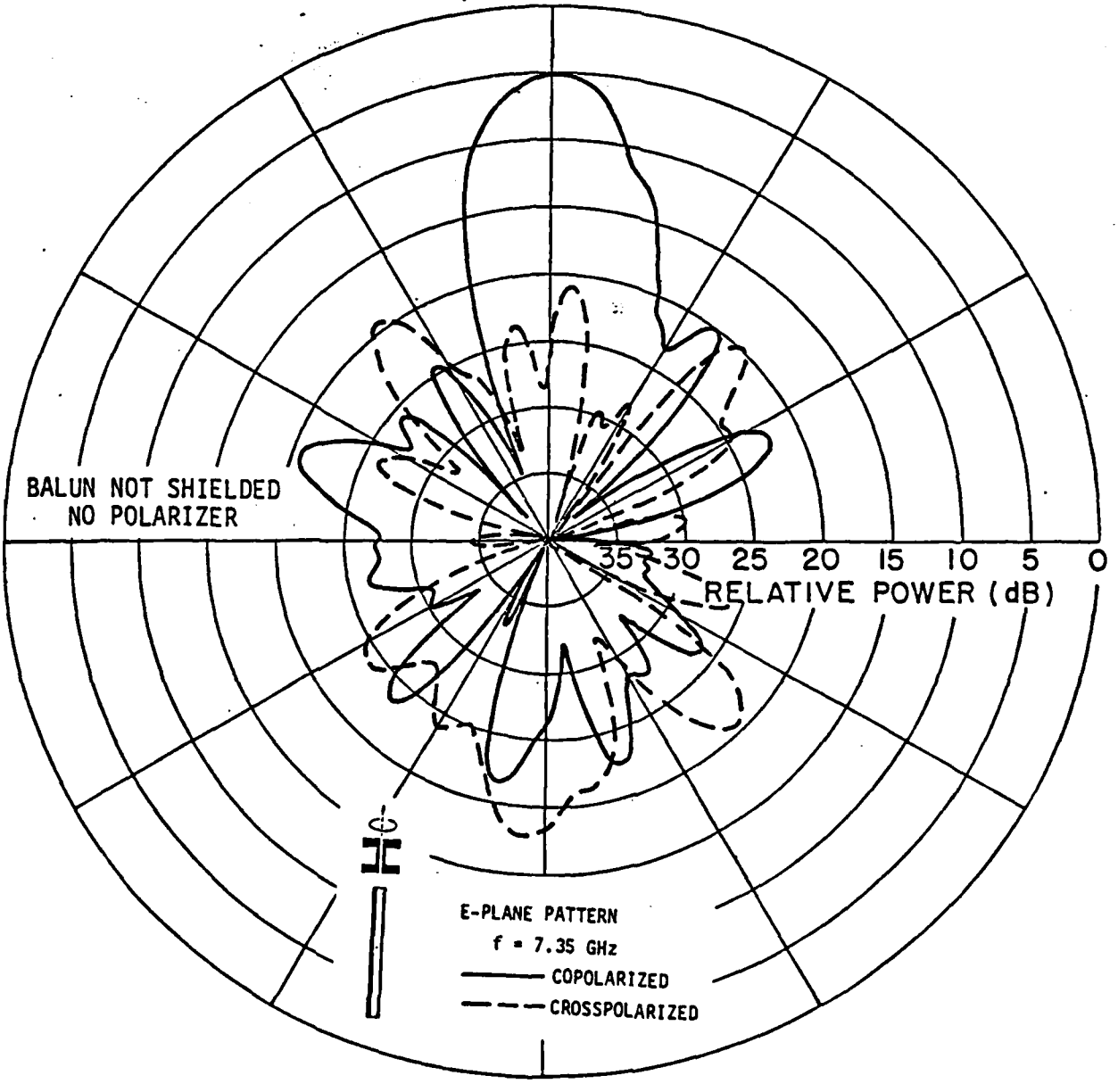

Figure 41. b. The radiation pattern of the X-band array without balun shielded. E-plane, f = 7.35 Ghz.

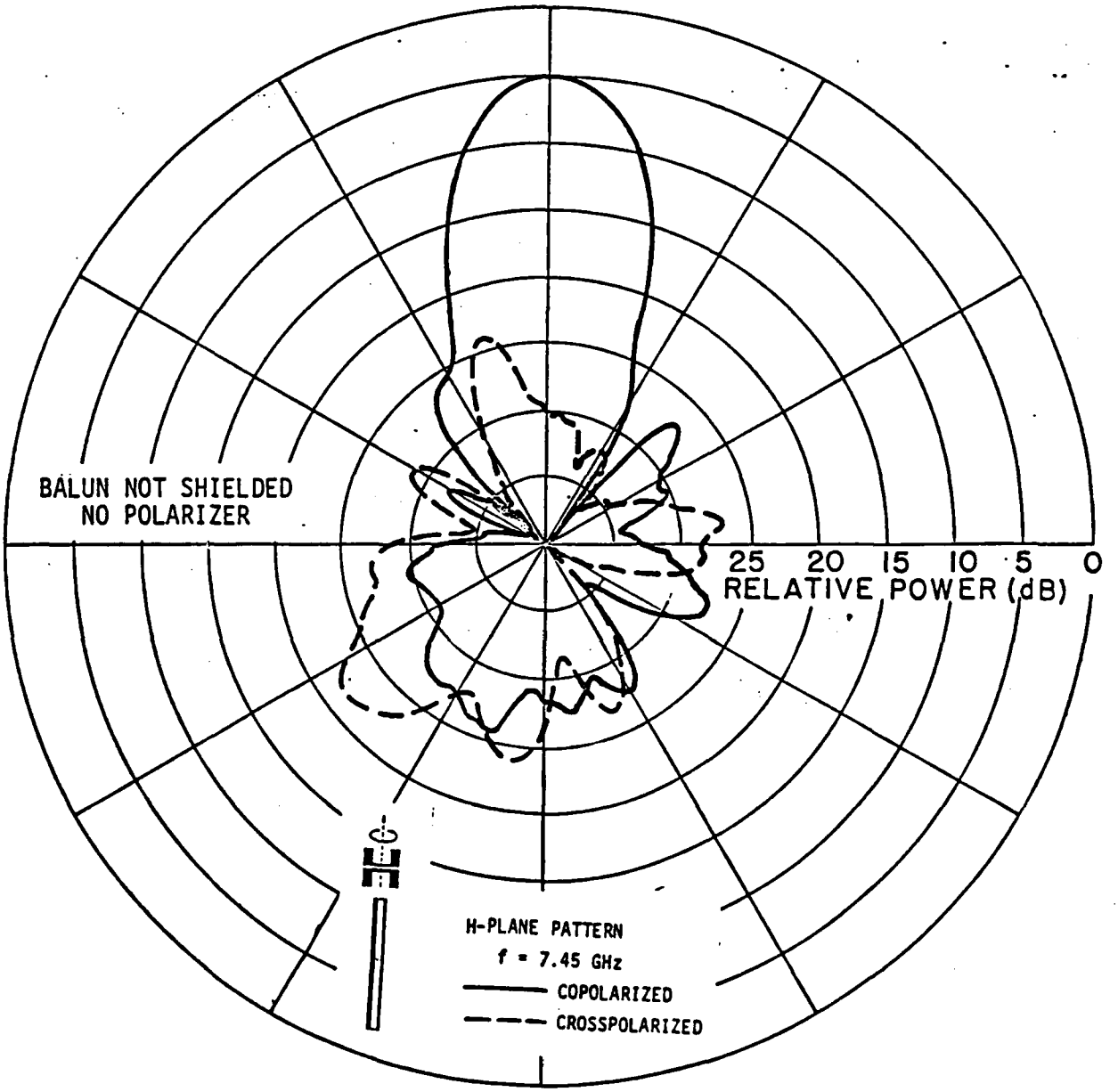

Figure 42. a. The radiation pattern of the X-band array without balun shielded. H-plane, f = 7.45 GHz.

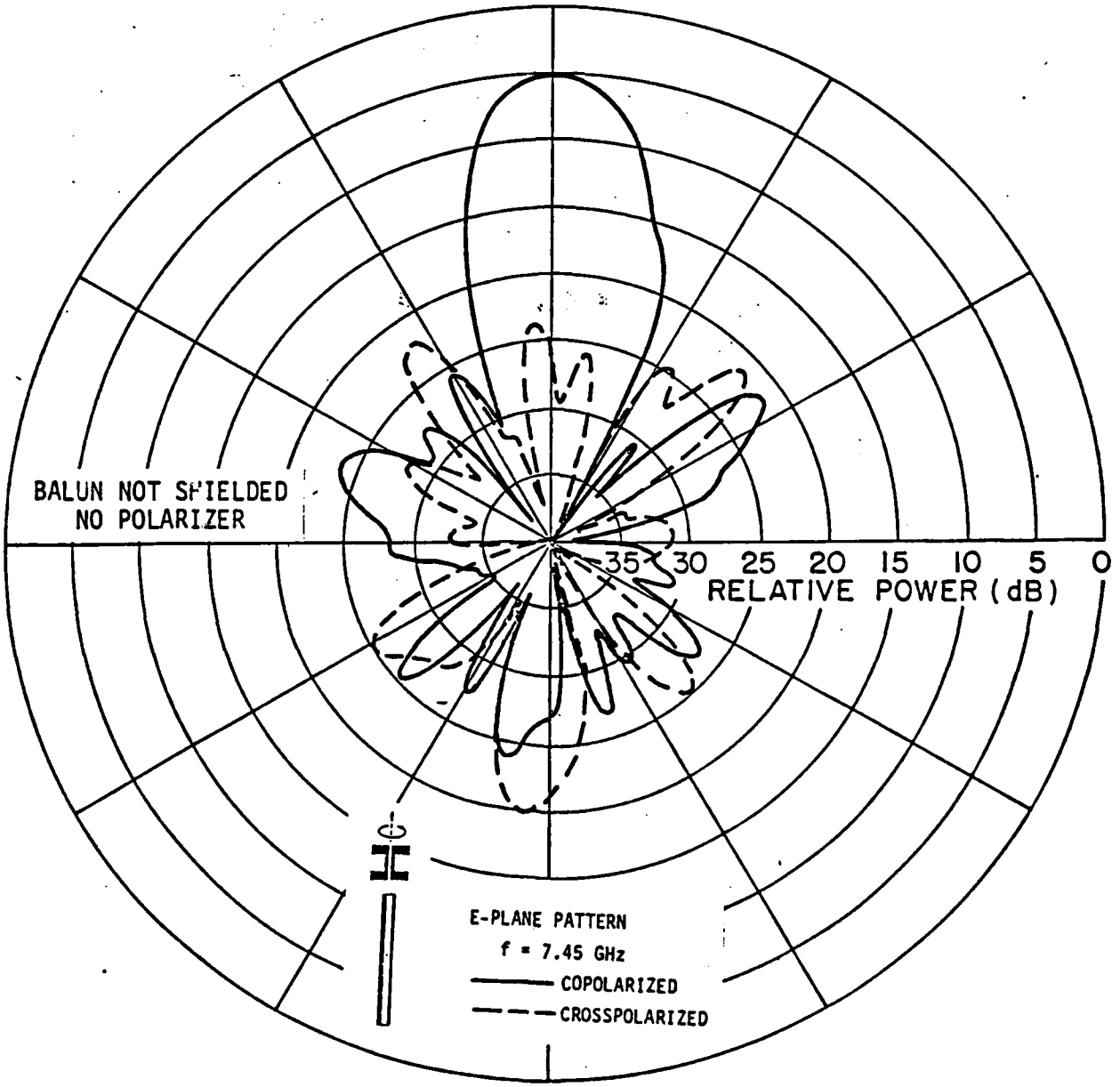

Figure 42. b. The radiation pattern of the X-band array without balun shielded. E-plane, f = 7.45 GHz.

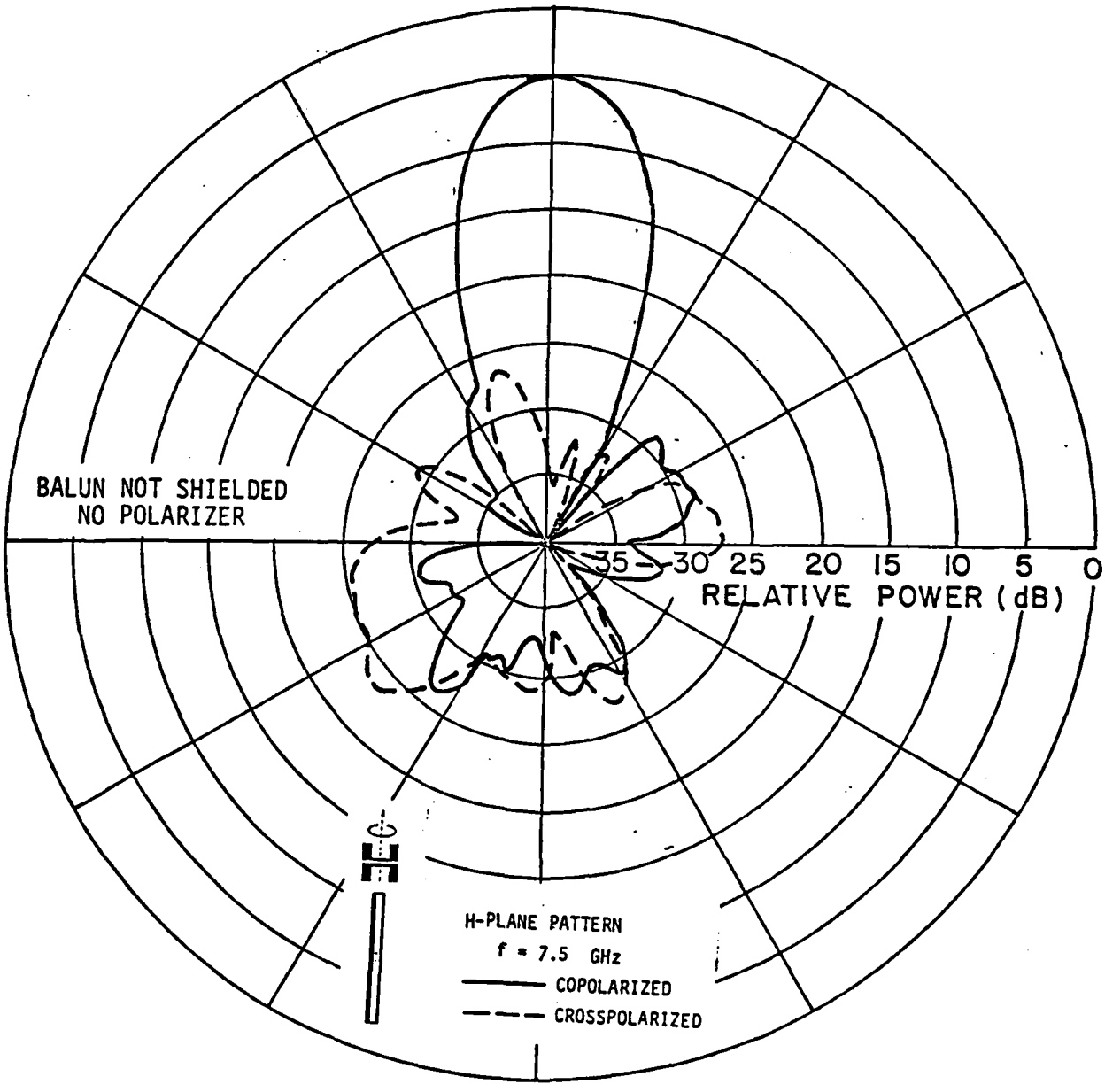

Figure 43. a. The radiation pattern of the X-band array without balun shielded. H-plane, f = 7.5 GHz.

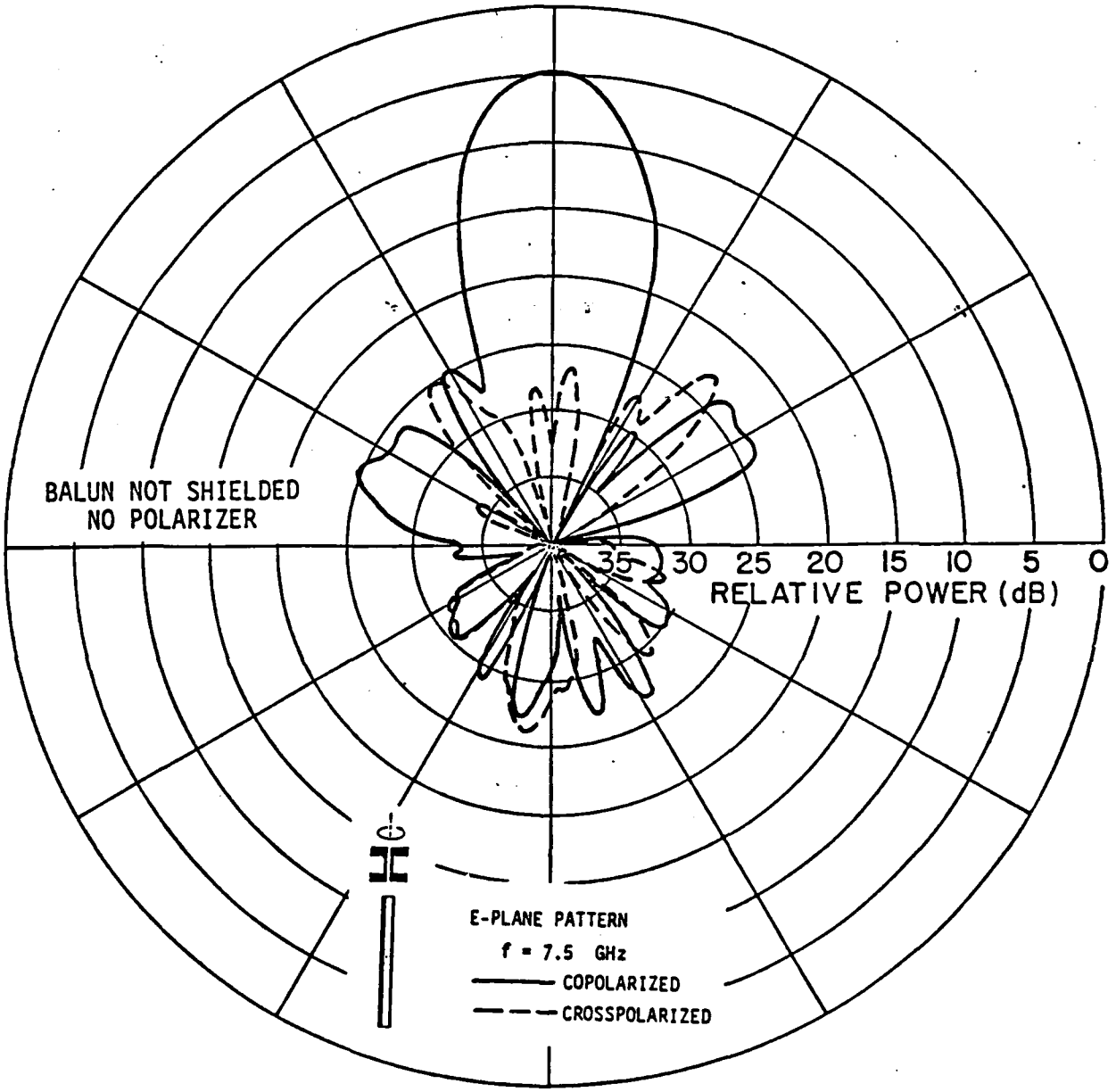

Figure 43. b. The radiation pattern of the X-band array without balun shielded. E-plane, f = 7.5 GHz.

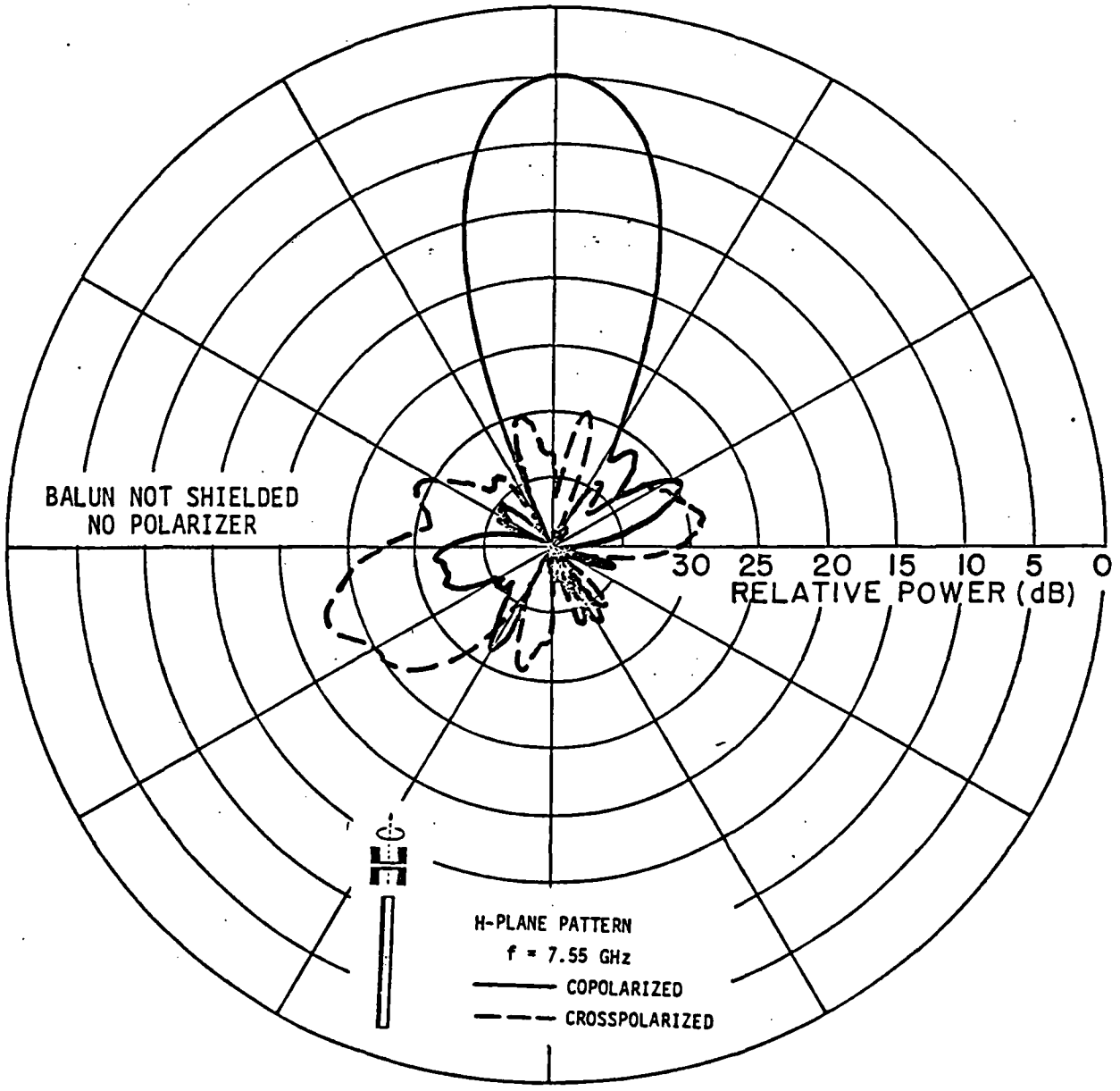

Figure 44. a. The radiation pattern of the X-band array without balun shielded. H-plane, f = 7.55 GHz.

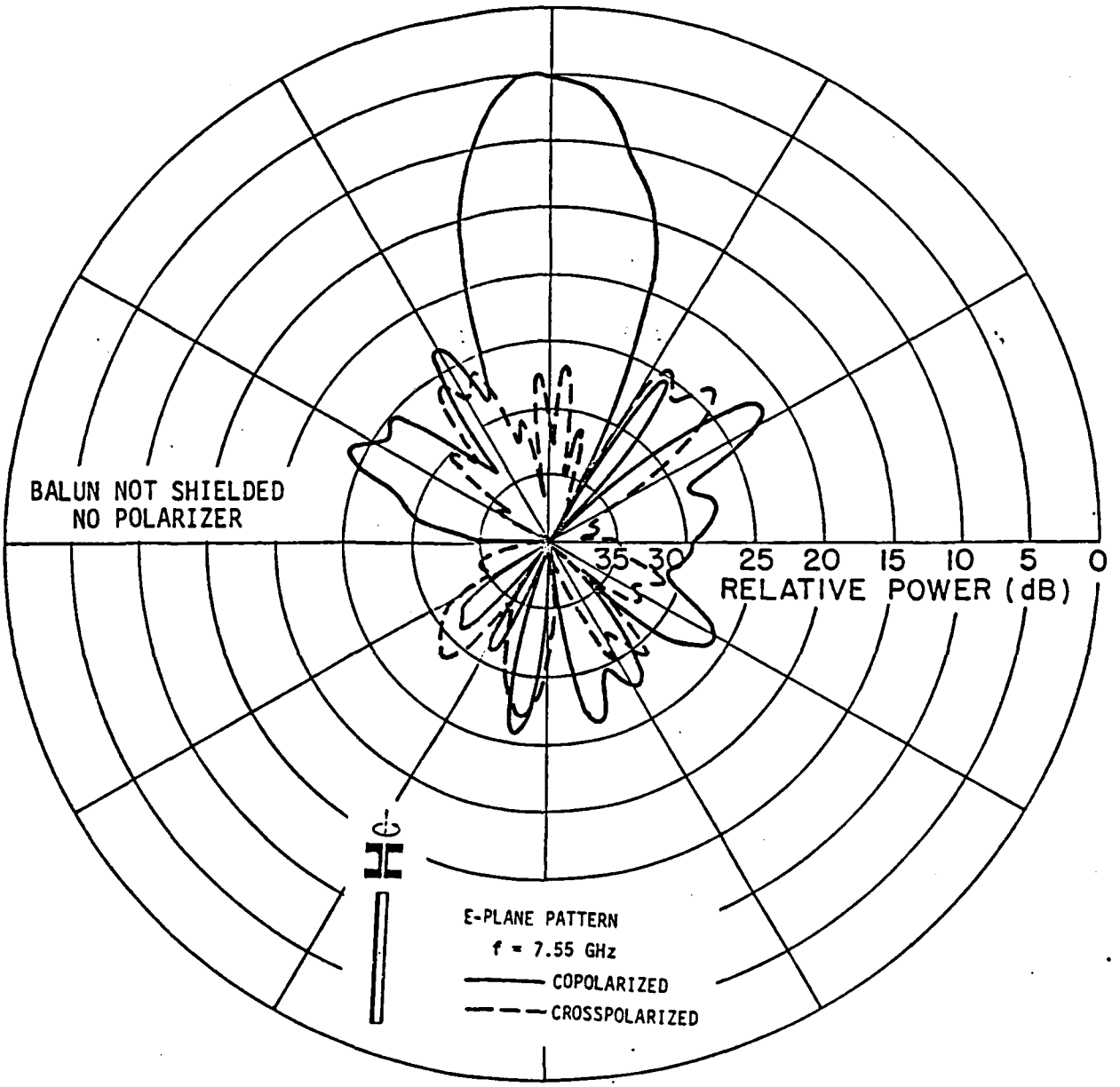

Figure 44. b. The radiation pattern of the X-band array without balun shielded. E-plane, f = 7.55 GHz.

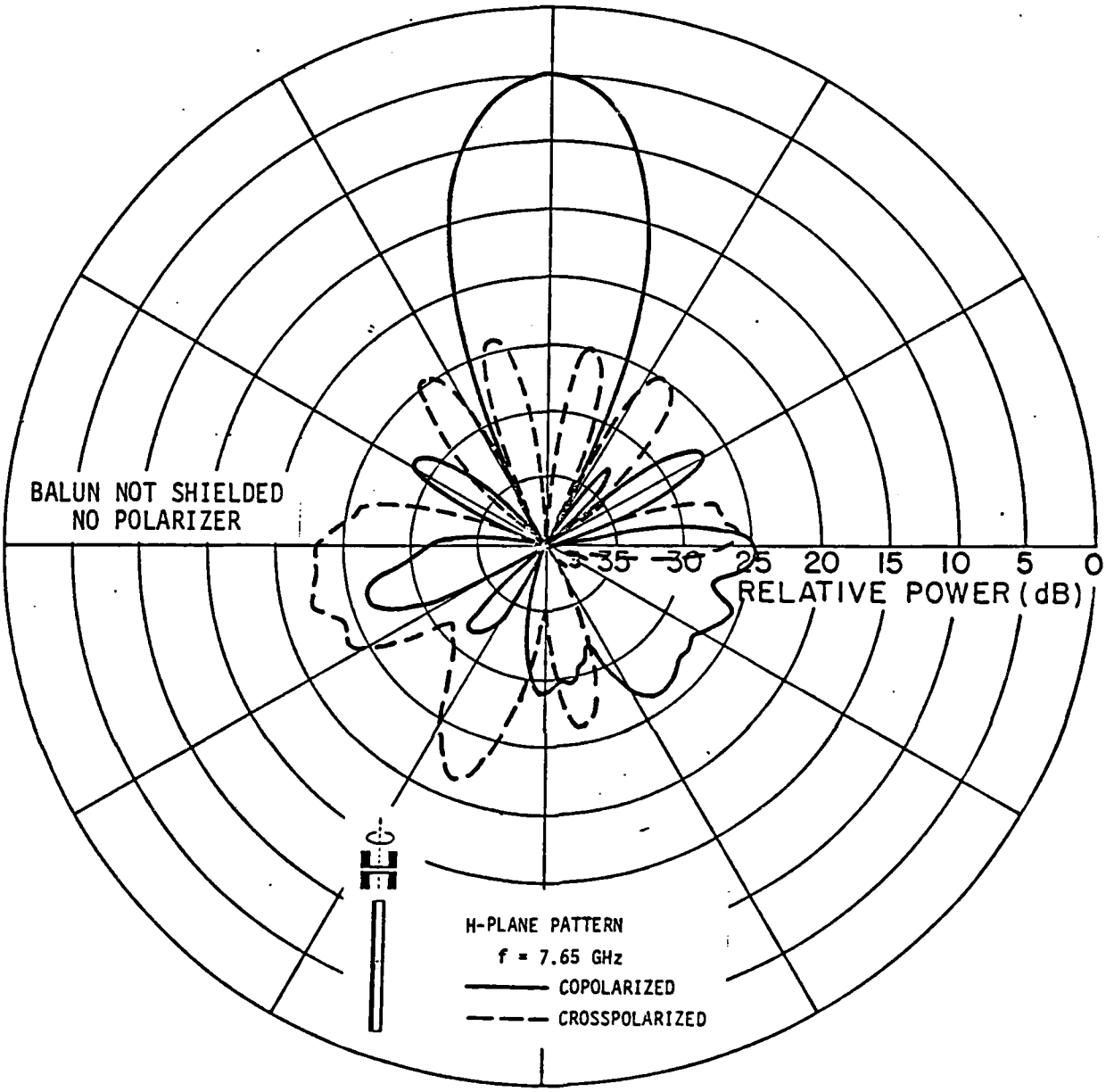

Figure 45. a. The radiation pattern of the X-band array without balun shielded. H-plane, f = 7.65 GHz.

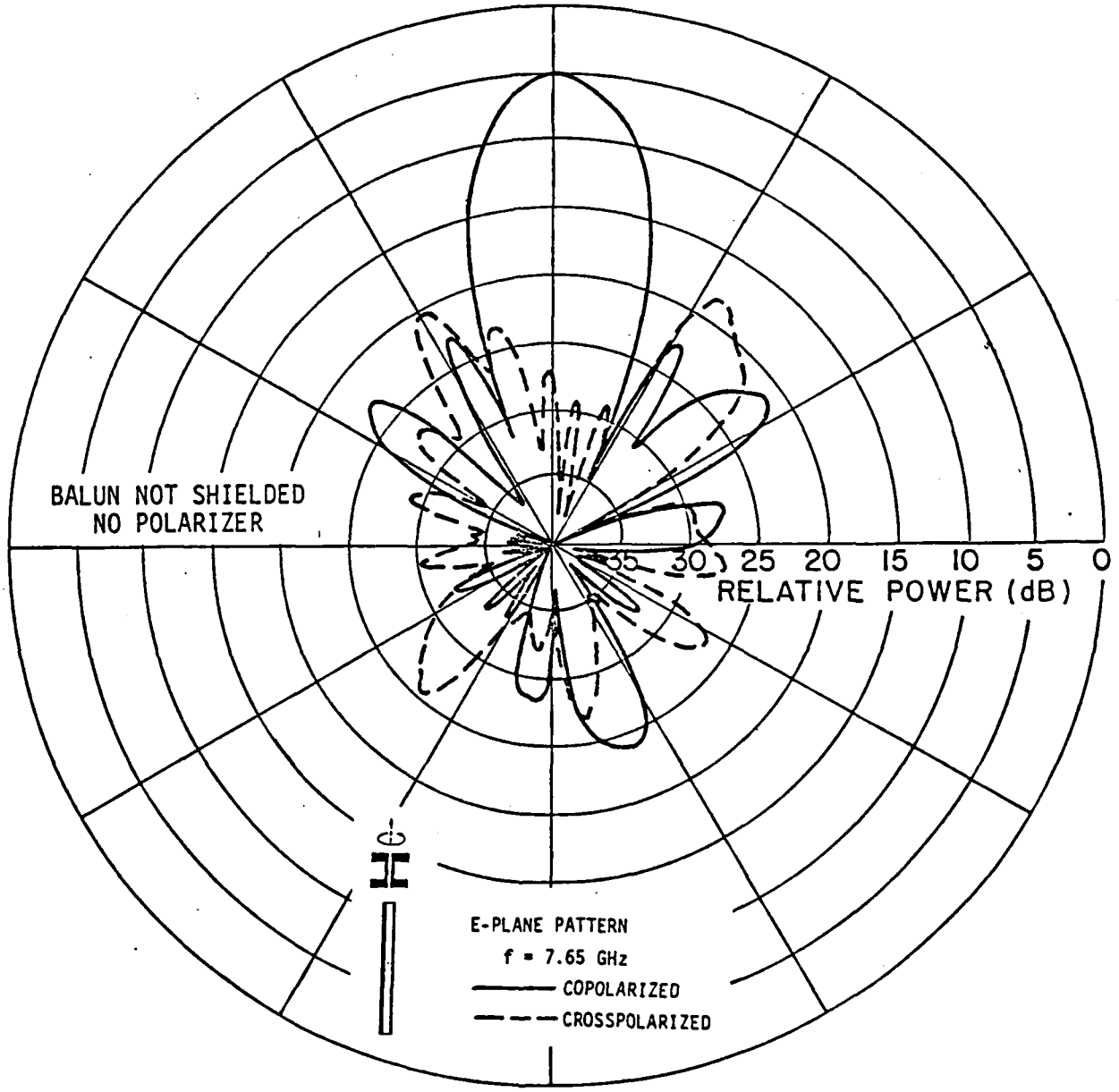

Figure 45. b. The radiation pattern of the X-band array without balun shielded. E-plane, f = 7.65 GHz.

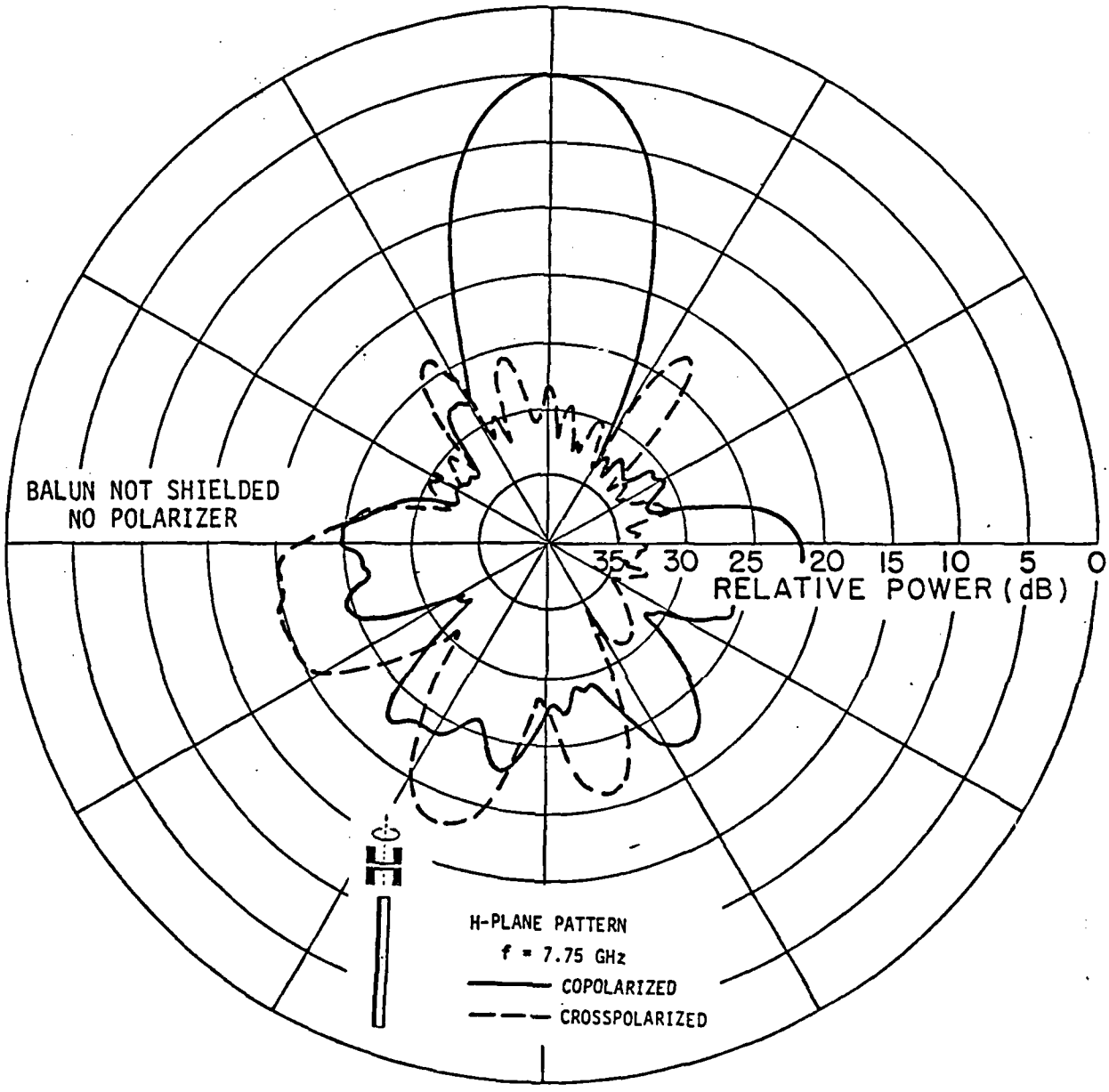

Figure 46. a. The radiation pattern of the X-band array without balun shielded. H-plane, f = 7.75 GHz.

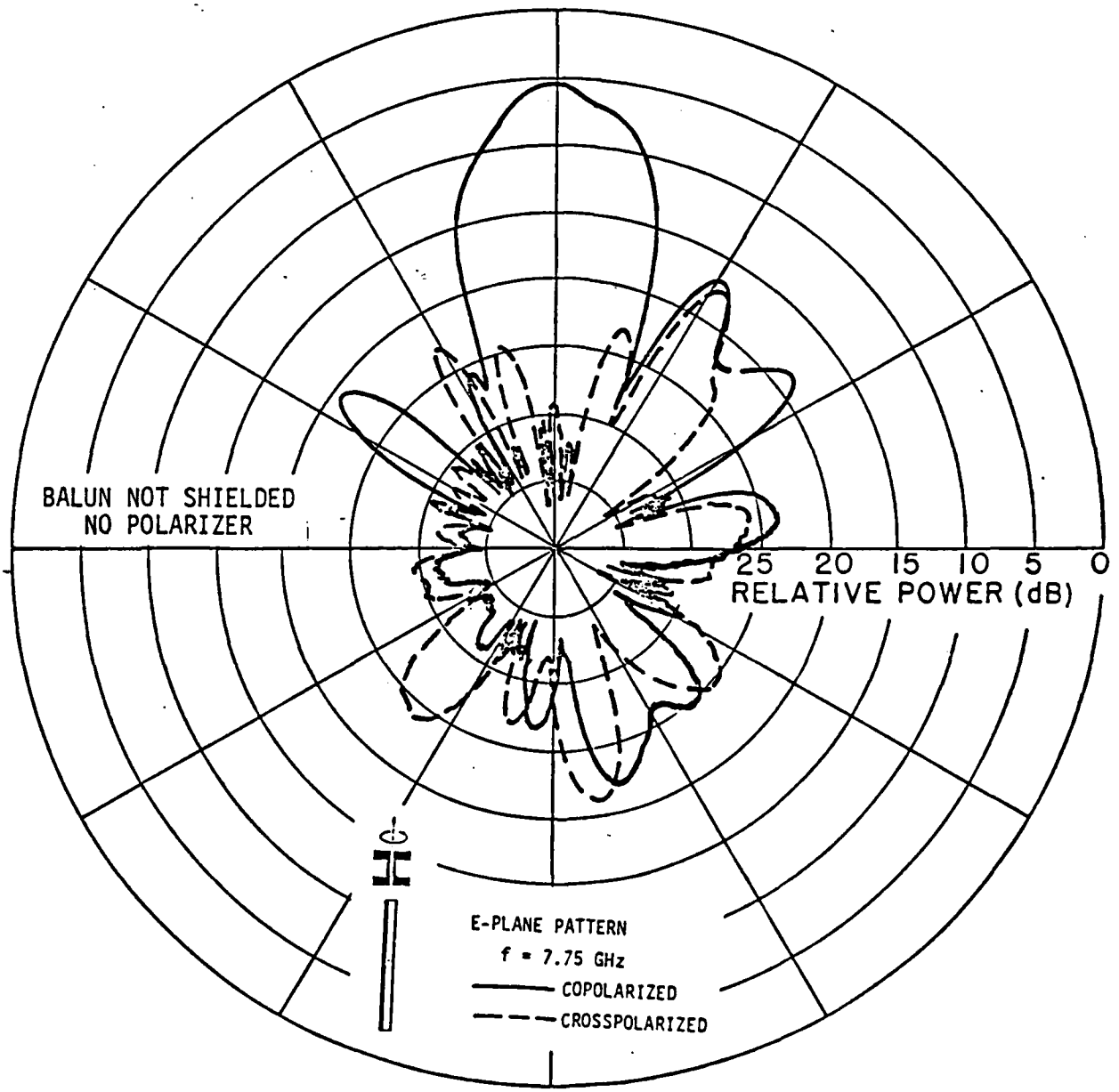

Figure 46. b. The radiation pattern of the X-band array without balun shielded. E-plane, f = 7.75 GHz.

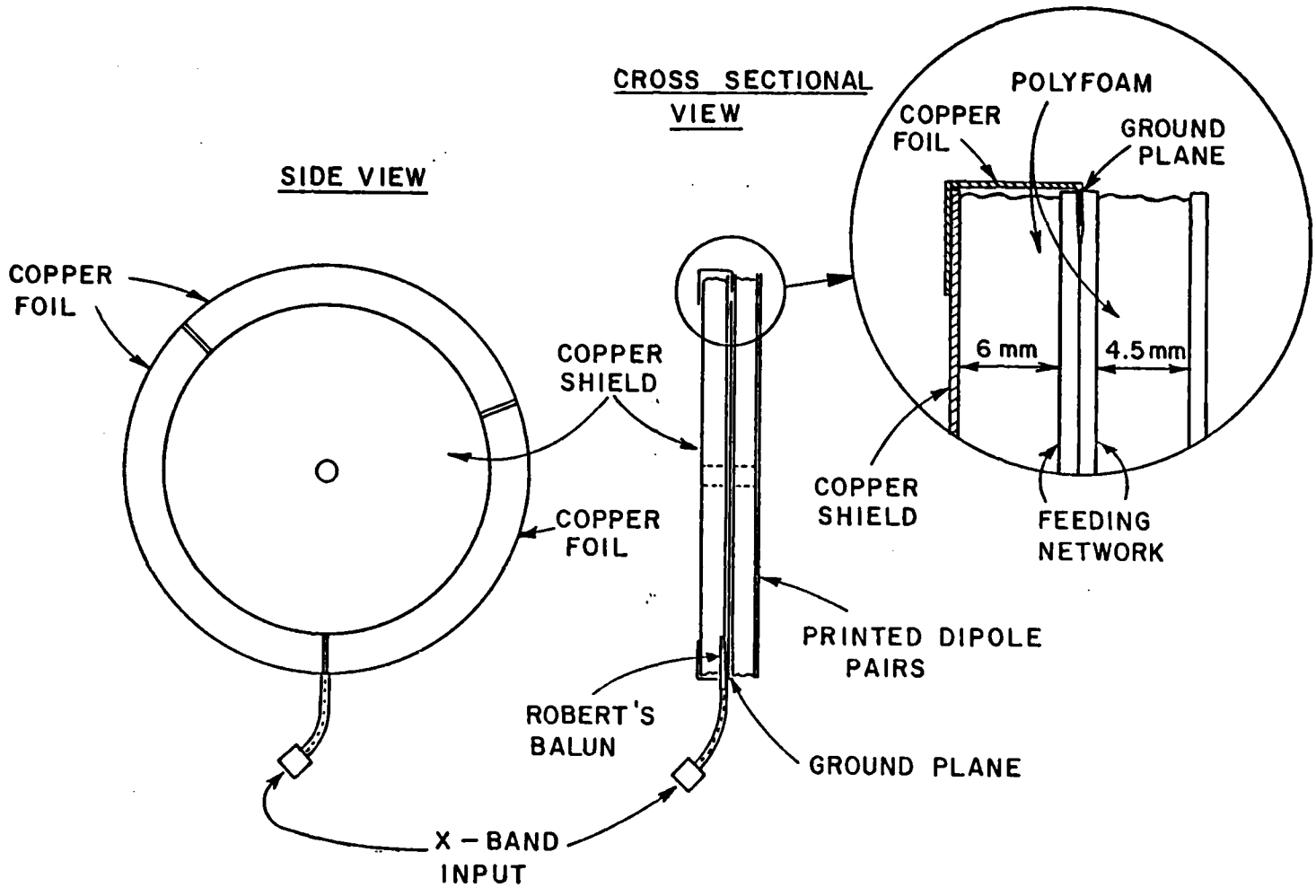

Figure 47. The construction of the copper shield. It is made of a circular copper plate attached to the groundplane by three sections of copper foil.

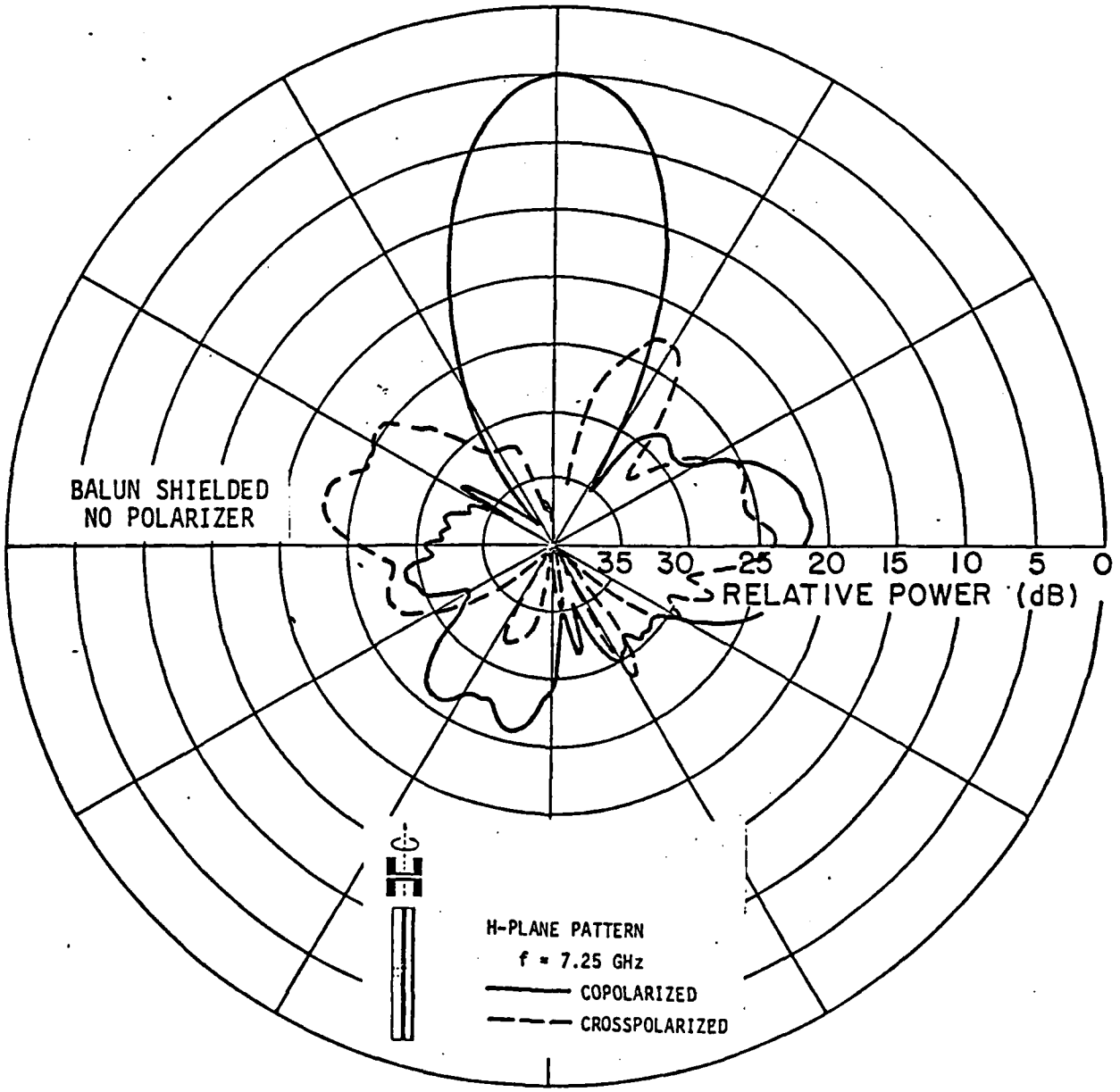

Figure 48. a. The radiation pattern of the X-band array with balun shielded. H-plane, f = 7.25 GHz.

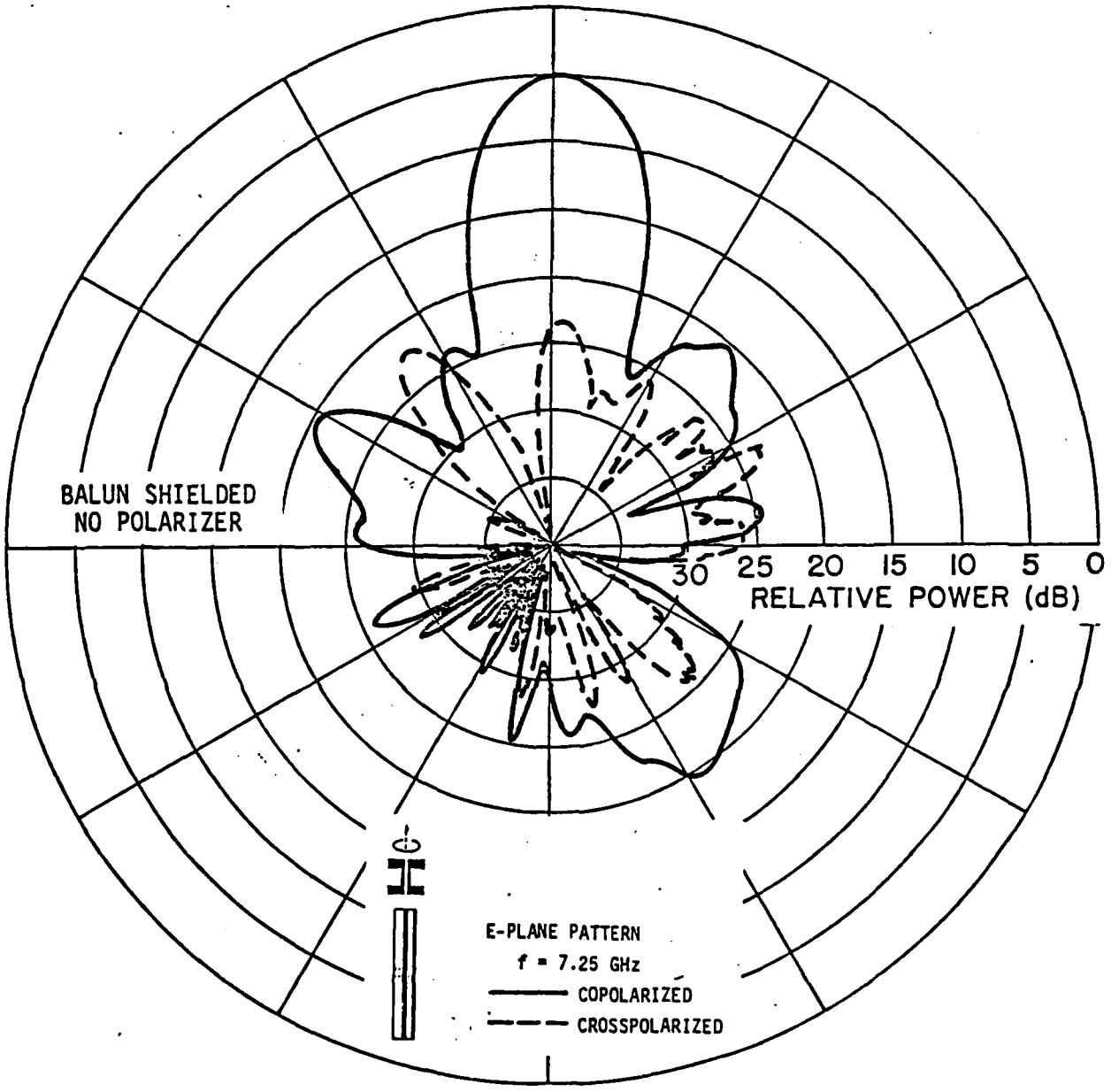

Figure 48. b. The radiation pattern of the X-band array with balun shielded. E-plane, f = 7.25 GHz.

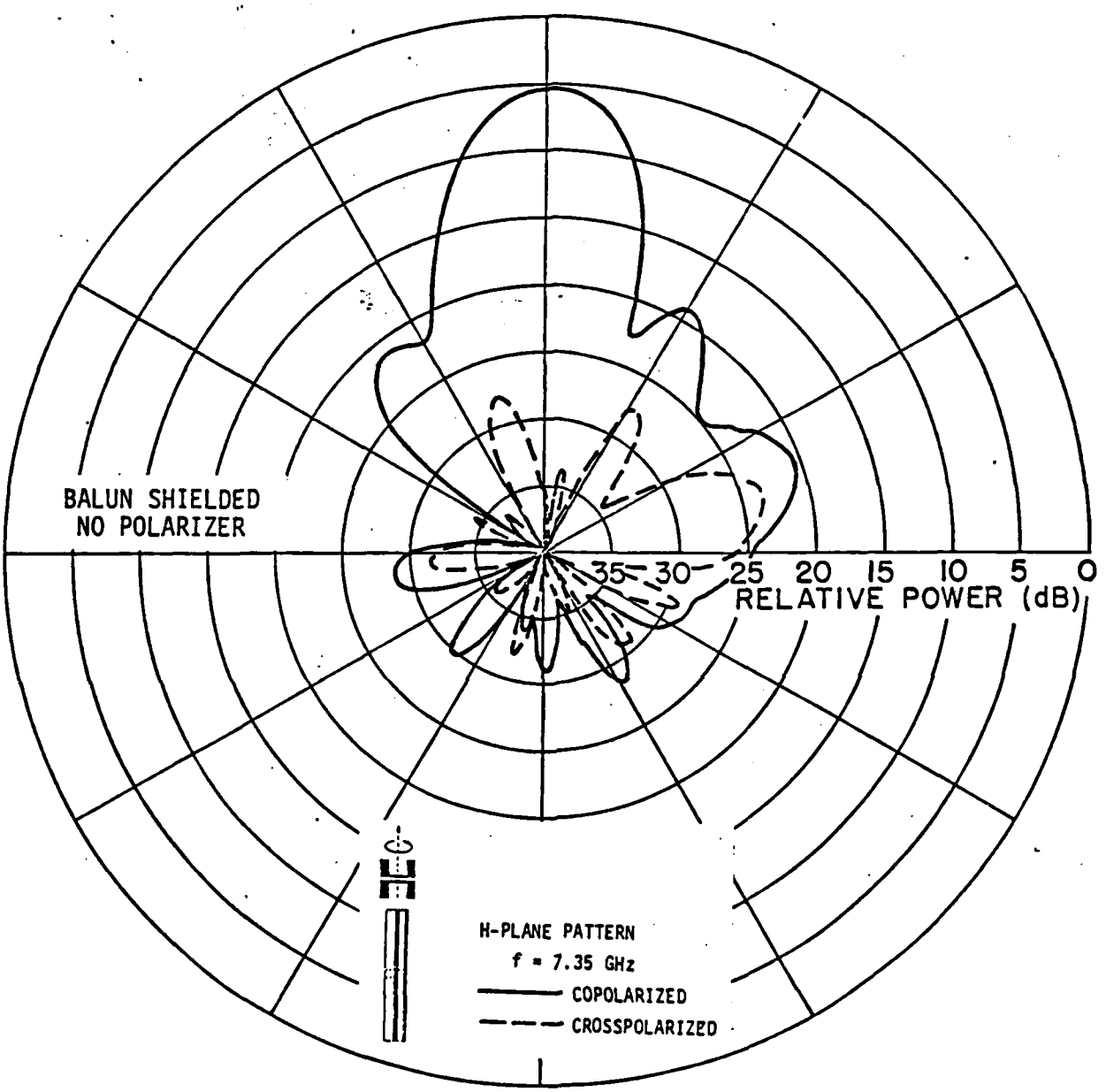

Figure 49. a. The radiation pattern of the X-band array with balun shielded. H-plane, f = 7.35 GHz.

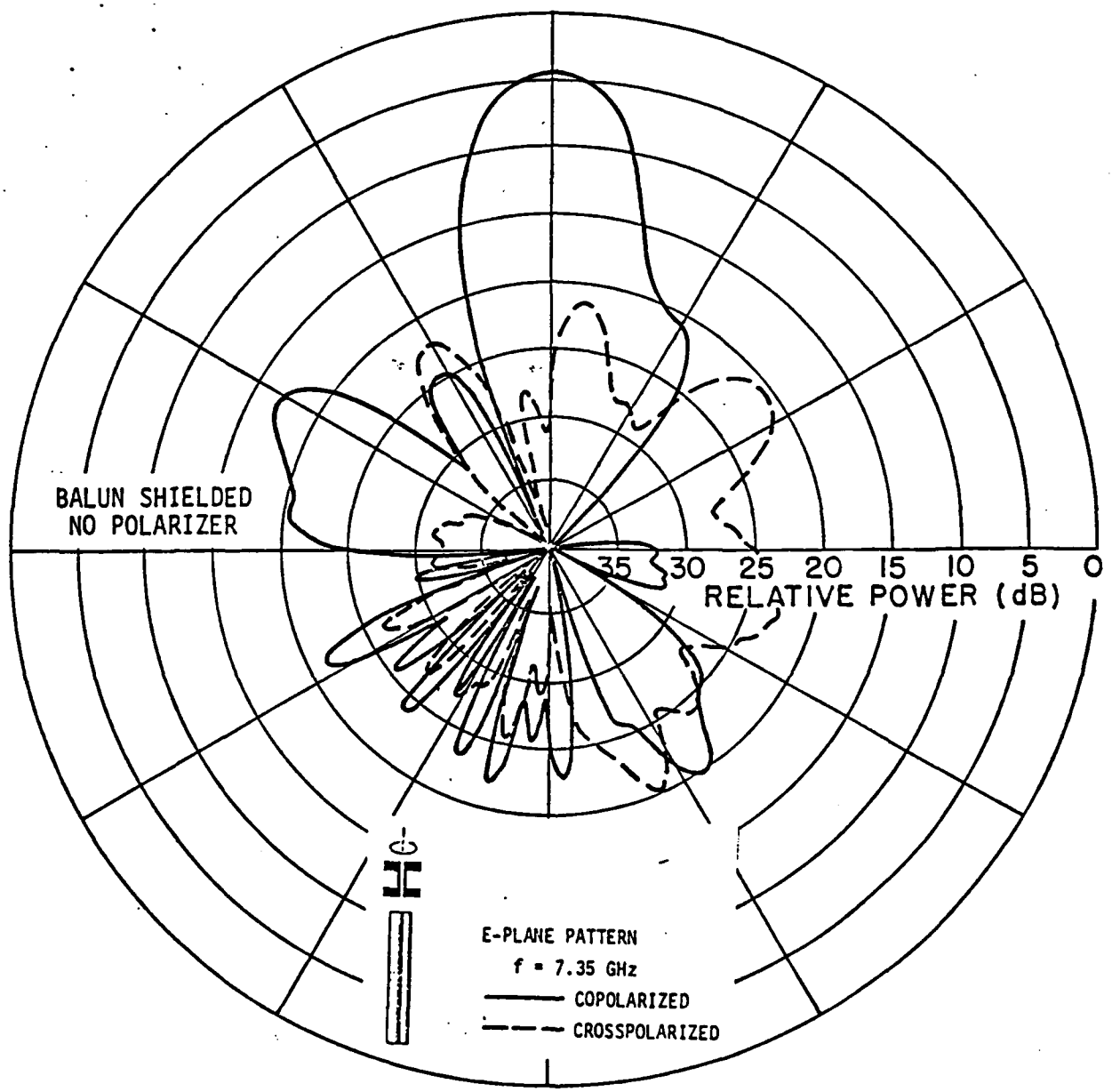

Figure 49. b. The radiation pattern of the X-band array with balun shielded. E-plane, f = 7.35 GHz.

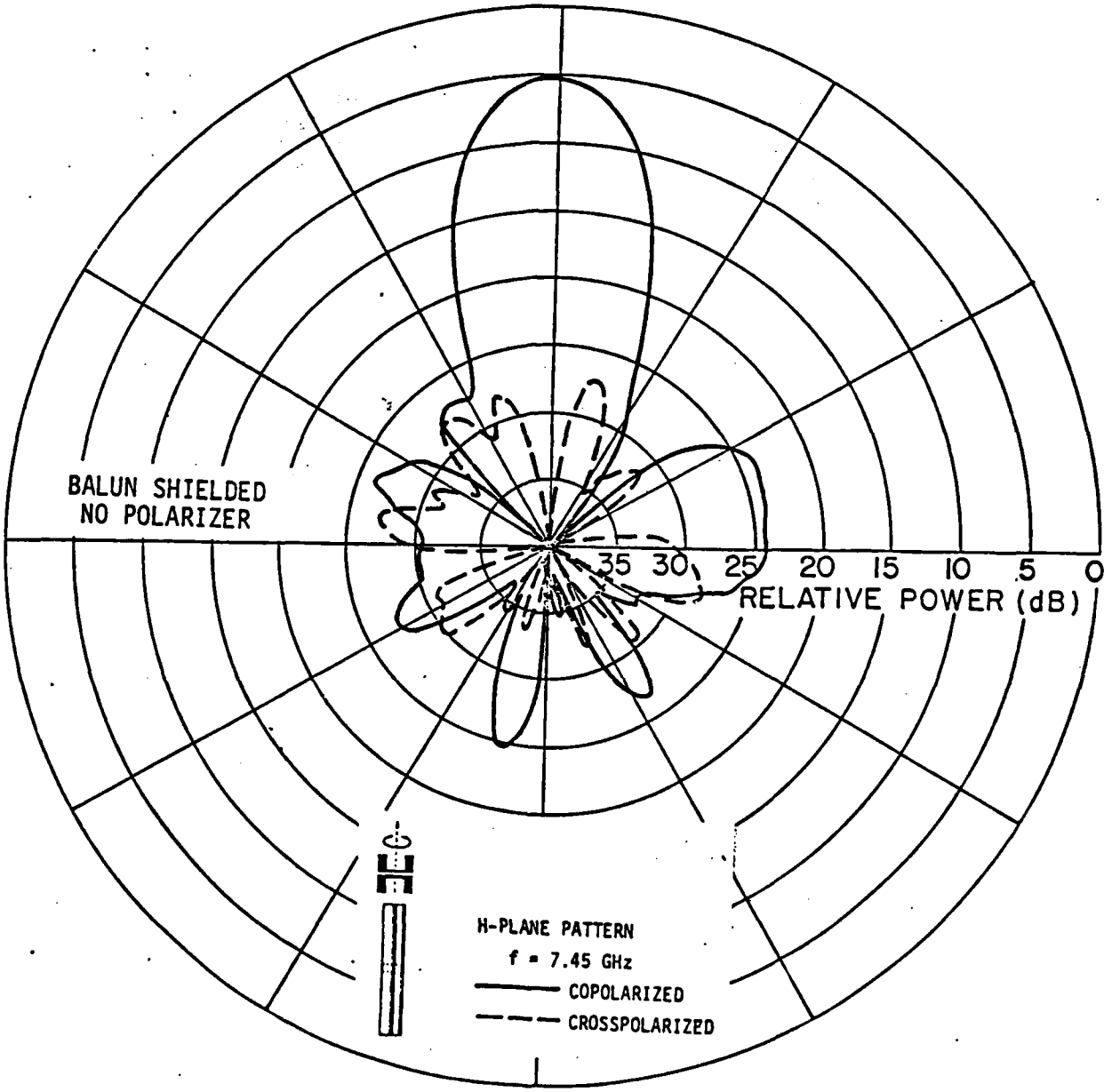

Figure 50. a. The radiation pattern of the X-band array with balun shielded. H-plane, f = 7.45 GHz.

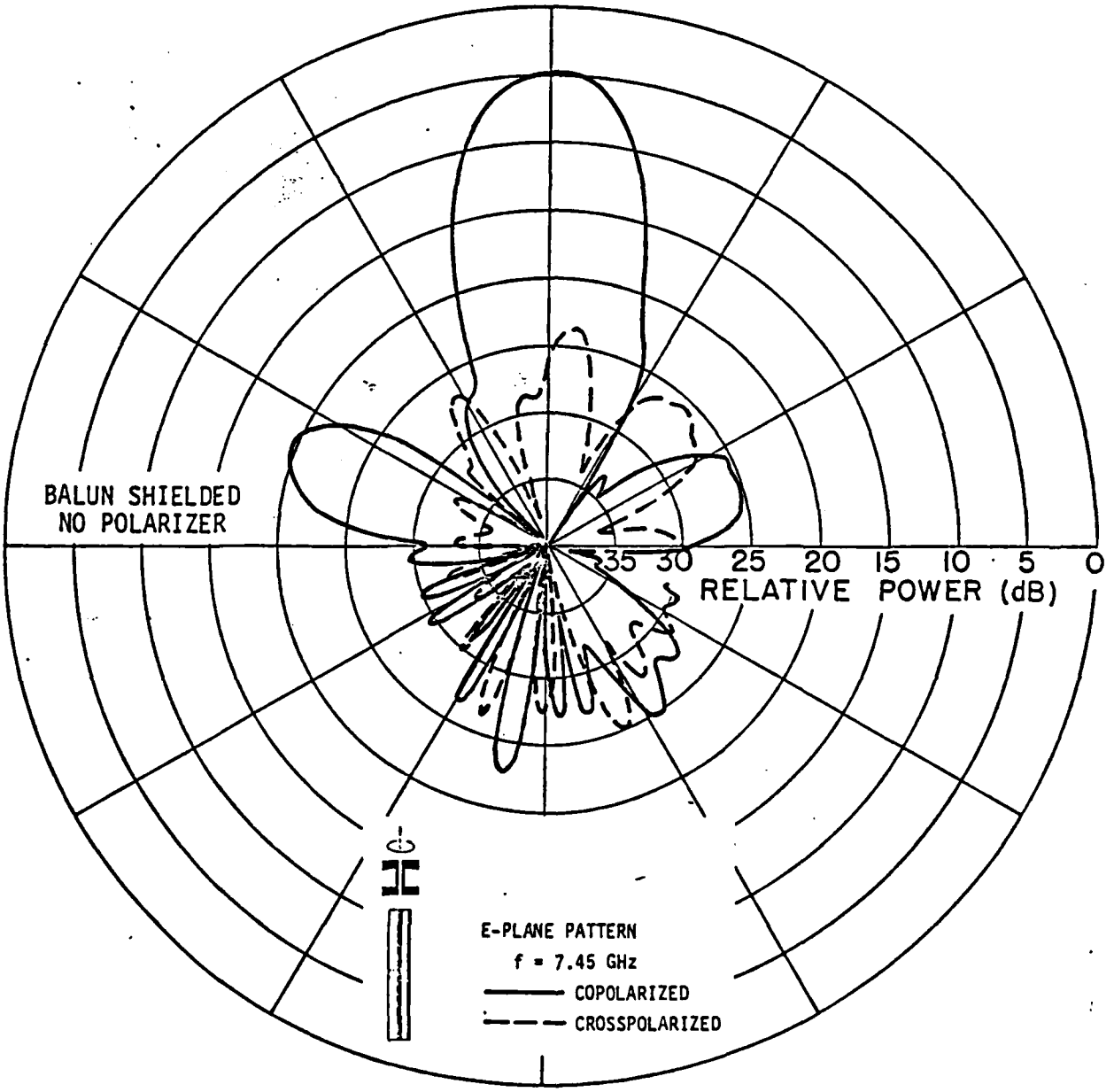

Figure 50. b. The radiation pattern of the X-band array with balun shielded. E-plane, f = 7.45 GHz.

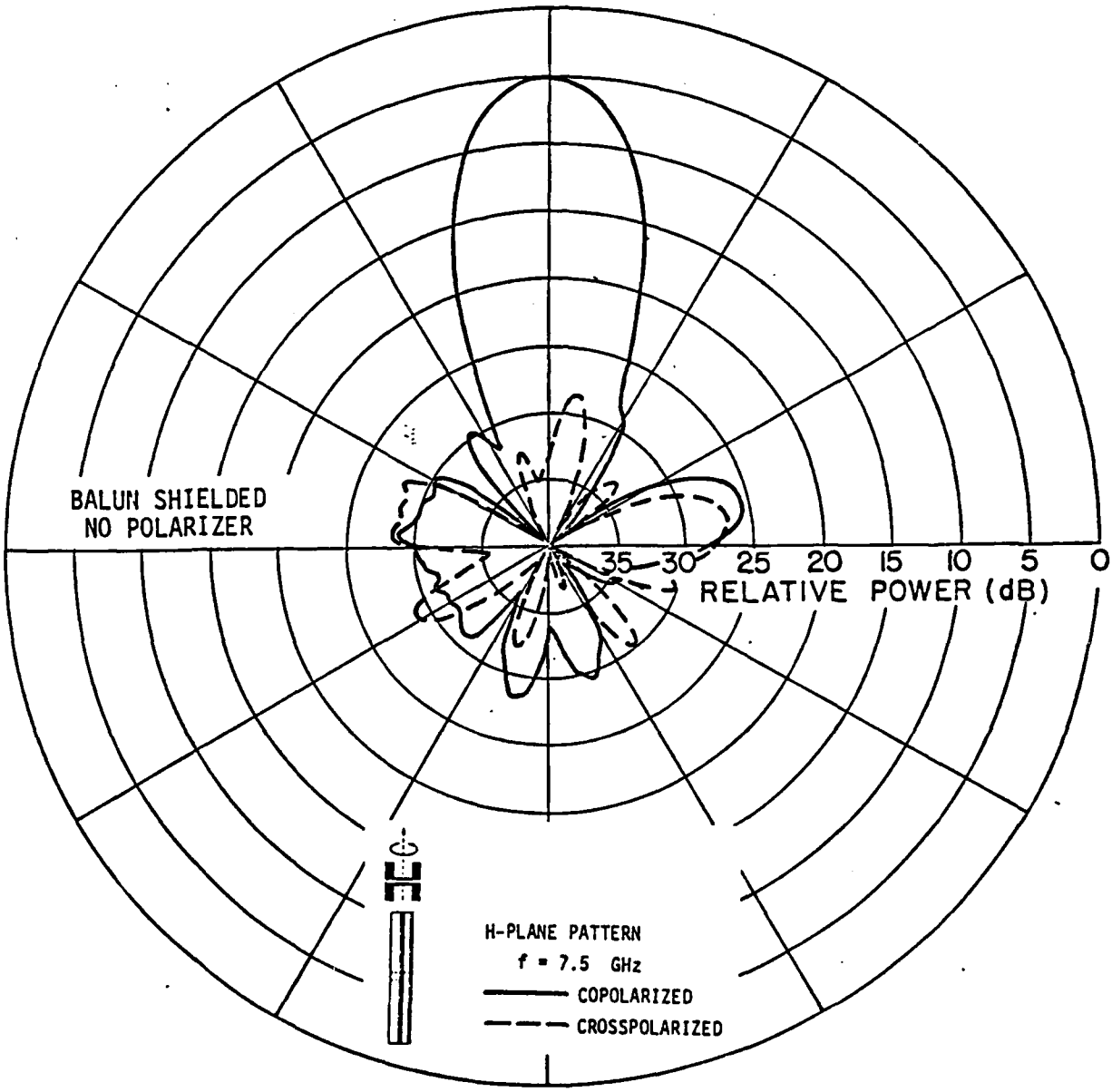

Figure 51. a. The radiation pattern of the X-band array with balun shielded. H-plane, f = 7.5 GHz.

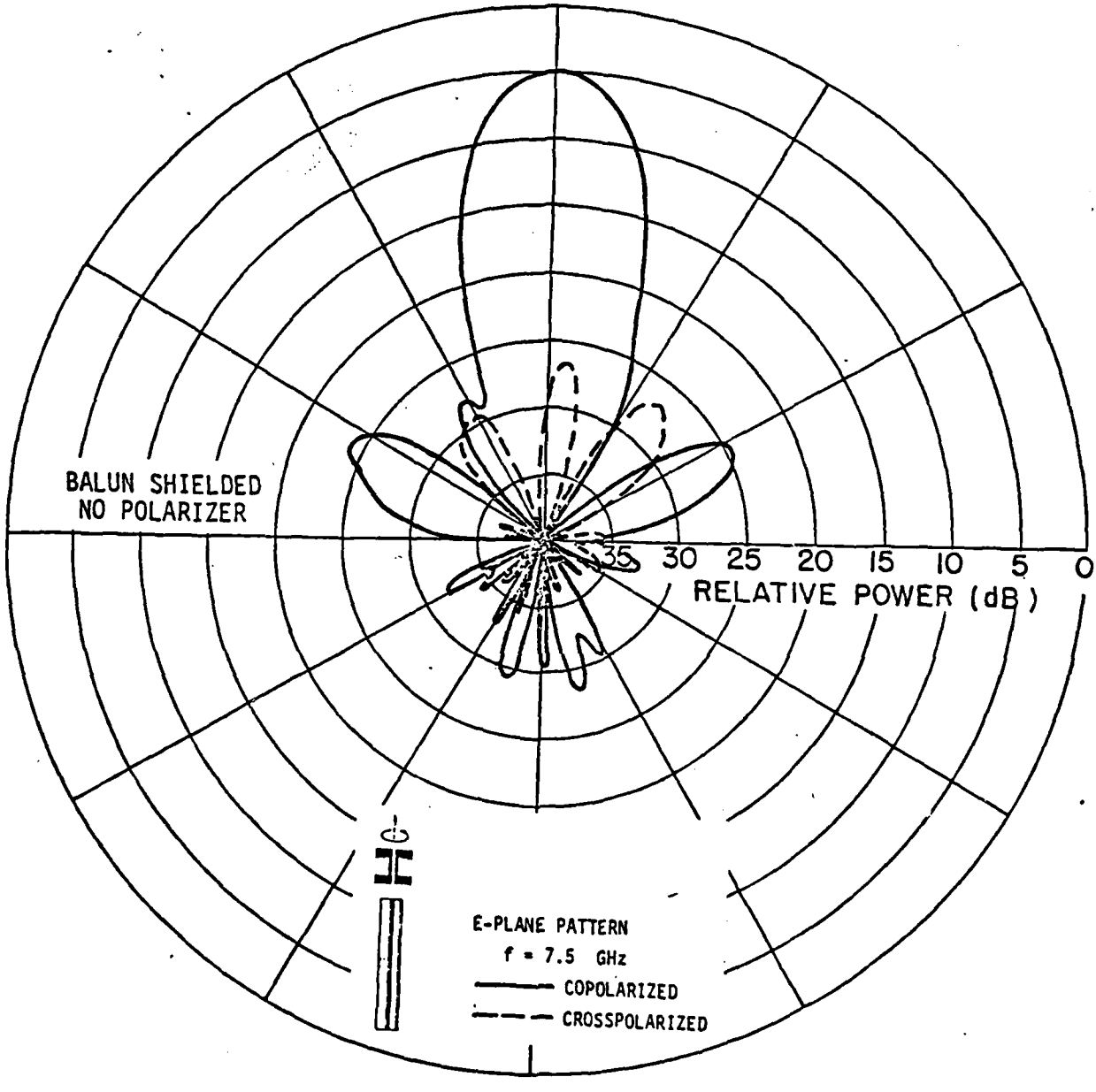

Figure 51. b. The radiation pattern of the X-band array with balun shielded. E-plane, f = 7.5 GHz.

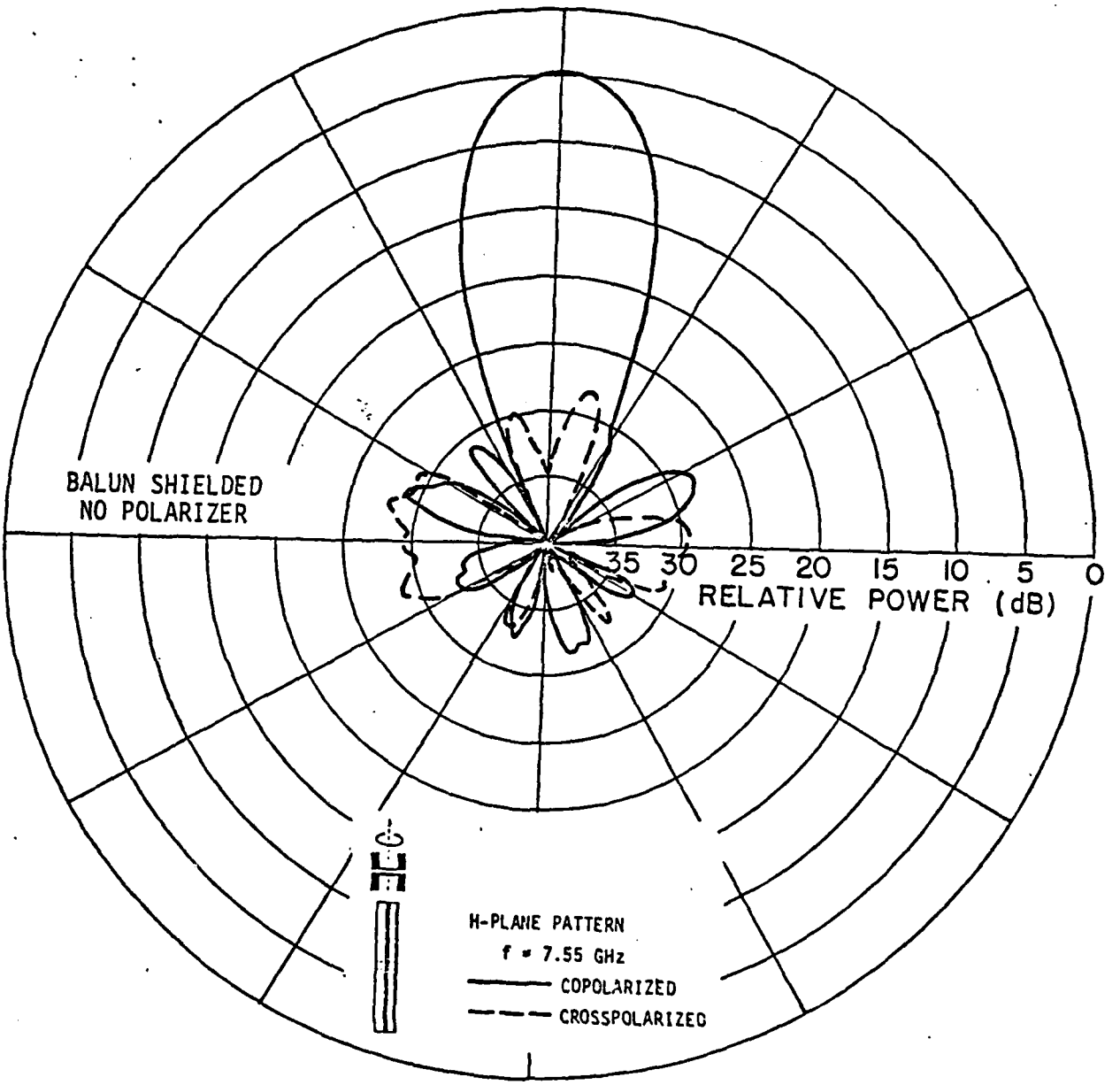

Figure 52. a. The radiation pattern of the X-band array with balun shielded. H-plane, f = 7.55 GHz.

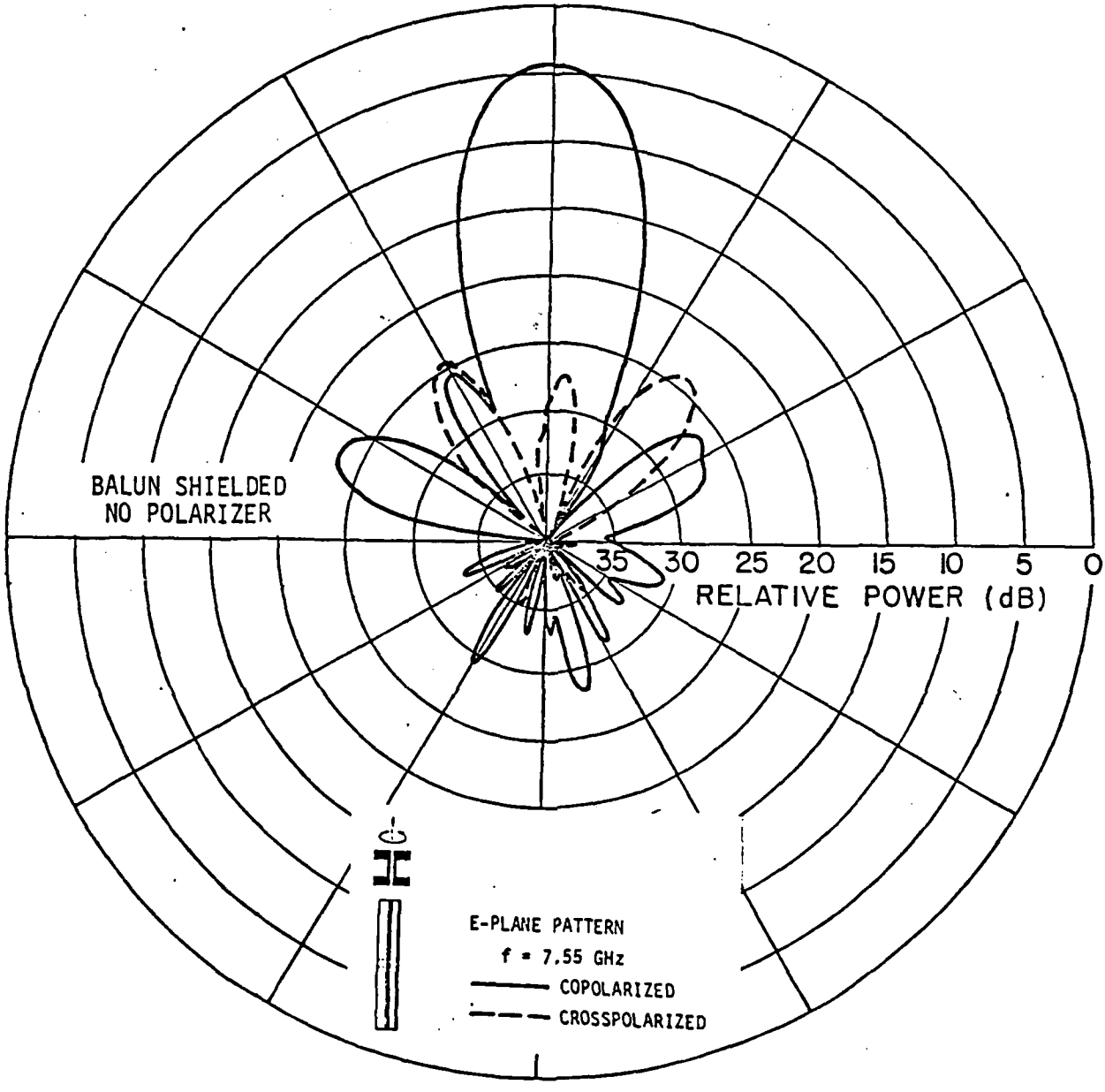

Figure 52. b. The radiation pattern of the X-band array with balun shielded. E-plane, f = 7.55 GHz.

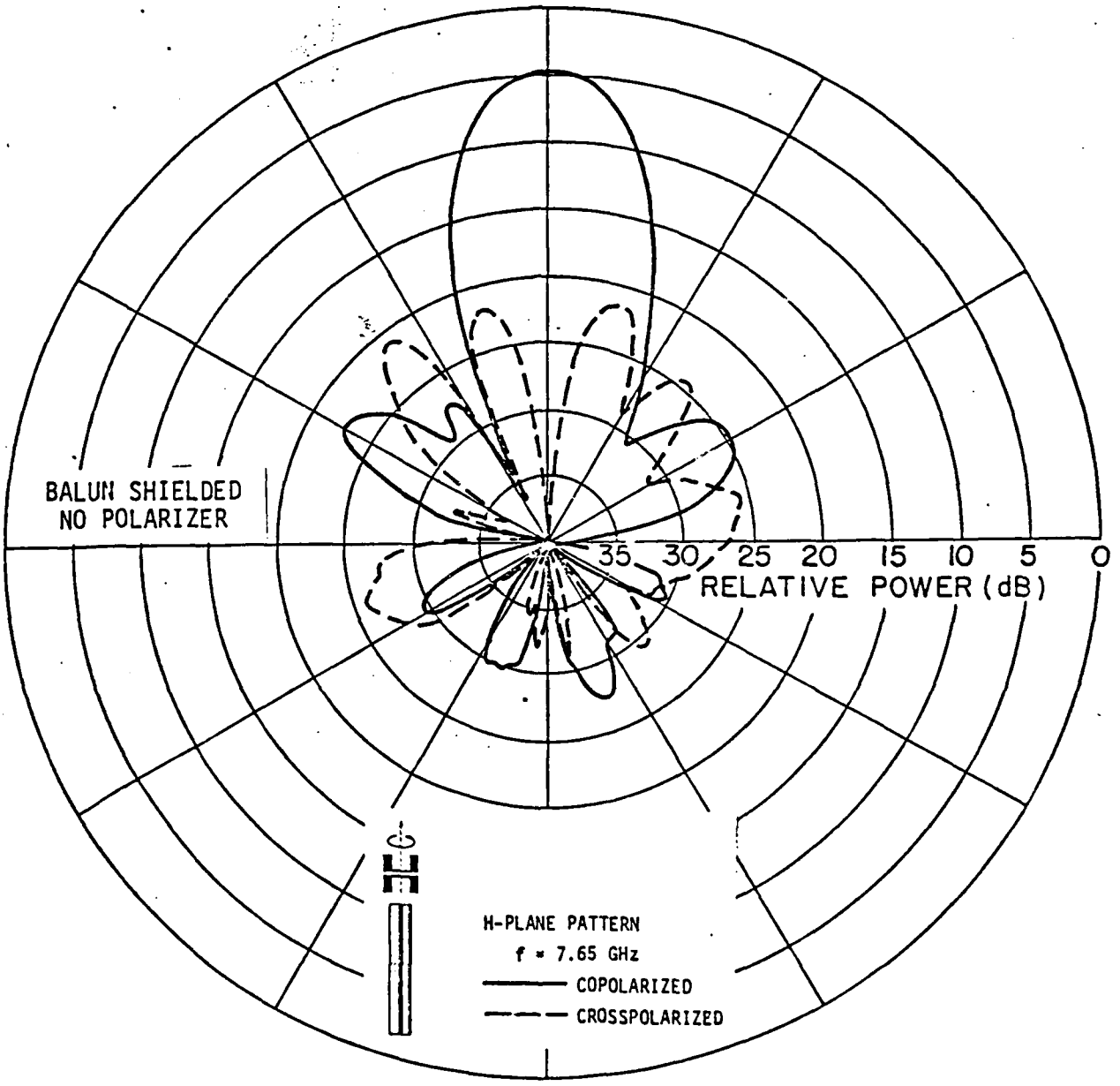

Figure 53. a. The radiation pattern of the X-band array with balun shielded. H-plane, f = 7.65 GHz.

AD-A132 575 A COMPACT SATCOM ANTENNA FOR X- AND Q-BAND(U) OHIO STATE UNIV COLUMBUS ELECTROSCIENCE LAB S J LIN ET AL. APR 82 ESL-713302-1 N00173-80-C-0367 2/2

UNCLASSIFIED F/G 9/5 NL

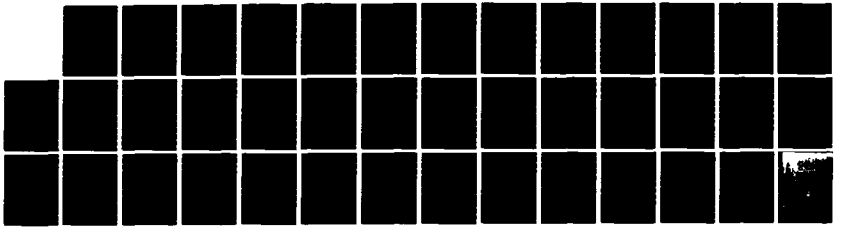

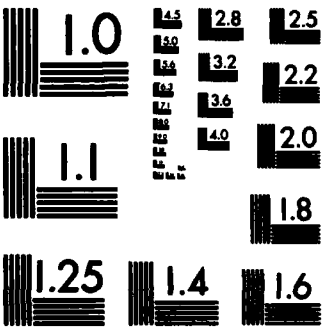

MICROCOPY RESOLUTION TEST CHART
NATIONAL BUREAU OF STANDARDS-1963-A

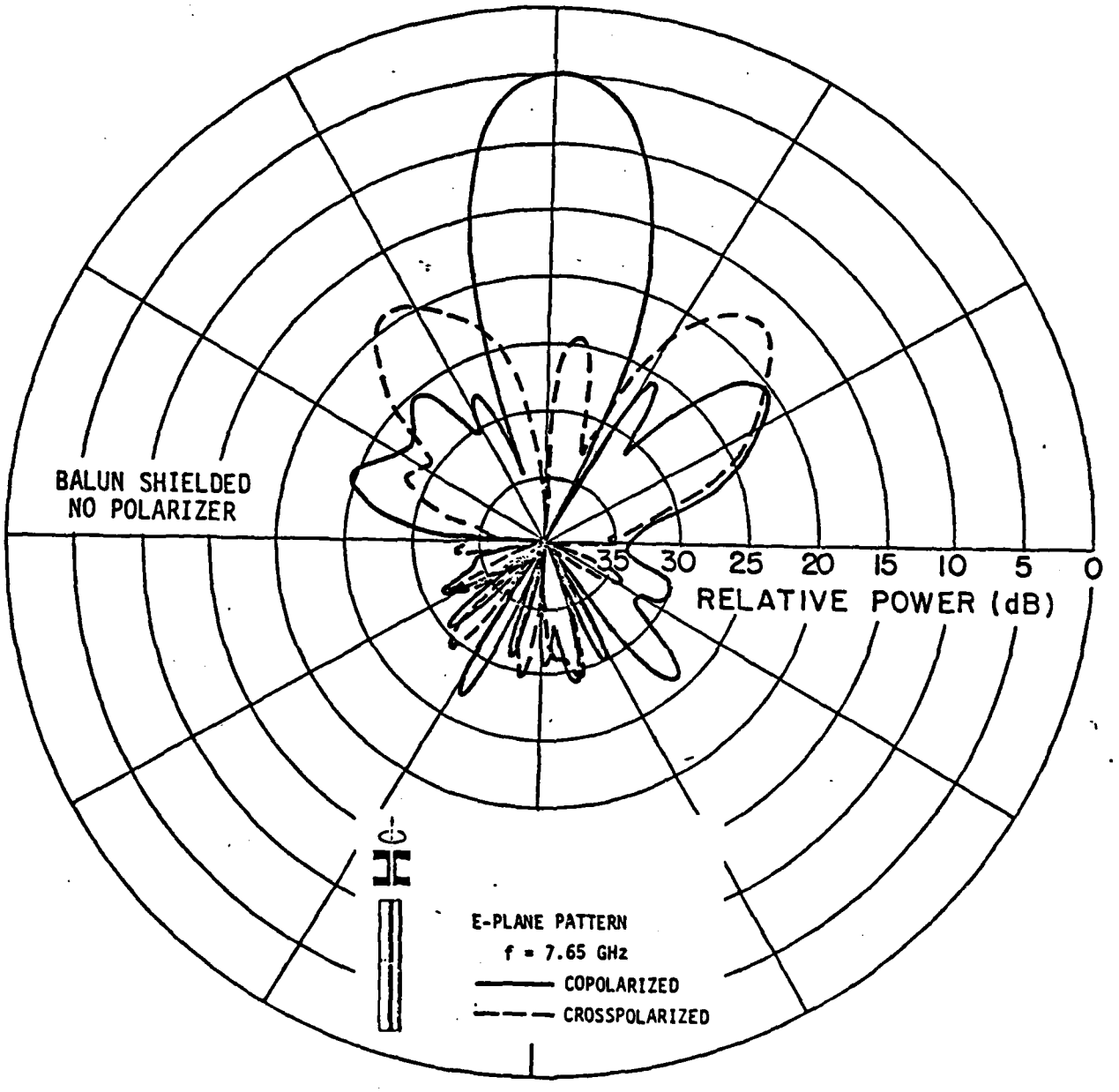

Figure 53. b. The radiation pattern of the X-band array with balun shielded. E-plane, f = 7.65 GHz.

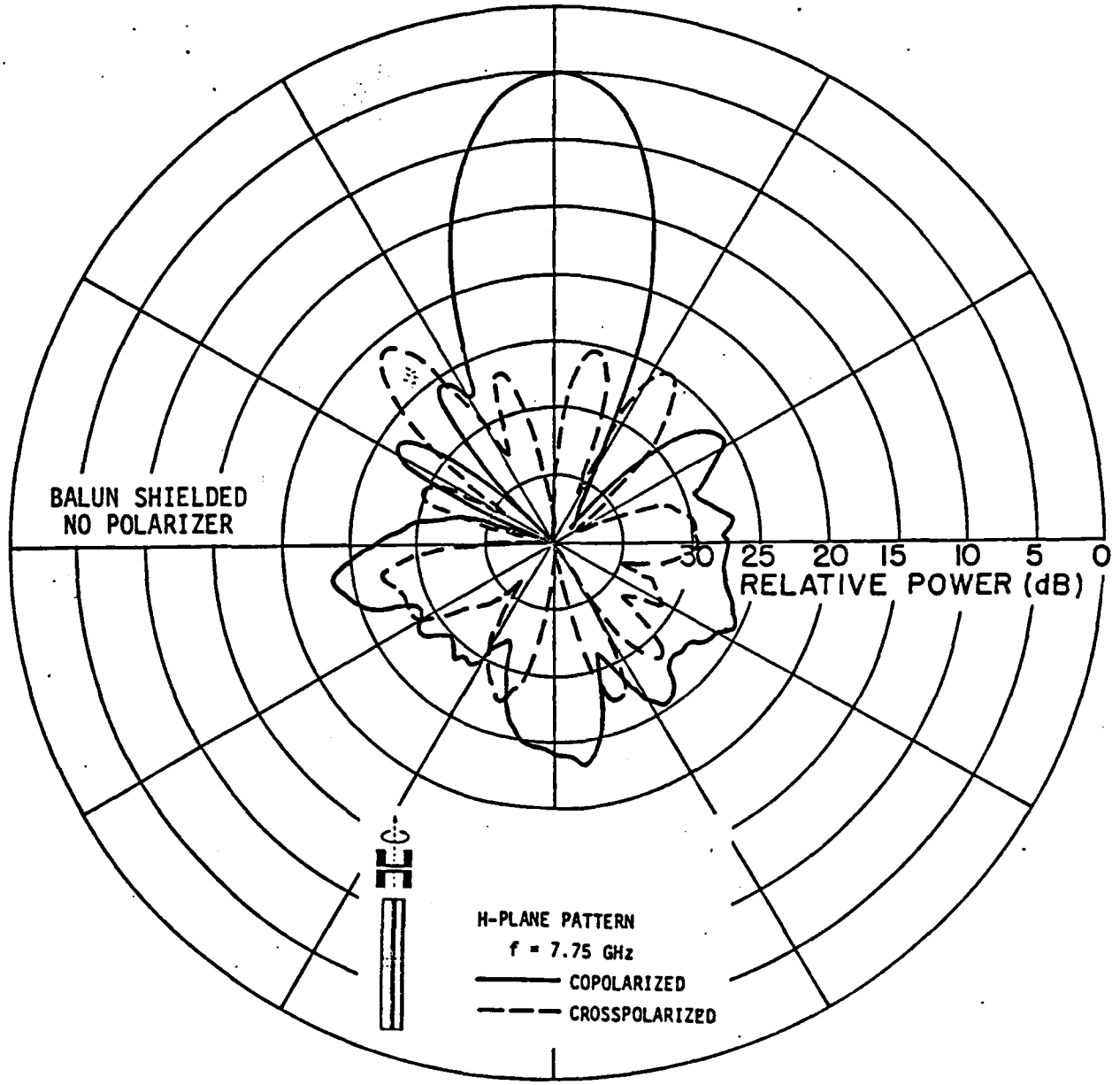

Figure 54. a. The radiation pattern of the X-band array with balun shielded. H-plane, f = 7.75 GHz.

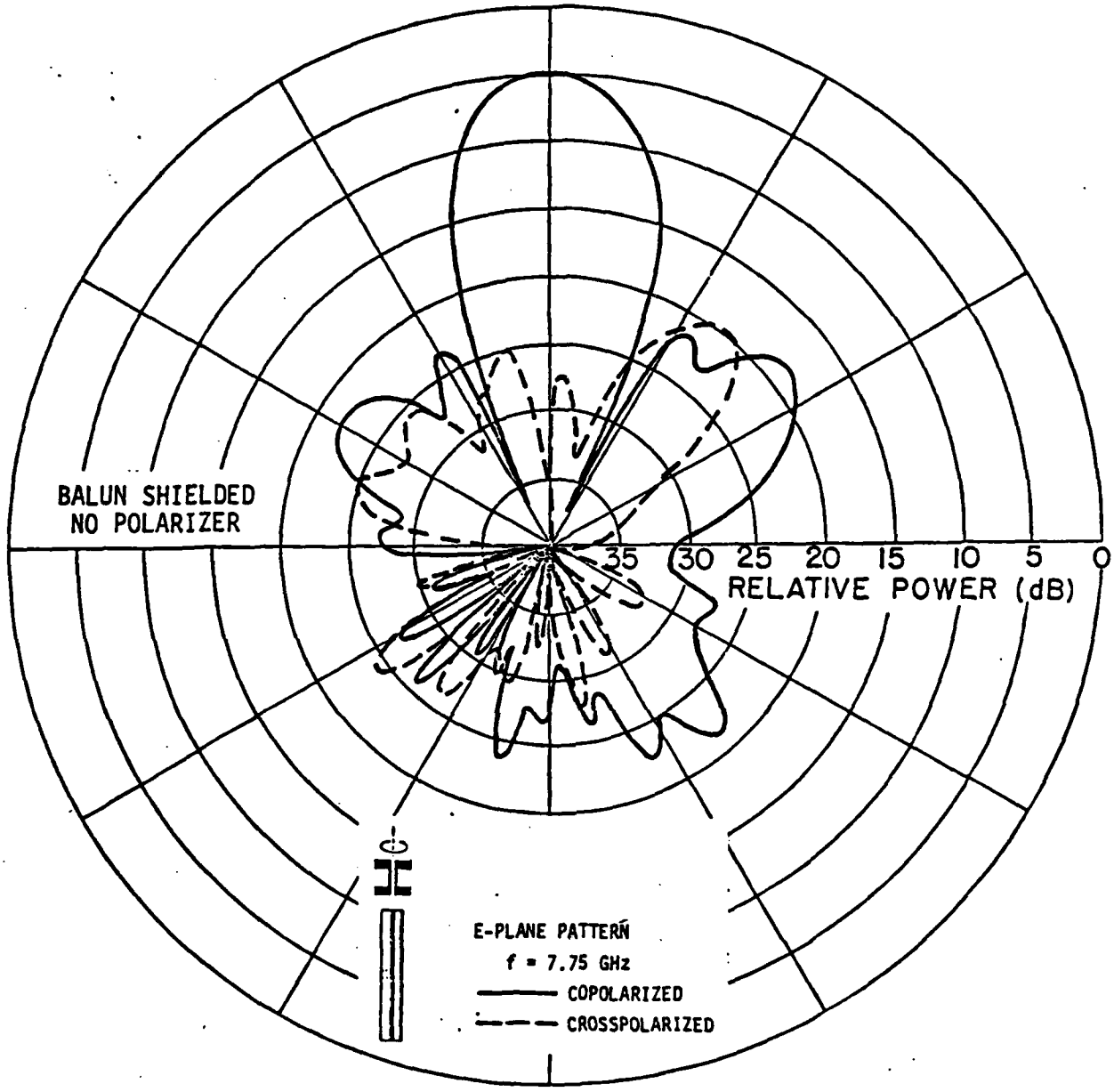

Figure 54. b. The radiation pattern of the X-band array with balun shielded. E-plane, f = 7.75 GHz.

The radiation patterns of the X-band array with the balun shielded are shown in Figures 48-54. We observe that the backlobe level is now 20 dB or more below the mainbeam over most of the operating band, and we also note that patterns are reduced to an acceptable level. Moreover, we also noted that the mainbeam and sidelobes level in the front direction were improved somewhat at some frequencies. The 20 dB backlobe level would be expected due to single defraction at the edge of the finite groundplane.

6. X-BAND RADIATION PATTERN WITH POLARIZER

The electric field radiating from the X-band dipole array is linearly polarized. However, due to its special application, the polarization should be transformed into CP. This is accomplished by a two-layer meanderline polarizer placed in front of the dipole array as shown in Figure 55a.

The two-layer meanderline polarizer was developed by our project sponsor, Naval Research Laboratory (NRL). It is made of two meanderline sheets spaced by a polyfoam slab 3.5 mm thick. The pattern of the meanderline is shown in Figure 55b. For normal operation, the meanderline polarizer is placed in front of the dipole array with the meanderlines making a 45° angle with respect to the principal axis of the dipole array as seen in Figure 55b.

The radiation patterns of the X-band dipole array with the meanderline polarizer in front were measured as presented in Figures 56-62. We observe that the main beam is quite well circularly polarized in the middle of the band but that some deterioration into eliptic

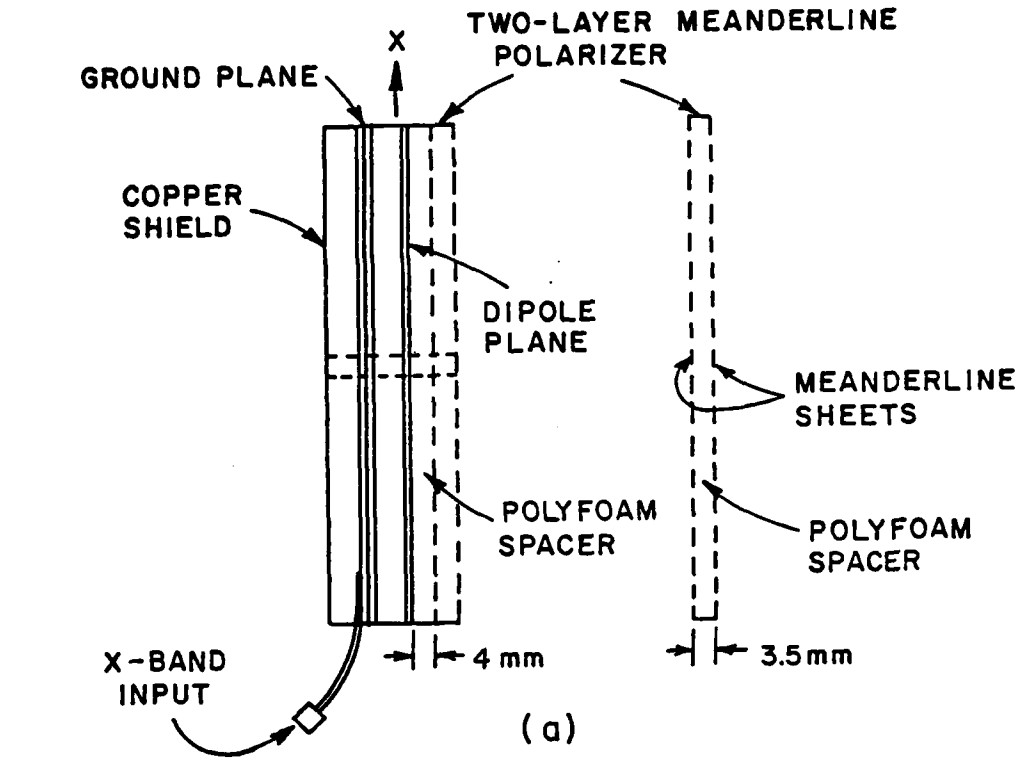

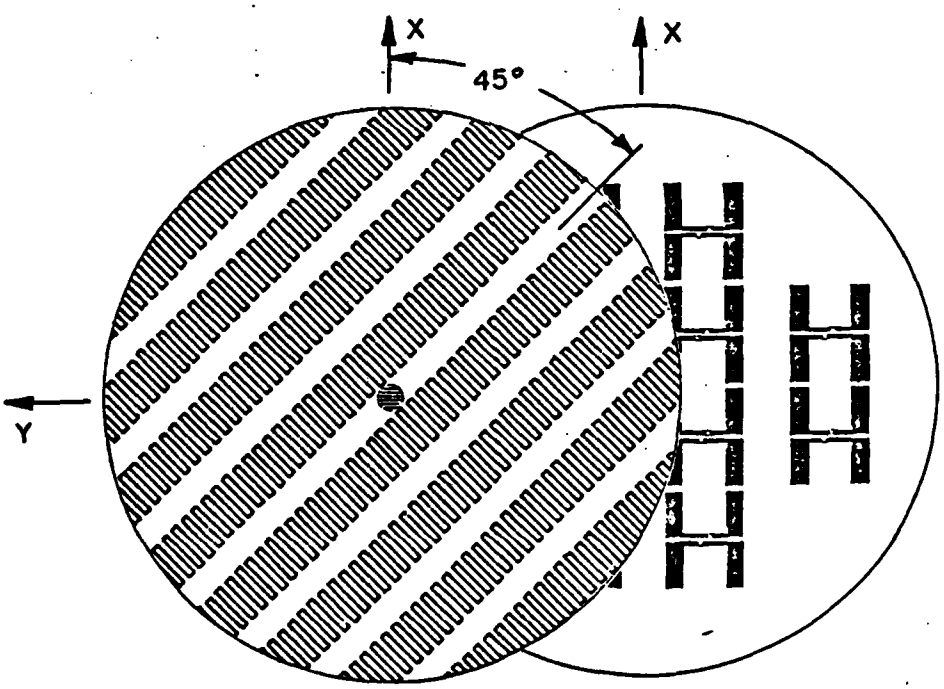

Figure 55. a. LEFT: The sideview showing the relative positions of the dipole array and the polarizer.
RIGHT: Configuration of the two-layer meanderline polarizer.
b. Schematic diagram showing the orientation between the meanderline and the dipoles.

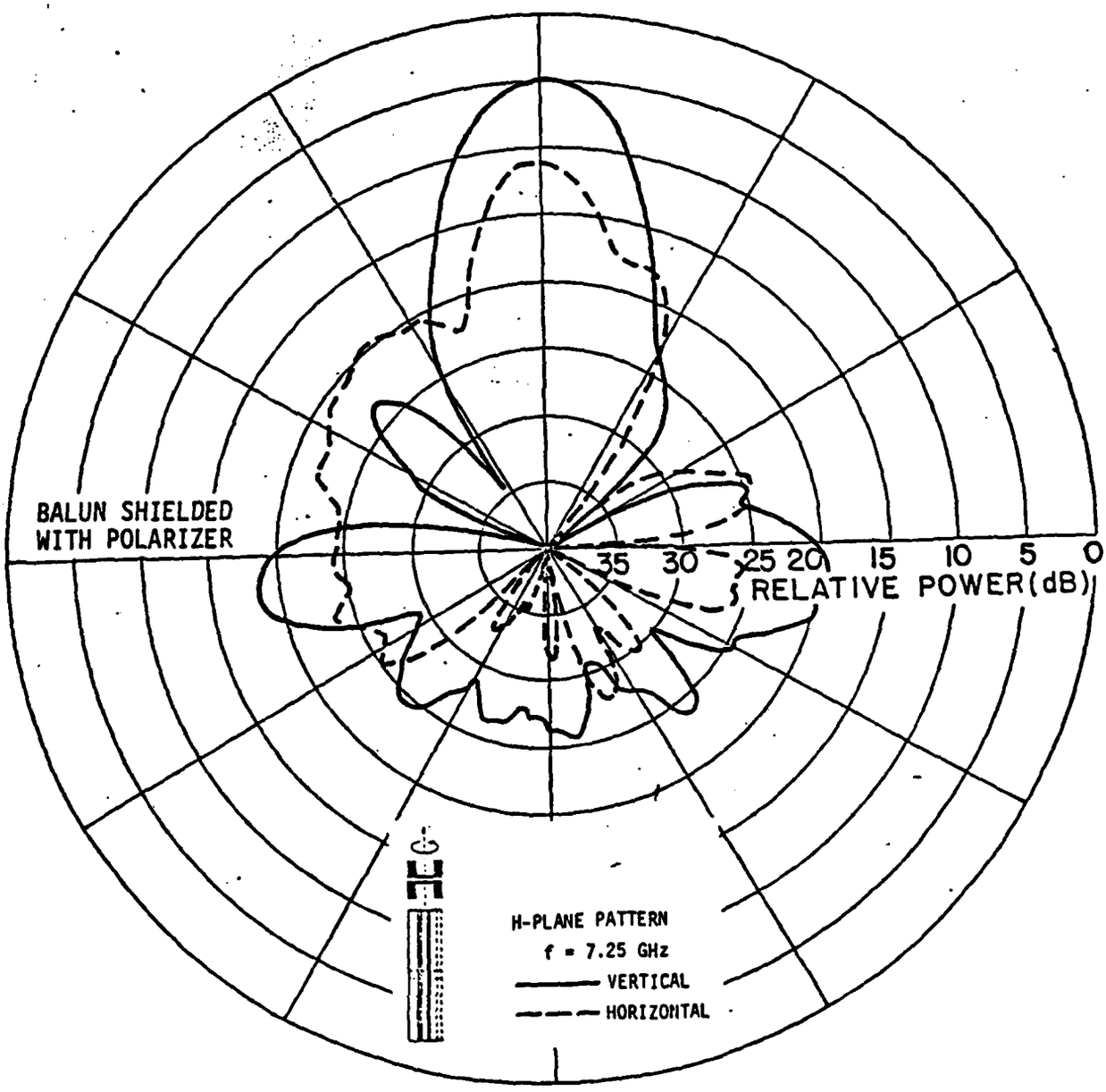

Figure 56. a. Two linear components of circularly polarized radiation pattern of the X-band array. H-plane, f = 7.25 GHz.

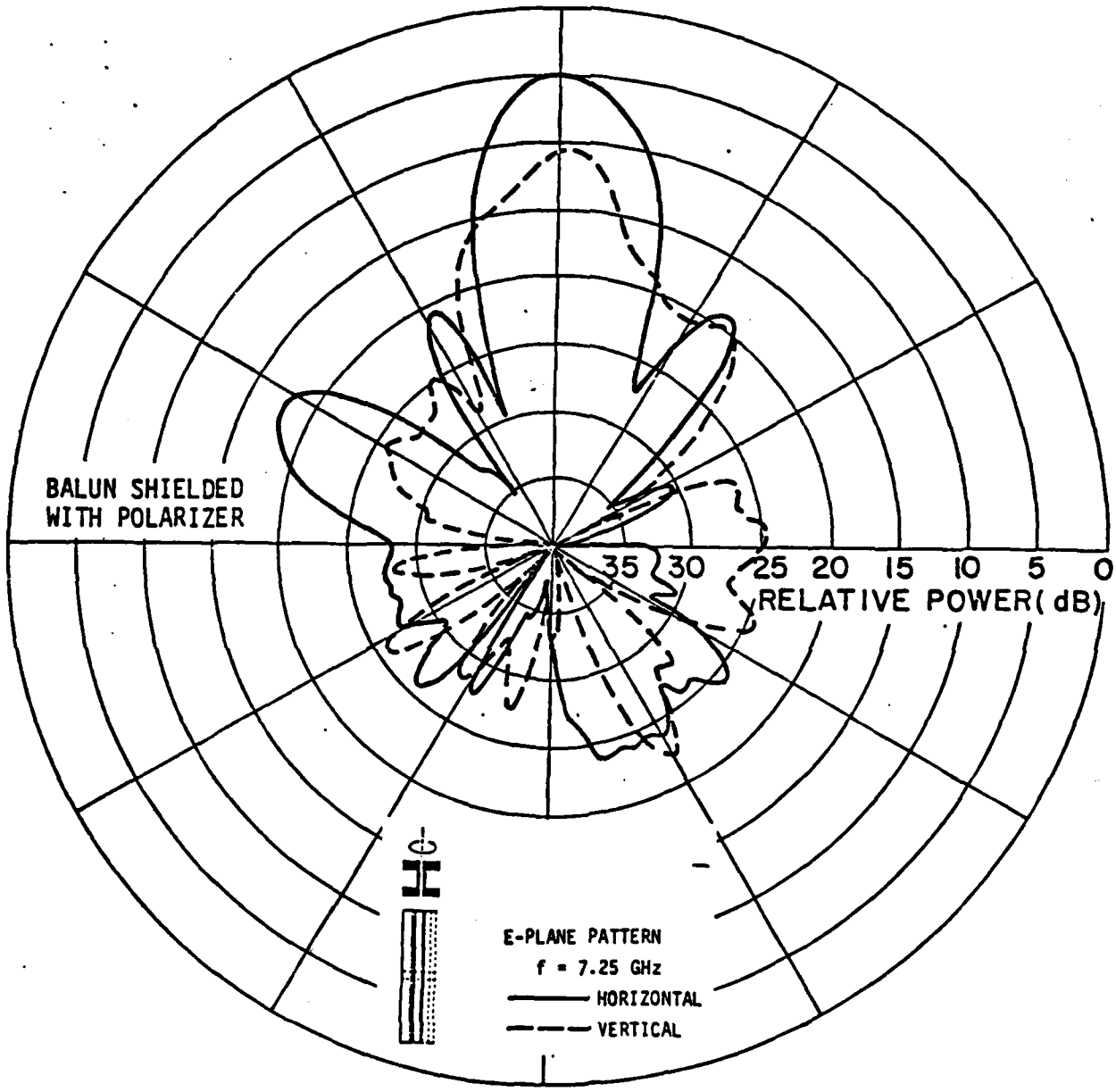

Figure 56. b. Two linear components of circularly polarized radiation pattern of the X-band array. E-plane, f = 7.25 GHz.

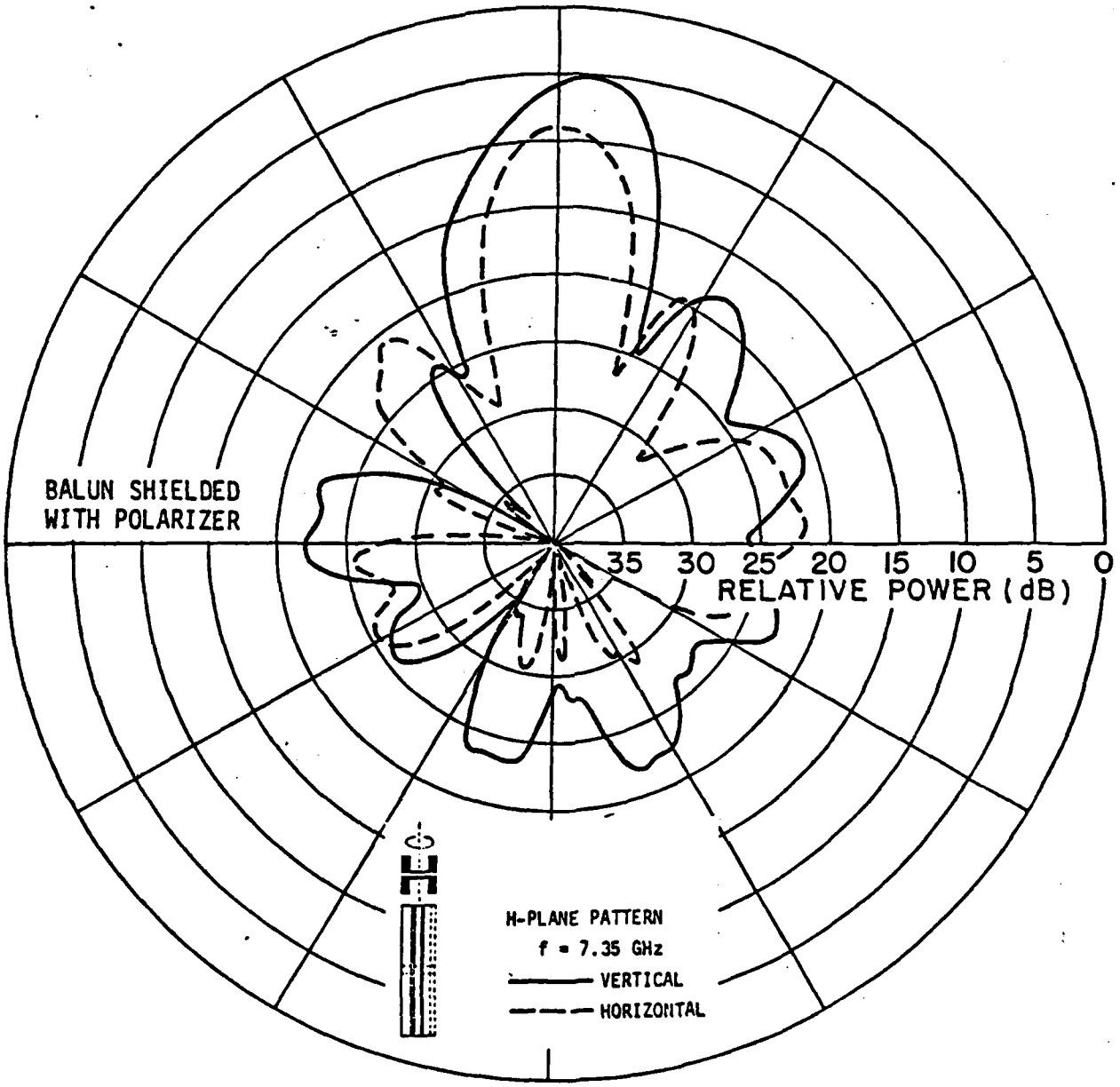

Figure 57. a. Two linear components of circularly polarized radiation pattern of the X-band array. H-plane, f = 7.35 GHz.

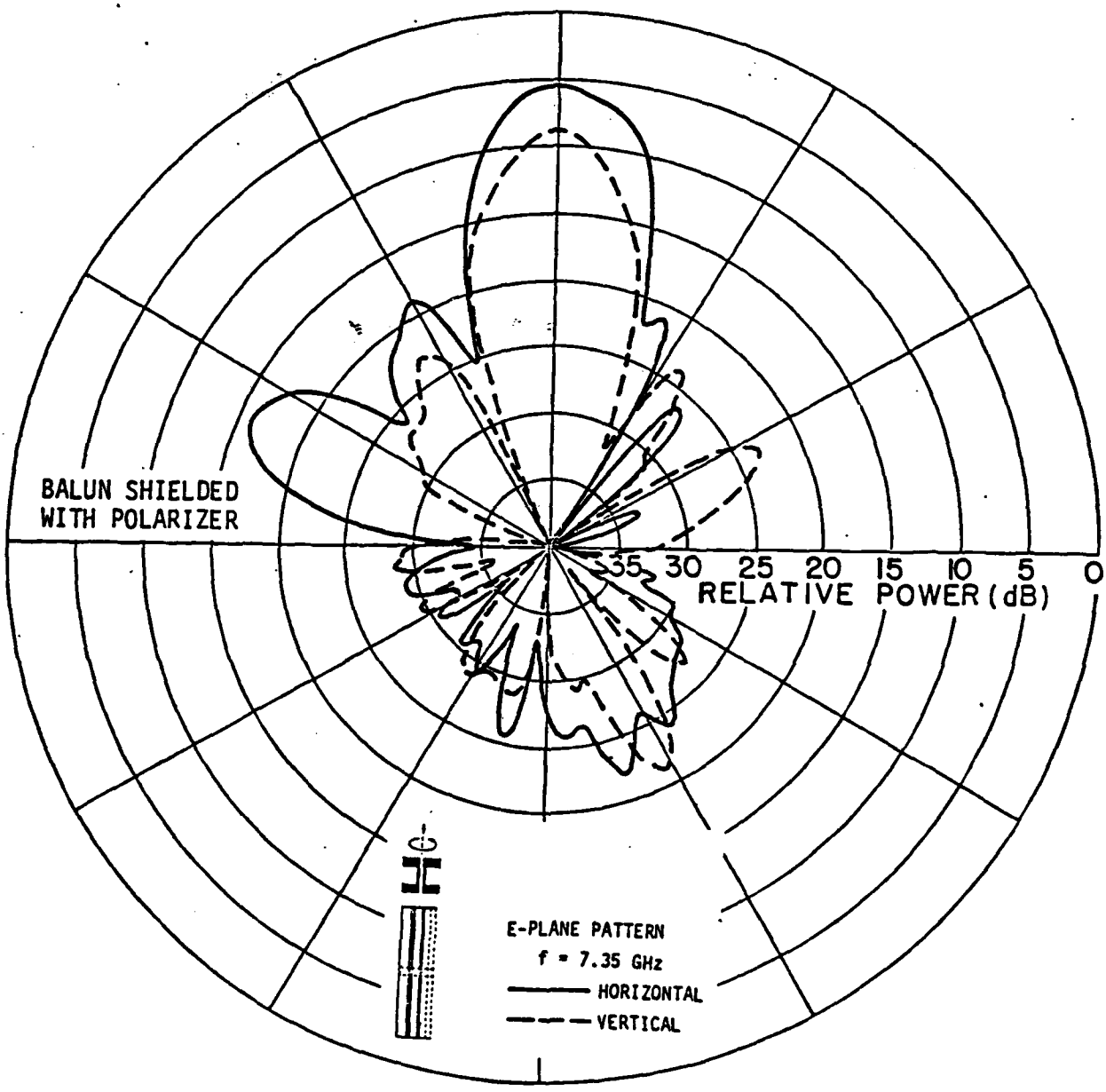

Figure 57. b. Two linear components of circularly polarized radiation pattern of the X-band array. E-plane, f = 7.35 GHz.

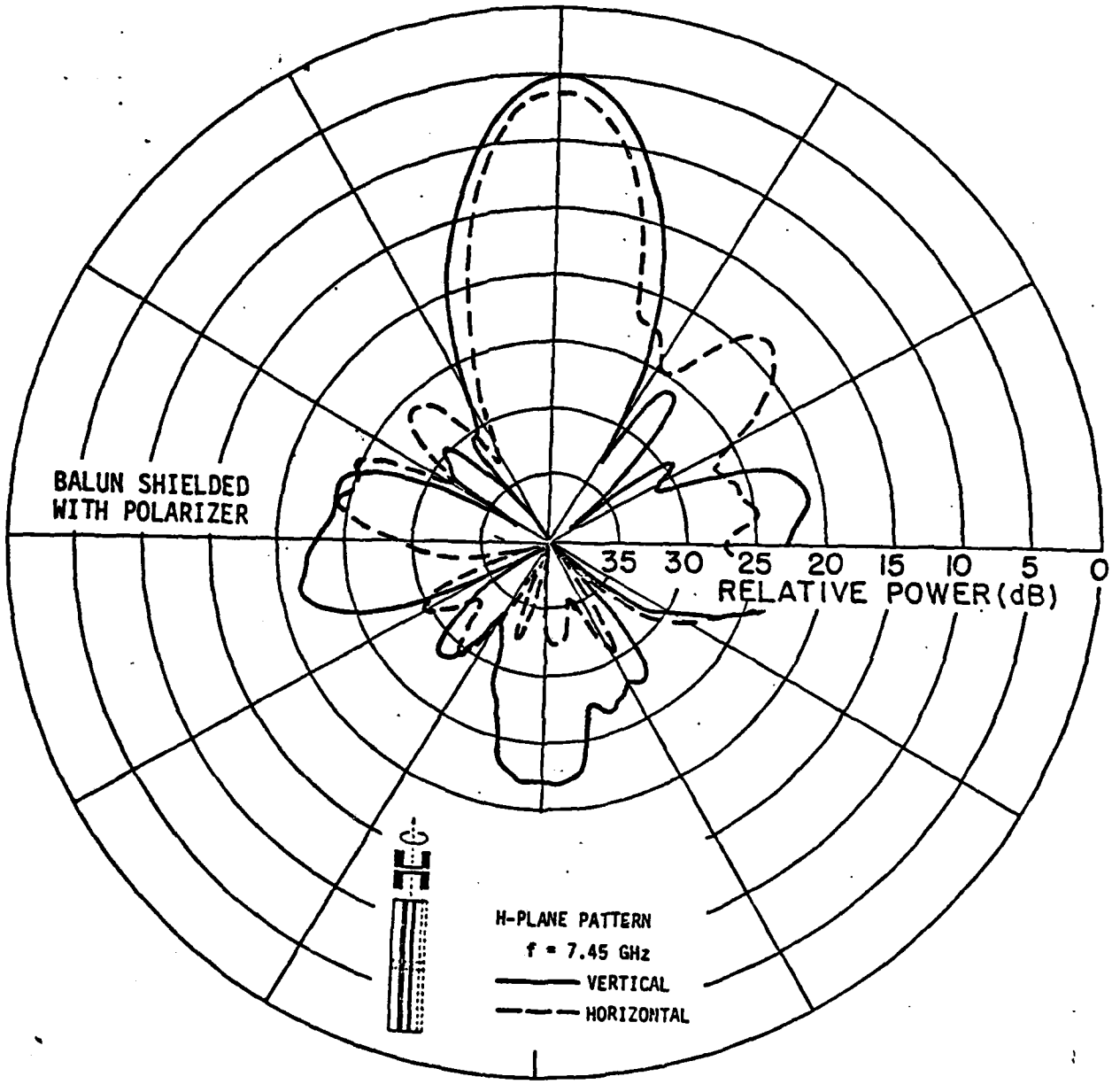

Figure 58. a. Two linear components of circularly polarized radiation pattern of the X-band array. H-plane, f = 7.45 GHz.

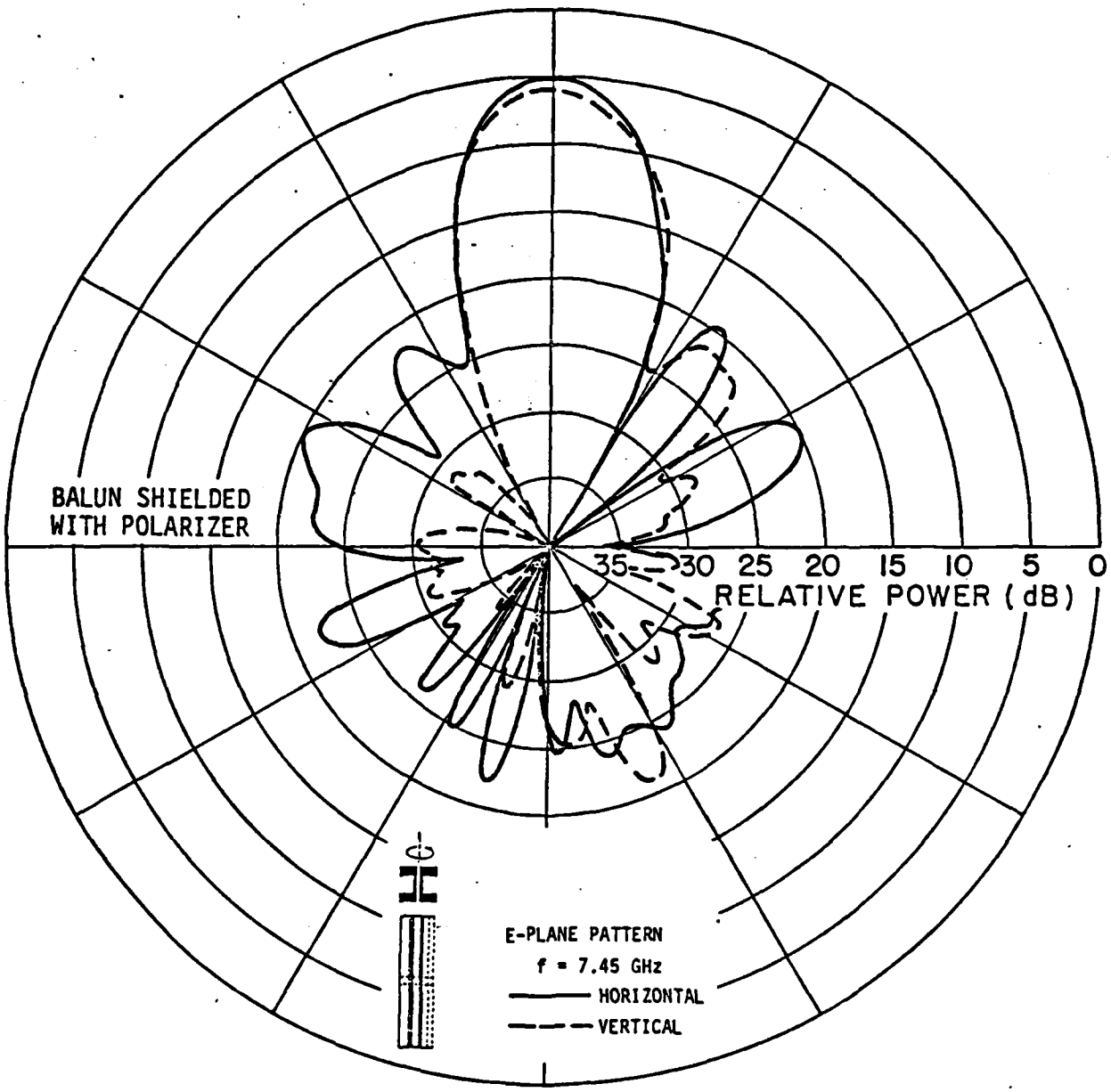

Figure 58. b. Two linear components of circularly polarized radiation pattern of the X-band array. E-plane, f = 7.45 GHz.

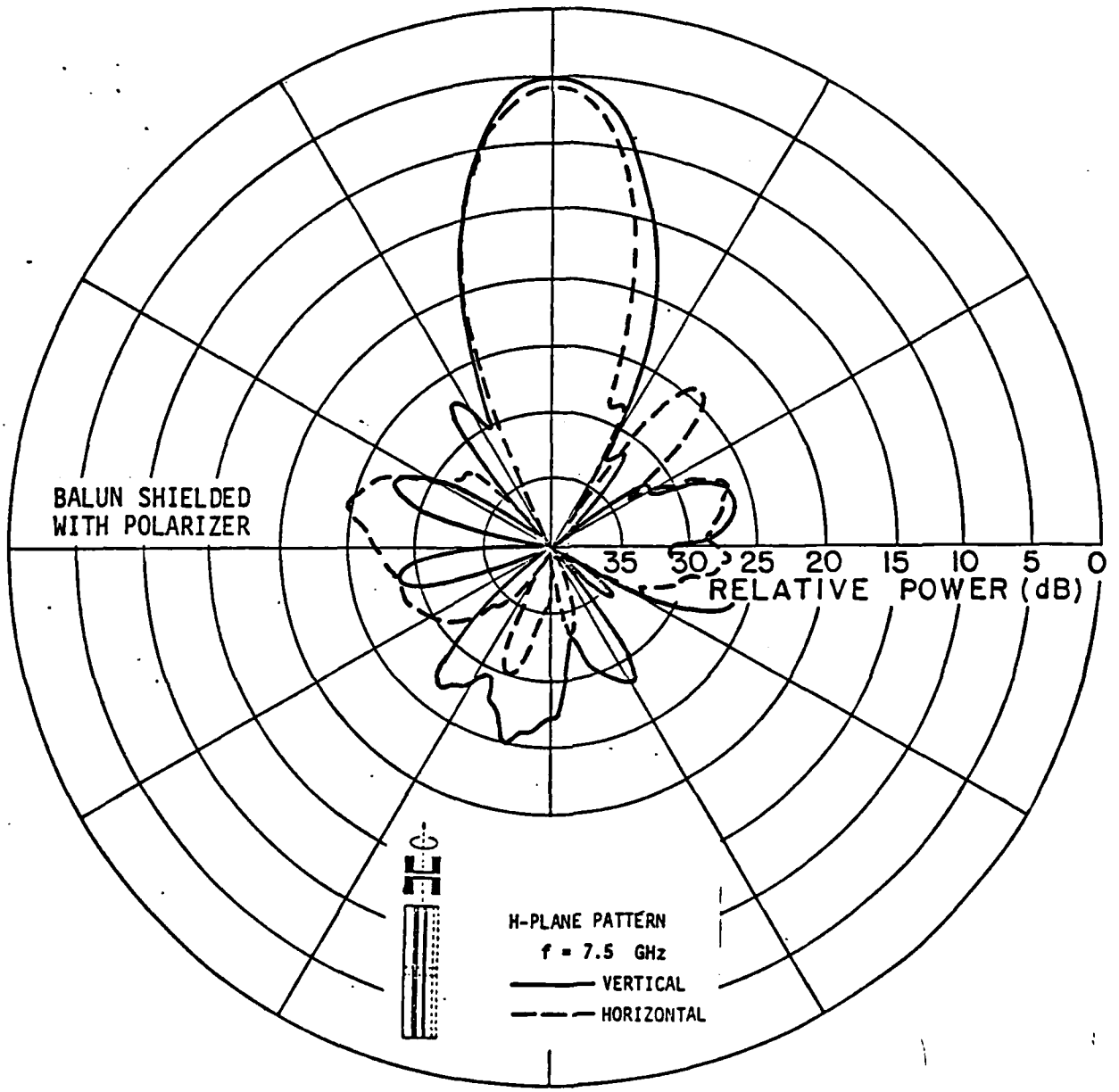

Figure 59. a. Two linear components of circularly polarized radiation pattern of the X-band array. H-plane, f = 7.5 GHz.

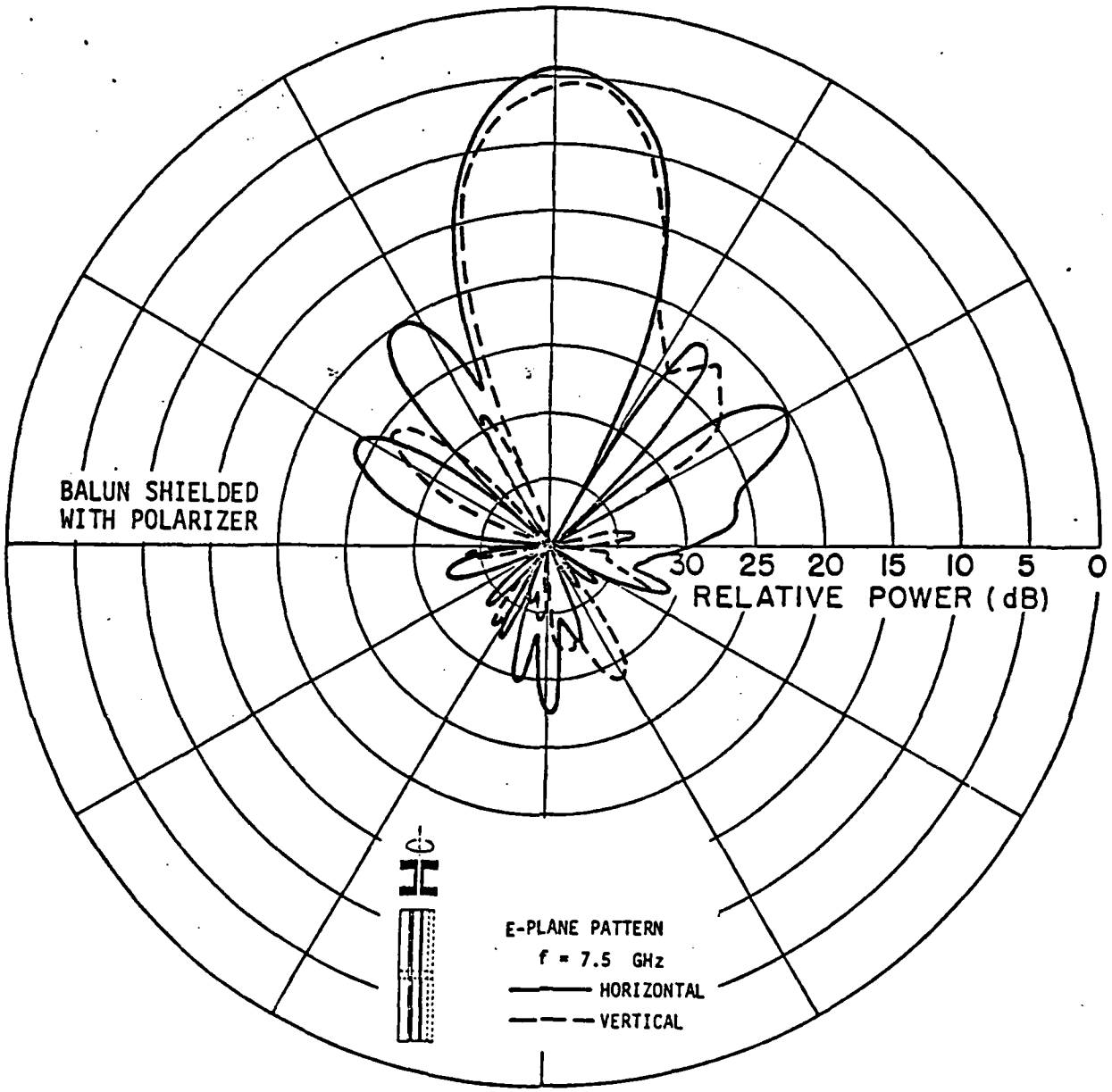

Figure 59. b. Two linear components of circularly polarized radiation pattern of the X-band array. E-plane, f = 7.5 GHz.

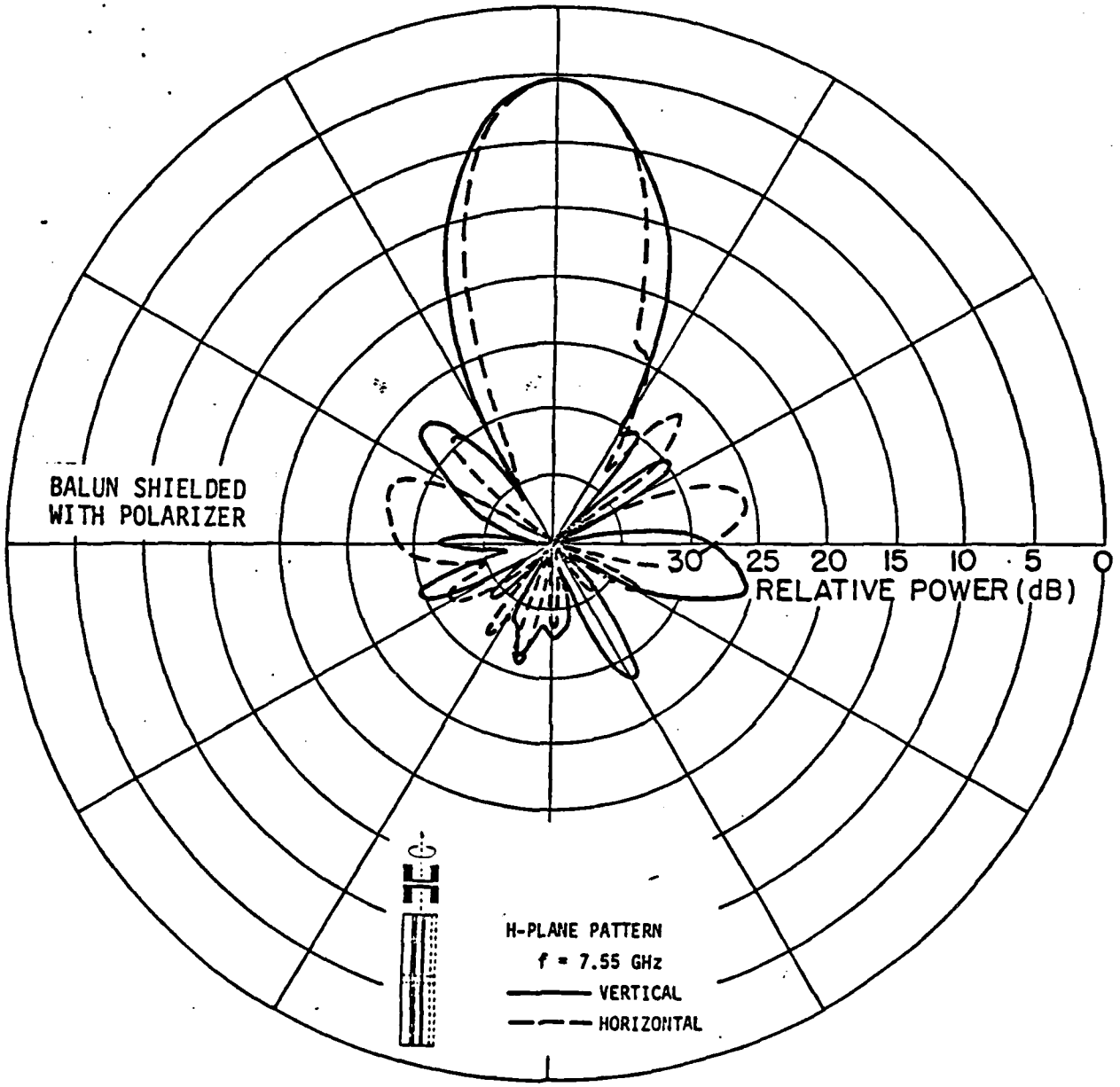

Figure 60. a. Two linear components of circularly polarized radiation pattern of the X-band array. H-plane, f = 7.55 GHz.

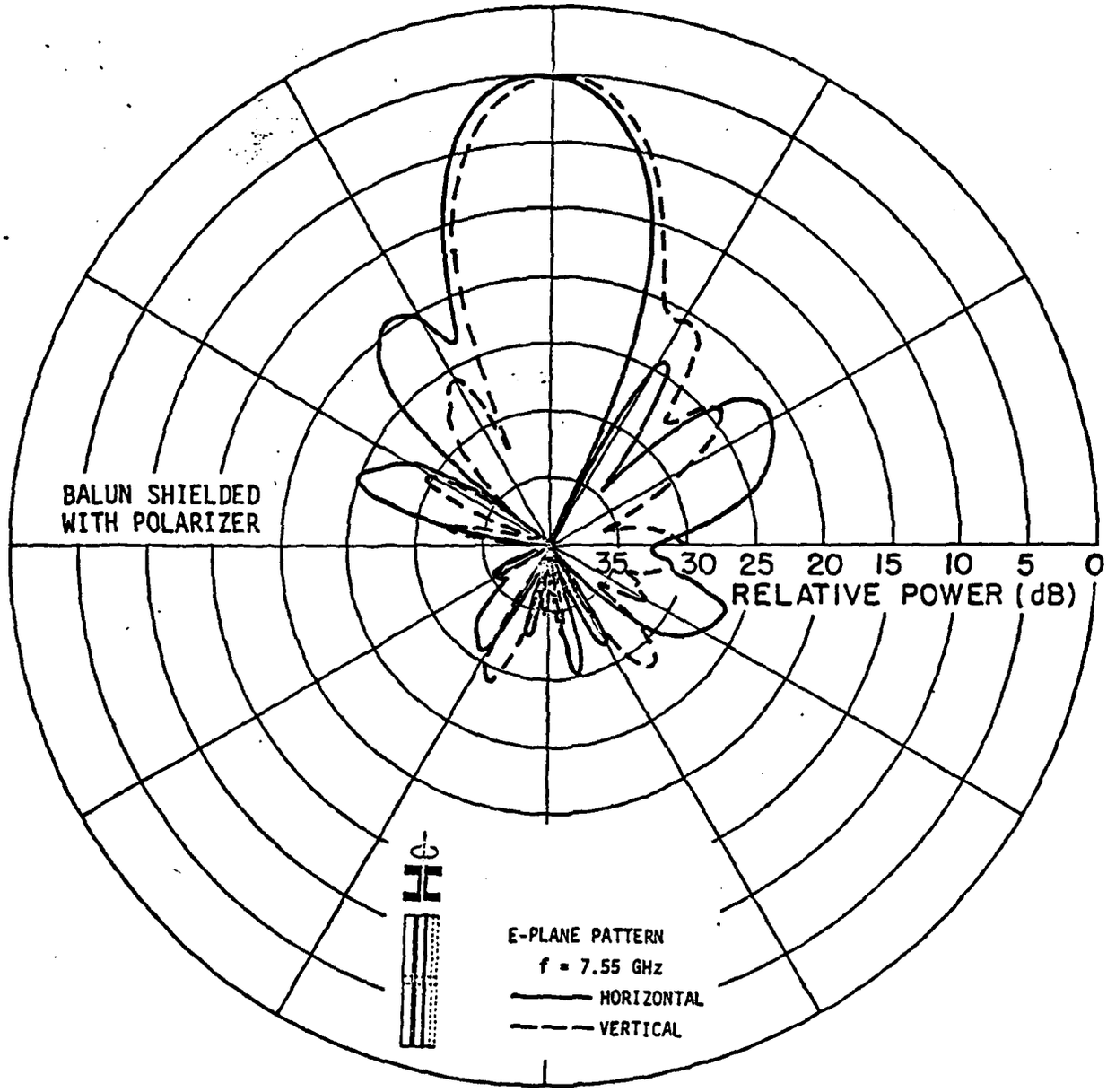

Figure 60. b. Two linear components of circularly polarized radiation pattern of the X-band array. E-plane, f = 7.55 GHz.

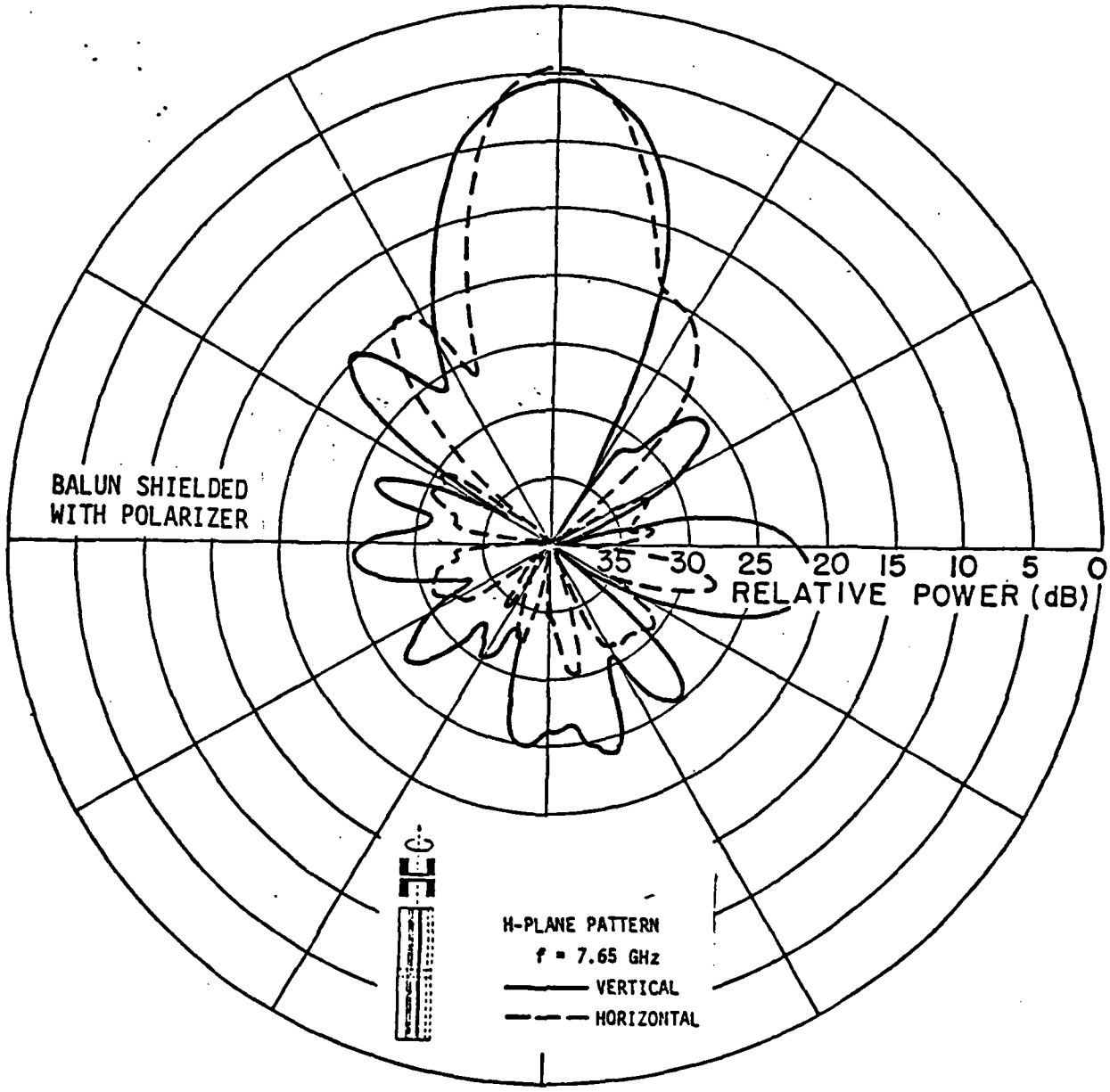

Figure 61. a. Two linear components of circularly polarized radiation pattern of the X-band array. H-plane, f = 7.65 GHz.

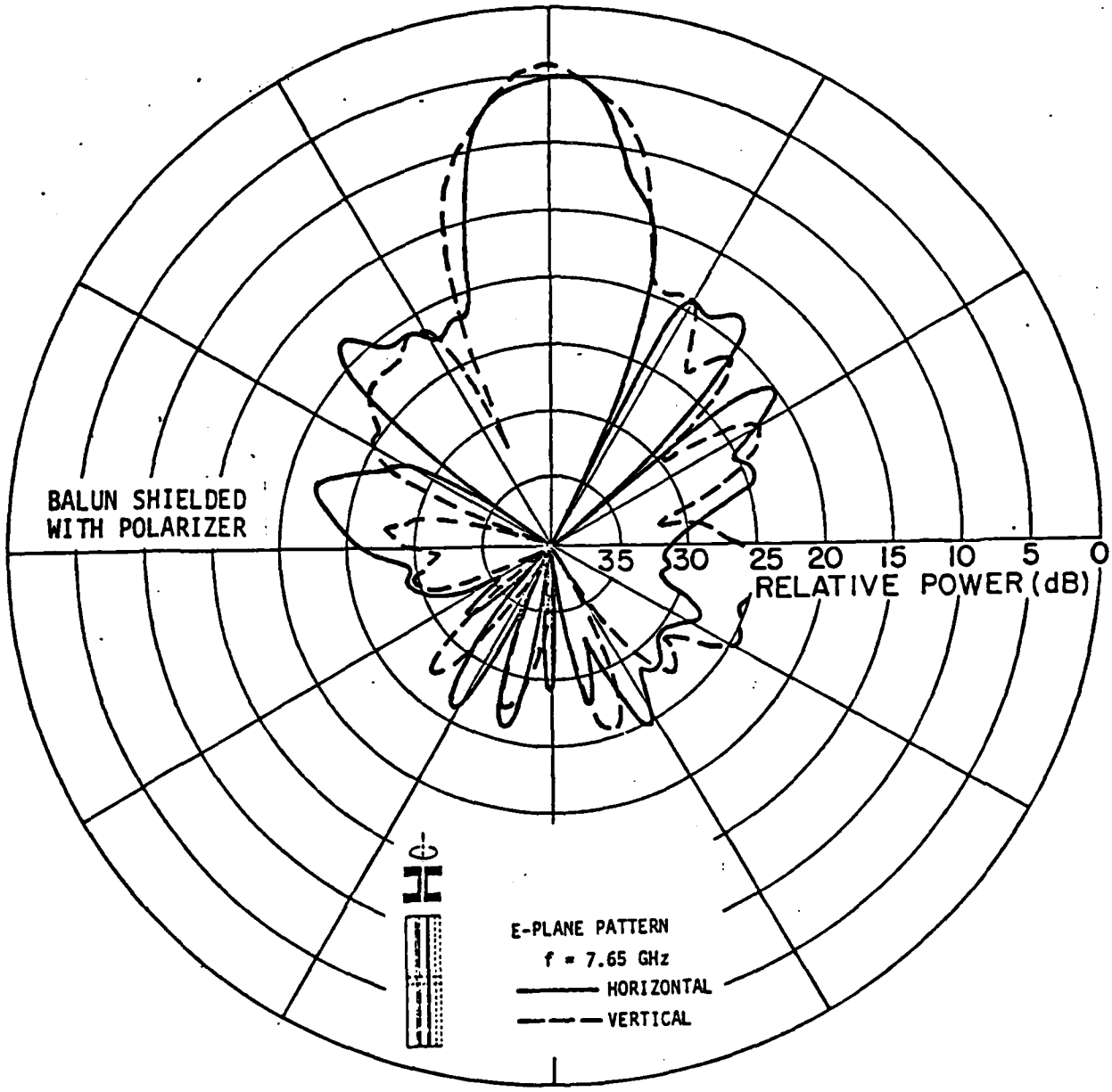

Figure 61. b. Two linear components of circularly polarized radiation pattern of the X-band array. E-plane, f = 7.65 GHz.

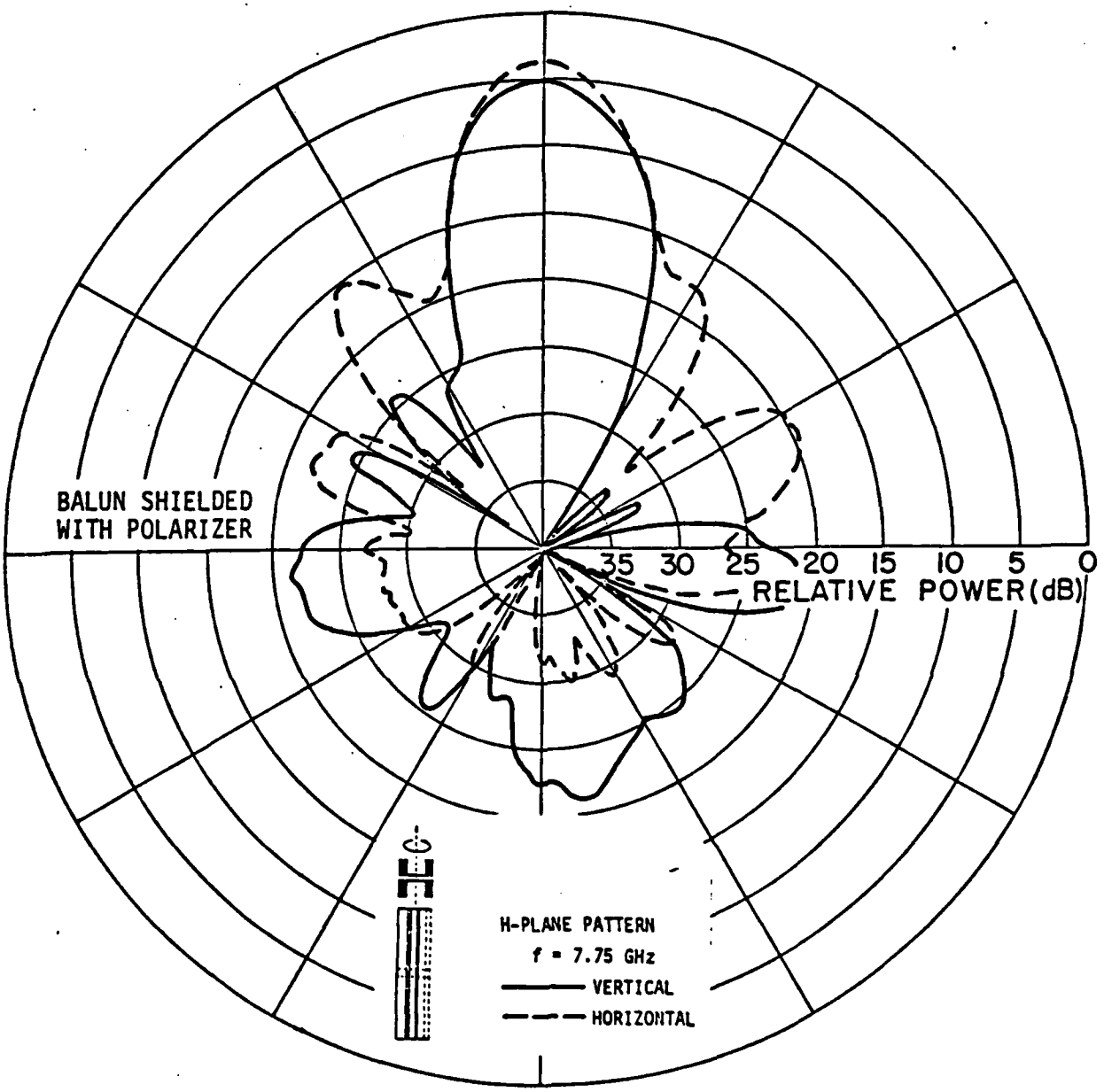

Figure 62. a. Two linear components of circularly polarized radiation pattern of the X-band array. H-plane, f = 7.75 GHz.

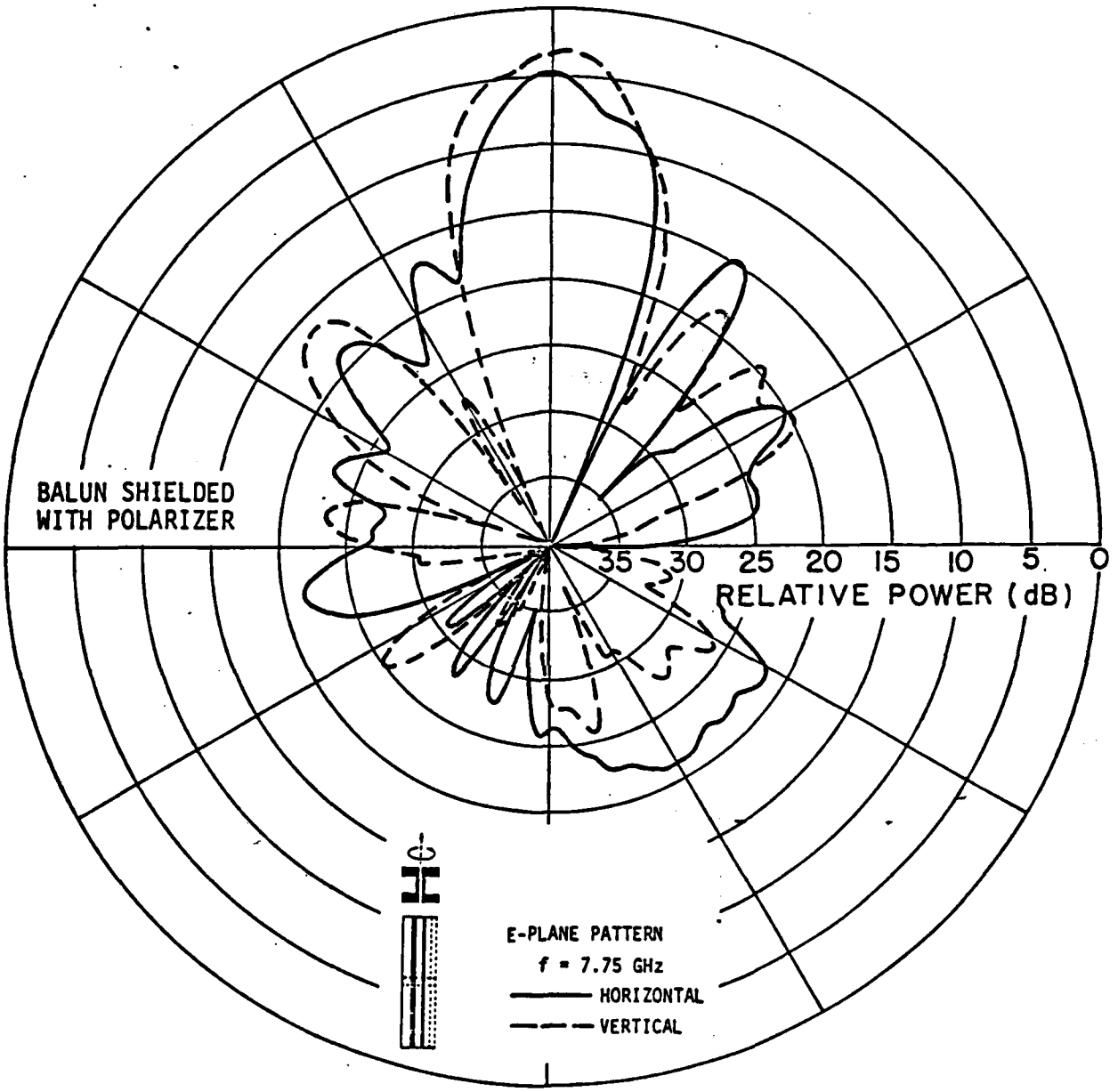

Figure 62. b. Two linear components of circularly polarized radiation pattern of the X-band array. E-plane, f = 7.75 GHz.

polarization is observed at the ends of the band. We should possibly have more meanderline layers instead of merely two. However, time did not permit our sponsor to pursue this possibility.

7. X-BAND RADIATION PATTERN WITH POLARIZER AND PARABOLIC DISH

Finally, the X-band dipole array with the meanderline polarizer was mounted in back of the parabolic dish as shown in Figure 63 . The parabolic dish is made of polyrethene and coated with a dichroic surface as desribed in Figure 63. This dichroic surface is designed to be a good reflector at 43-46 GHz and very transparent at the X-band frequencies (7.25-7.75 GHz). The meanderline polarizer and the parabolic dish are closely spaced. However, in order to avoid an undesired cavity effect between the X-band array and the parabolic dish, proper spacing between these two elements is necessary. The spacing, d, can be adjusted by moving the dipole array backward or forward along the metallic separation screws.

The spacing was first set at d=0.2 inch and a set of radiation patterns of the X-band array were measured. From the measured patterns, we noted that there were small ripples appearing in the mainbeam at the frequencies at the low end of the operating band (see Figure 64 for the patterns at f=7.25 GHz). These ripples might be caused by a certain cavity effect between the X-band array and the parabolic dish, which was due to the smaller d. When we changed the spacing to d=0.3 inch, the ripples disappeared. The measured radiation patterns of the X-band array with spacing d=0.3 inch are shown in Figures 65-71.

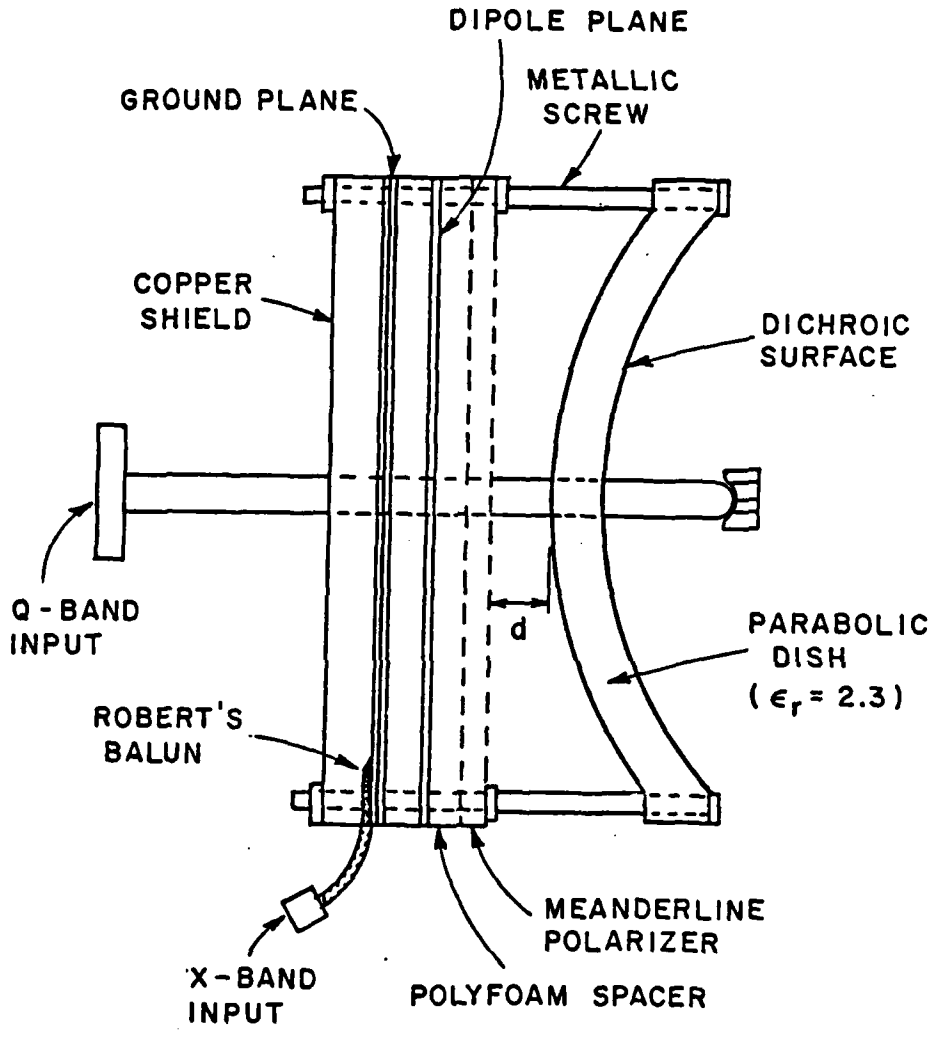

Figure 63. Completed assembly of the dual-band antenna. The X-band array and the polarizer are mounted in back of the parabolic dish with four metallic screws.

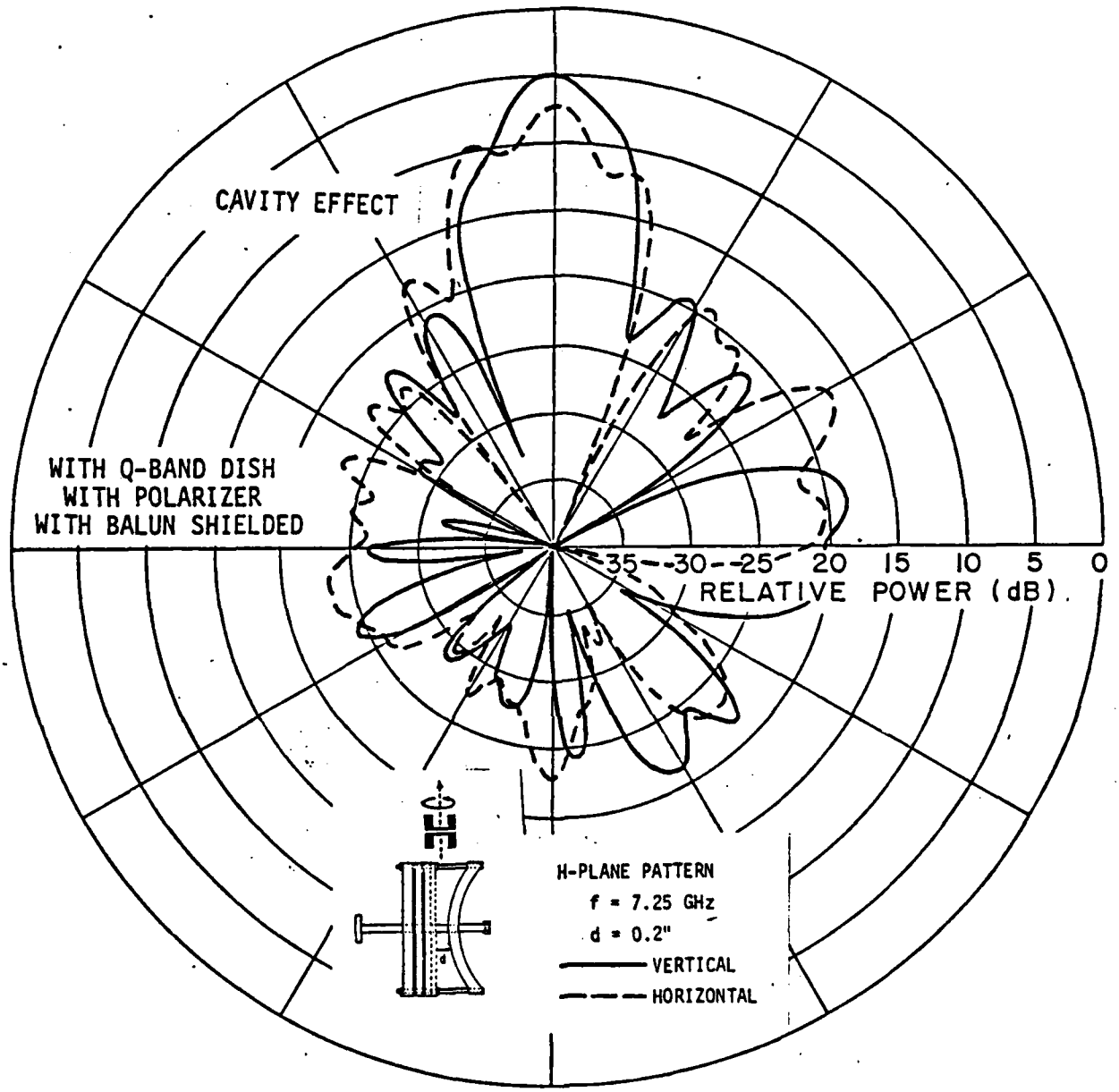

Figure 64. a. Two linear components of circularly polarized radiation pattern in the dipole H-plane, at f = 7.25 GHz, when d = 0.2". (W/polarizer + parabolic dish + Q-band feed). The ripples in the mainbeam are caused by the coupling between the X-band array and the parabolic dish, which is due to the smaller d.

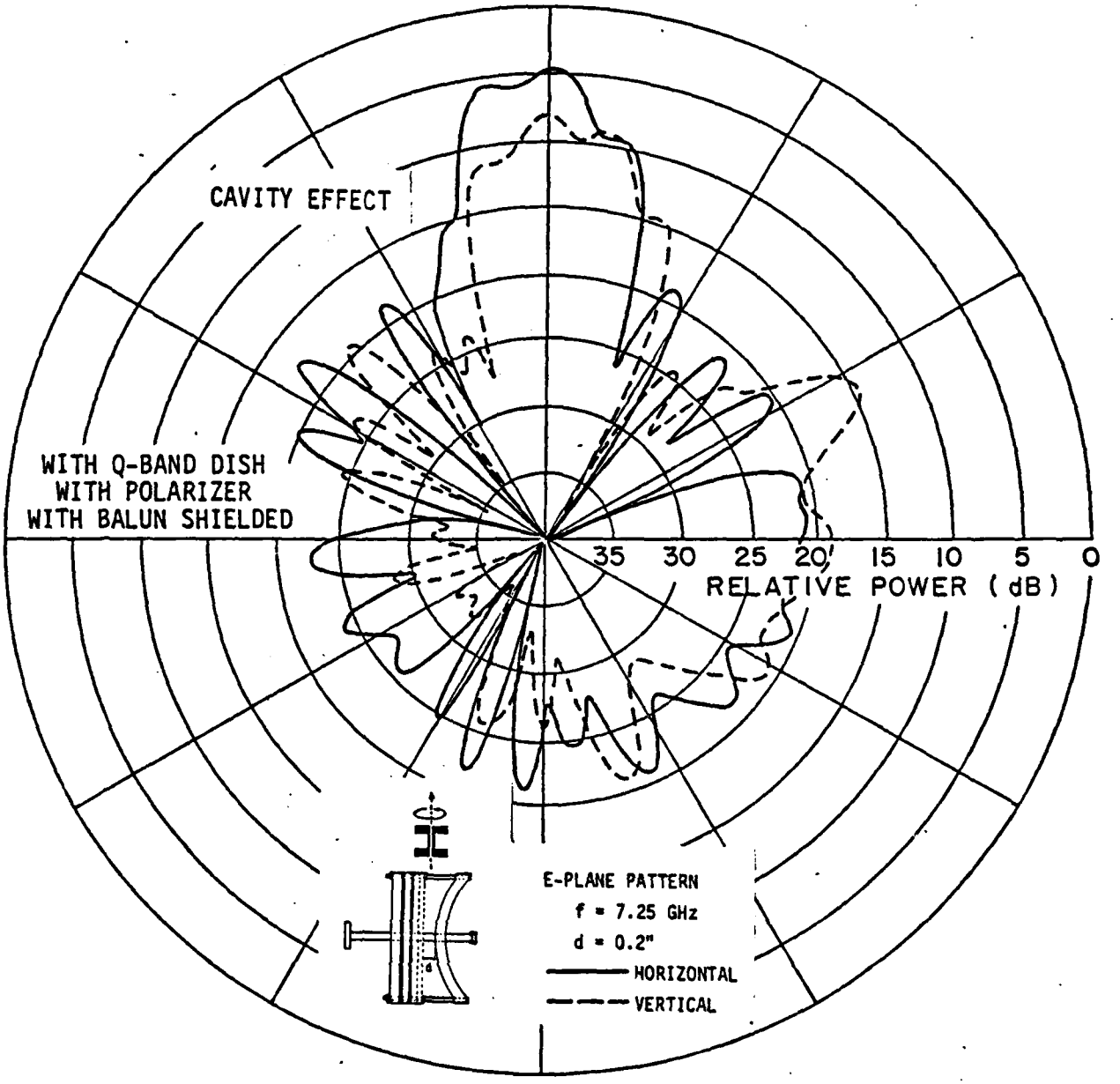

Figure 64. b. Two linear components of circularly polarized radiation pattern in the dipole E-plane, at f = 7.25 GHz, when d = 0.2". (W/polarizer + parabolic dish + Q-band feed). The ripples in the mainbeam are caused by the coupling between the X-band array and the parabolic dish, which is due to the smaller d.

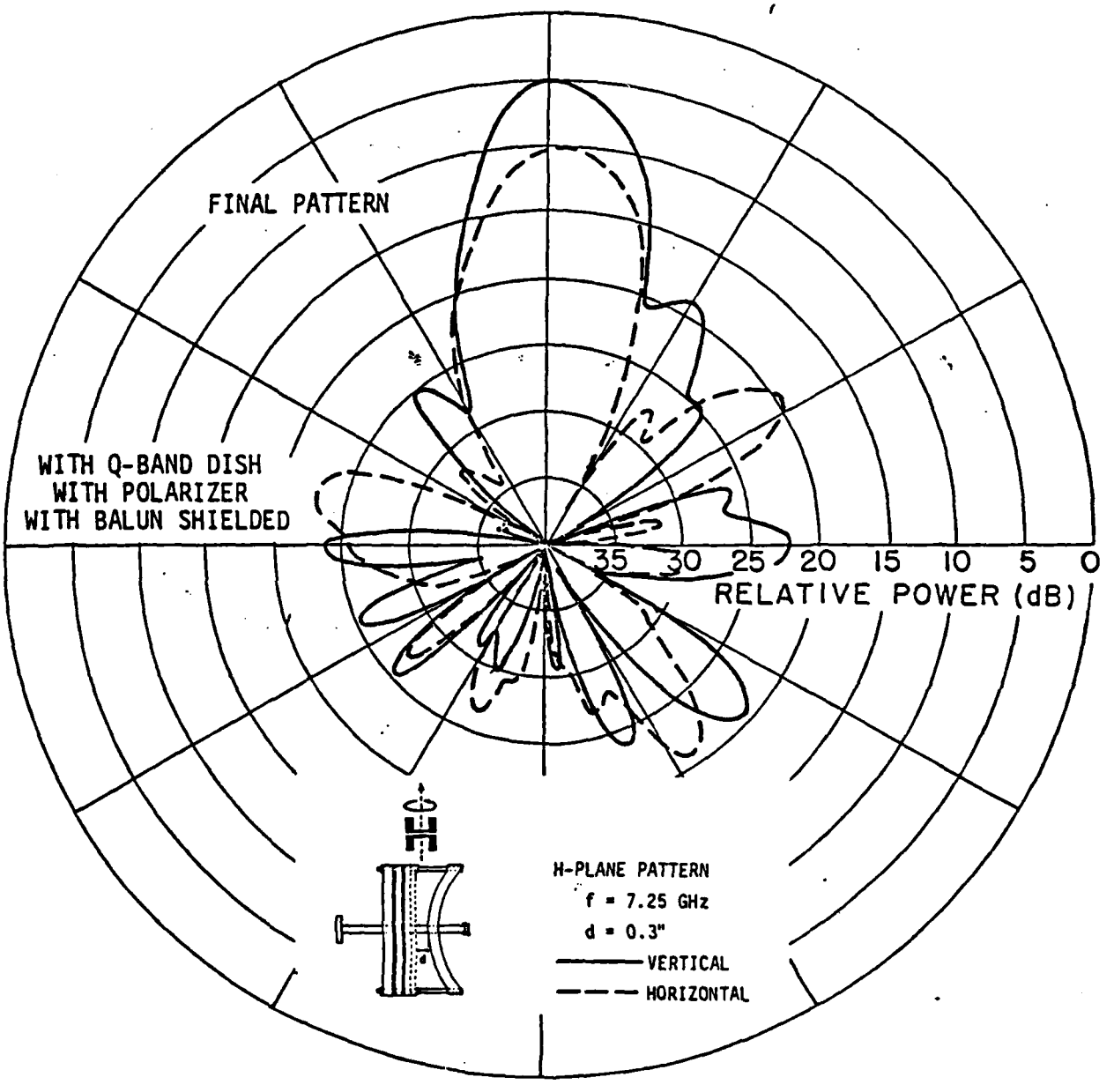

Figure 65. a. Two linear components of circularly polarized radiation pattern in the dipole H-plane, at f = 7.25 GHz, when d = 0.3". (W/ polarizer + parabolic dish + Q-band feed).

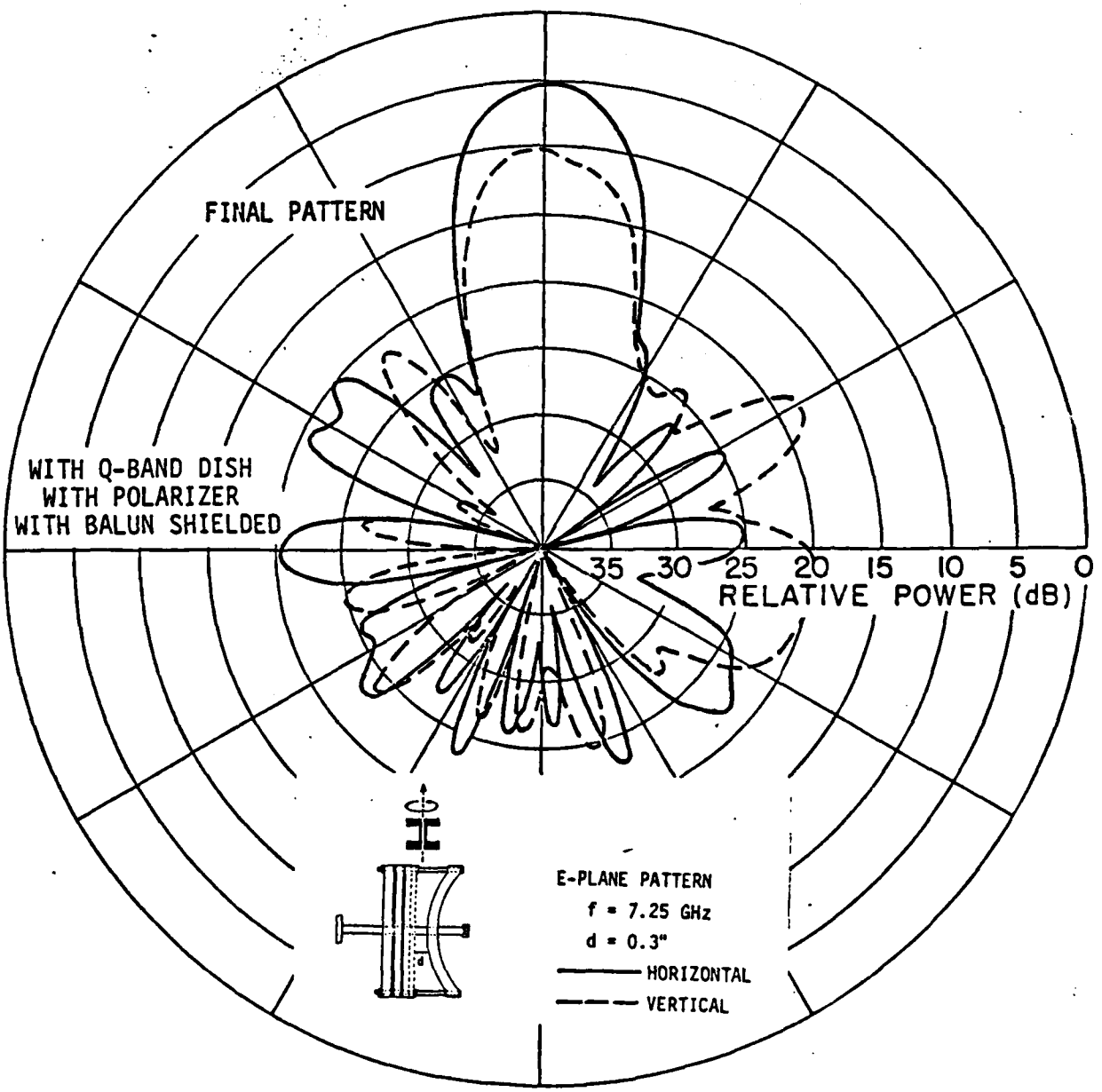

Figure 65. b. Two linear components of circularly polarized radiation pattern in the dipole E-plane, at f = 7.25 GHz, when d = 0.3". (W/ polarizer + parabolic dish + Q-band feed).

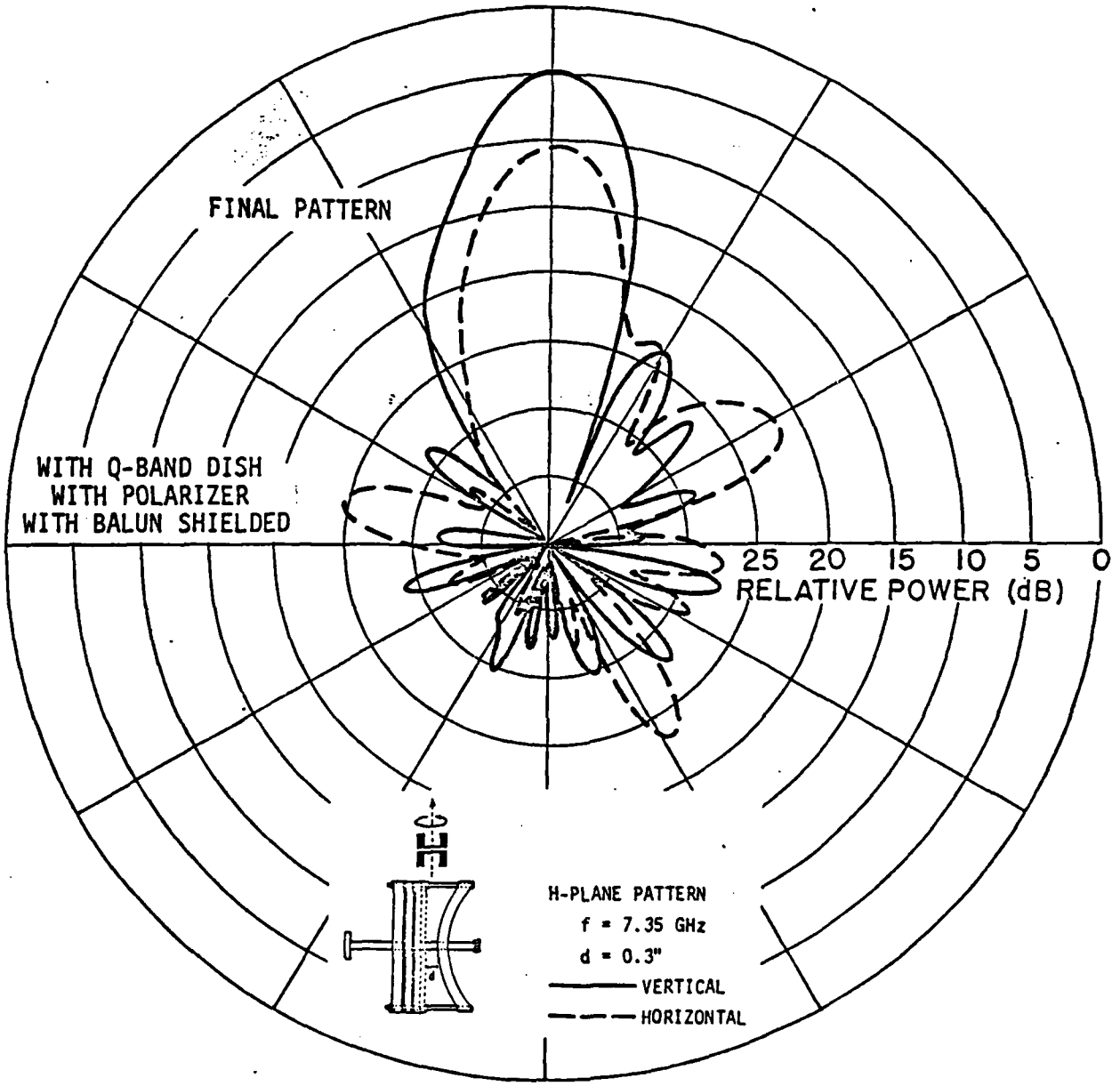

Figure 66. a. Two linear components of circularly polarized radiation pattern in the dipole H-plane, at f = 7.35 GHz, when d = 0.3". (W/ polarizer + parabolic dish + Q-band feed).

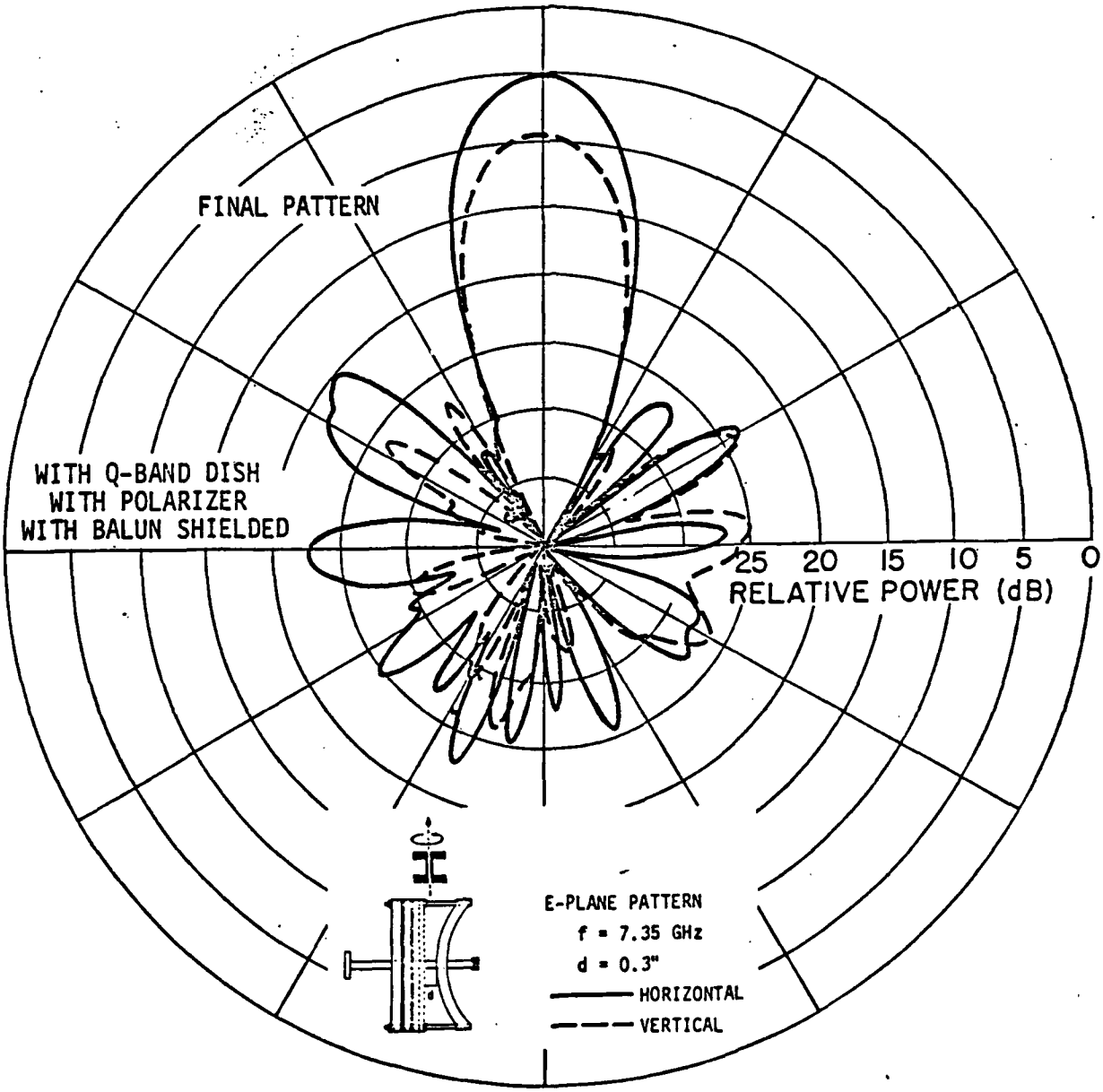

Figure 66. b. Two linear components of circularly polarized radiation pattern in the dipole E-plane, at f = 7.35 GHz, when d = 0.3". (W/ polarizer + parabolic dish + Q-band feed).

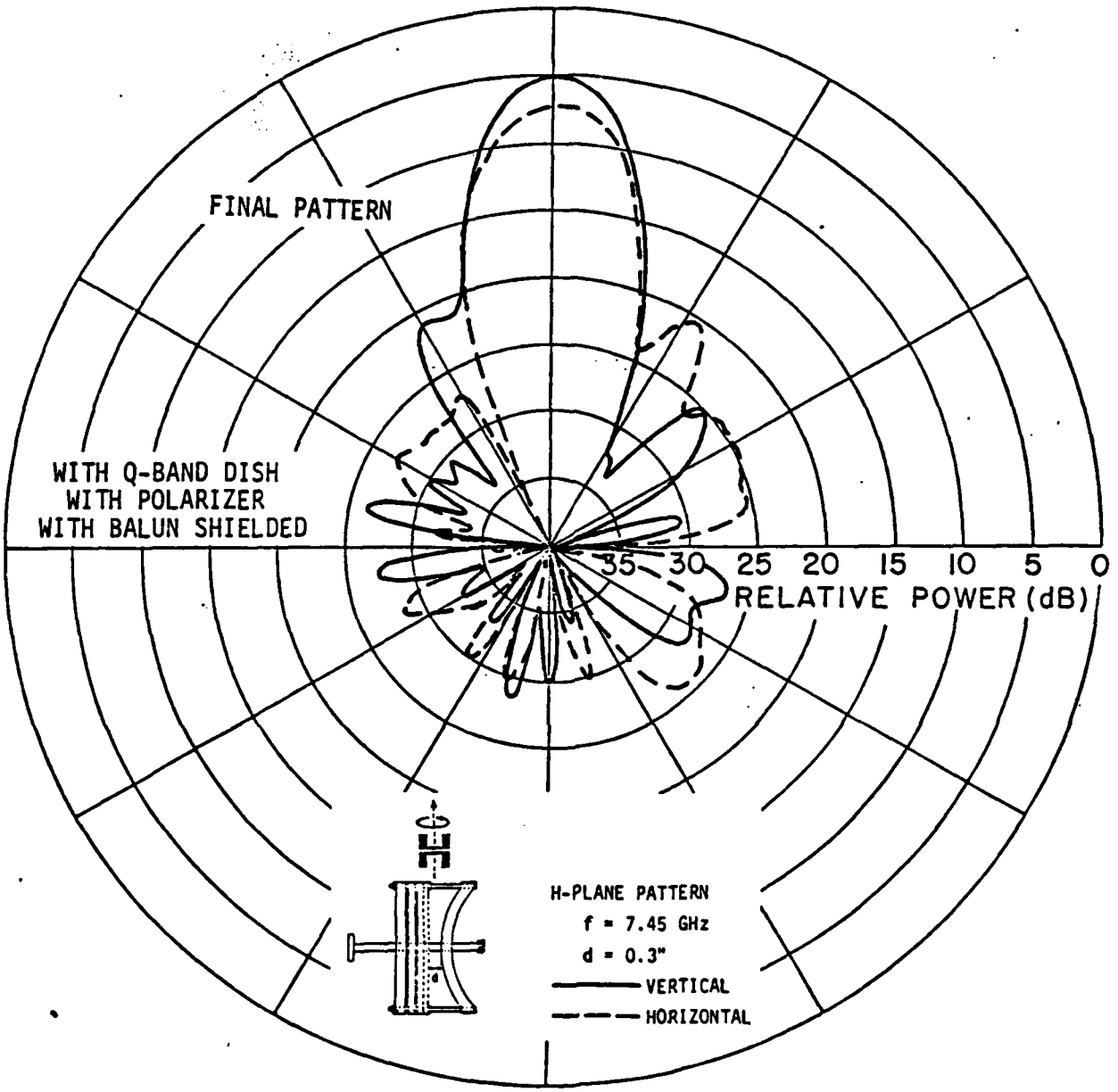

Figure 67. a. Two linear components of circularly polarized radiation pattern in the dipole H-plane, at f = 7.45 GHz, when d = 0.3". (W/ polarizer + parabolic dish + Q-band feed).

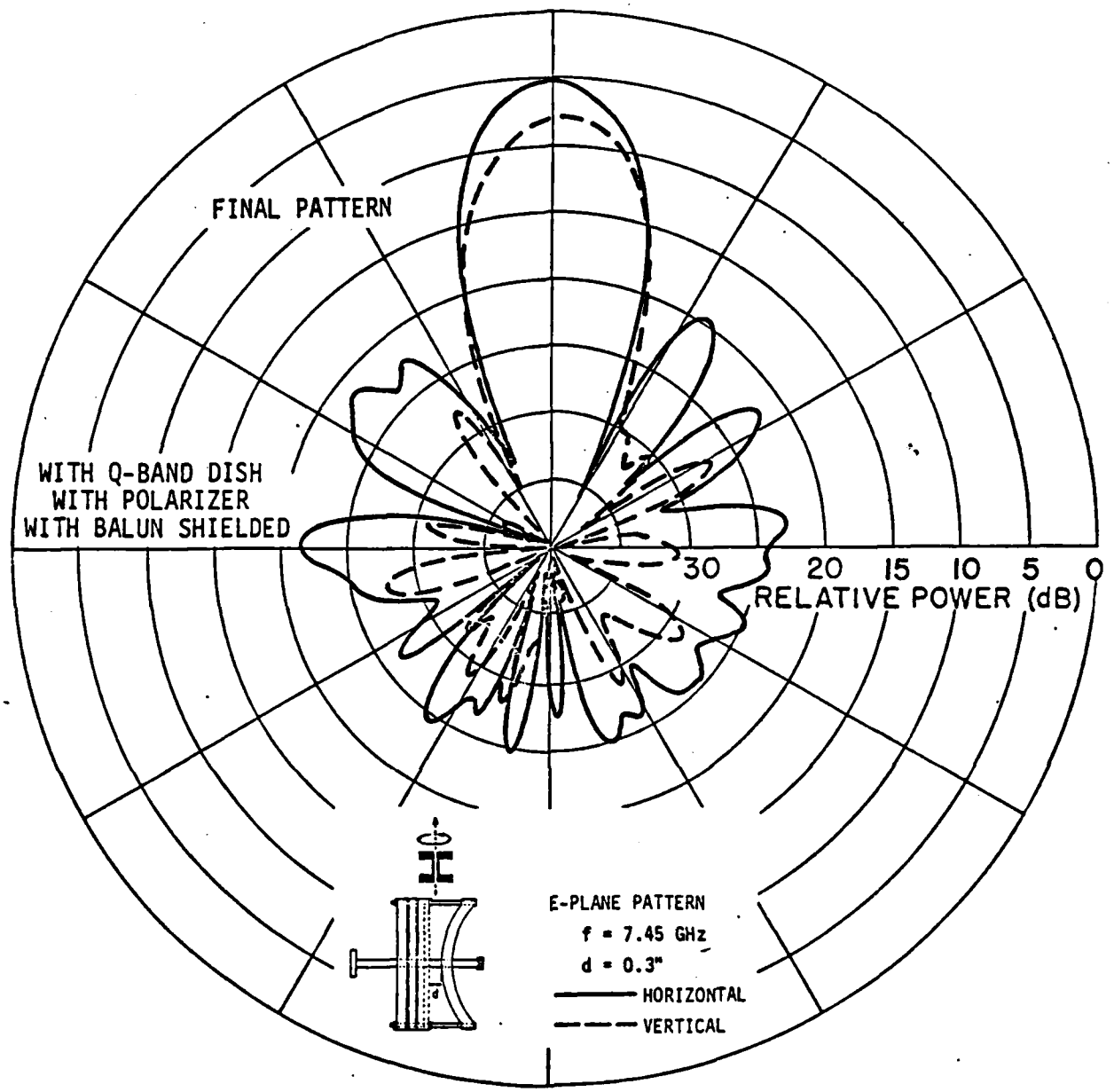

Figure 67. b. Two linear components of circularly polarized radiation pattern in the dipole E-plane, at f = 7.45 GHz, when d = 0.3". (W/ polarizer + parabolic dish + Q-band feed).

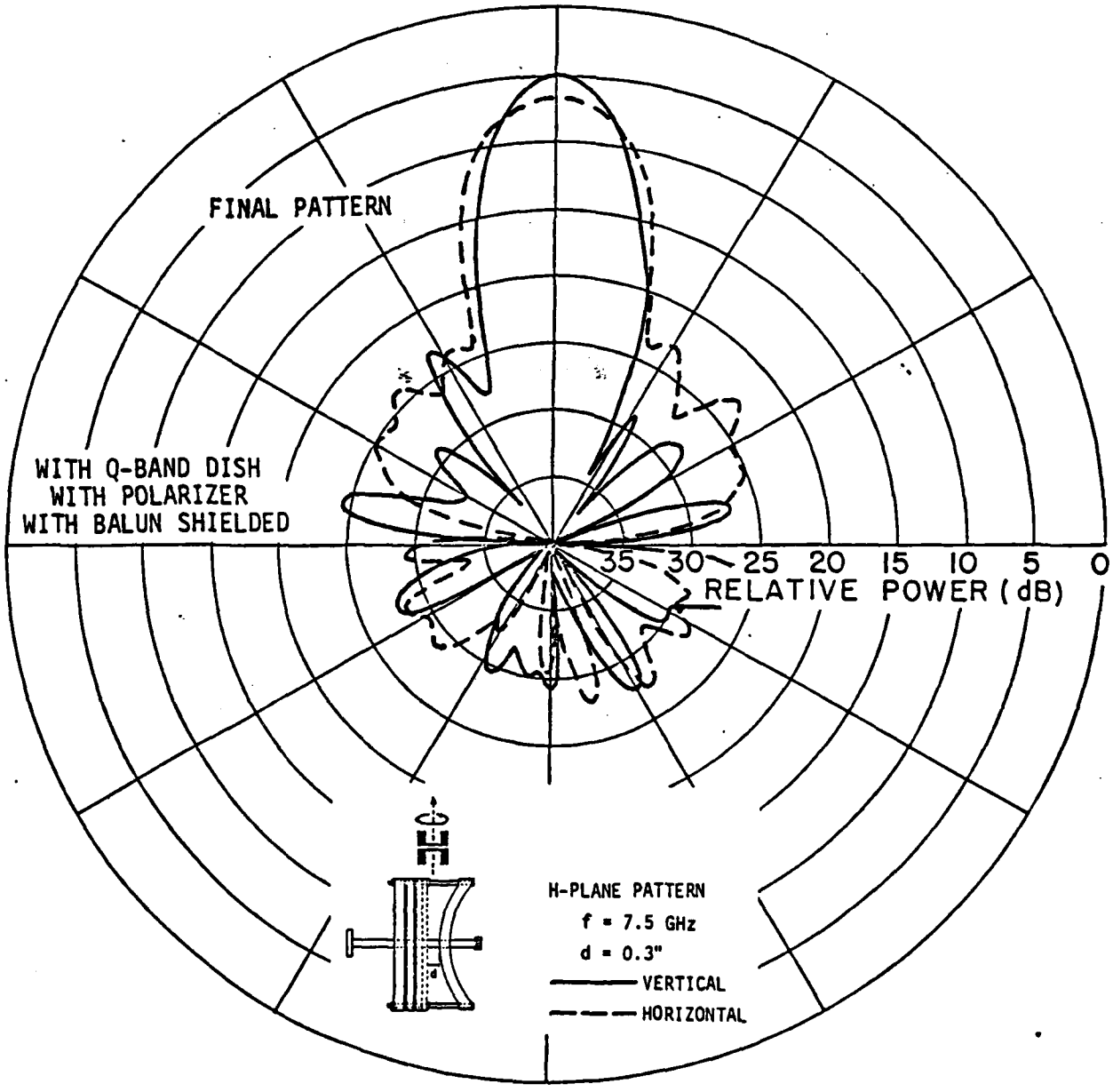

Figure 68. a. Two linear components of circularly polarized radiation pattern in the dipole H-plane, at f = 7.5 GHz, when d = 0.3". (W/ polarizer + parabolic dish + Q-band feed).

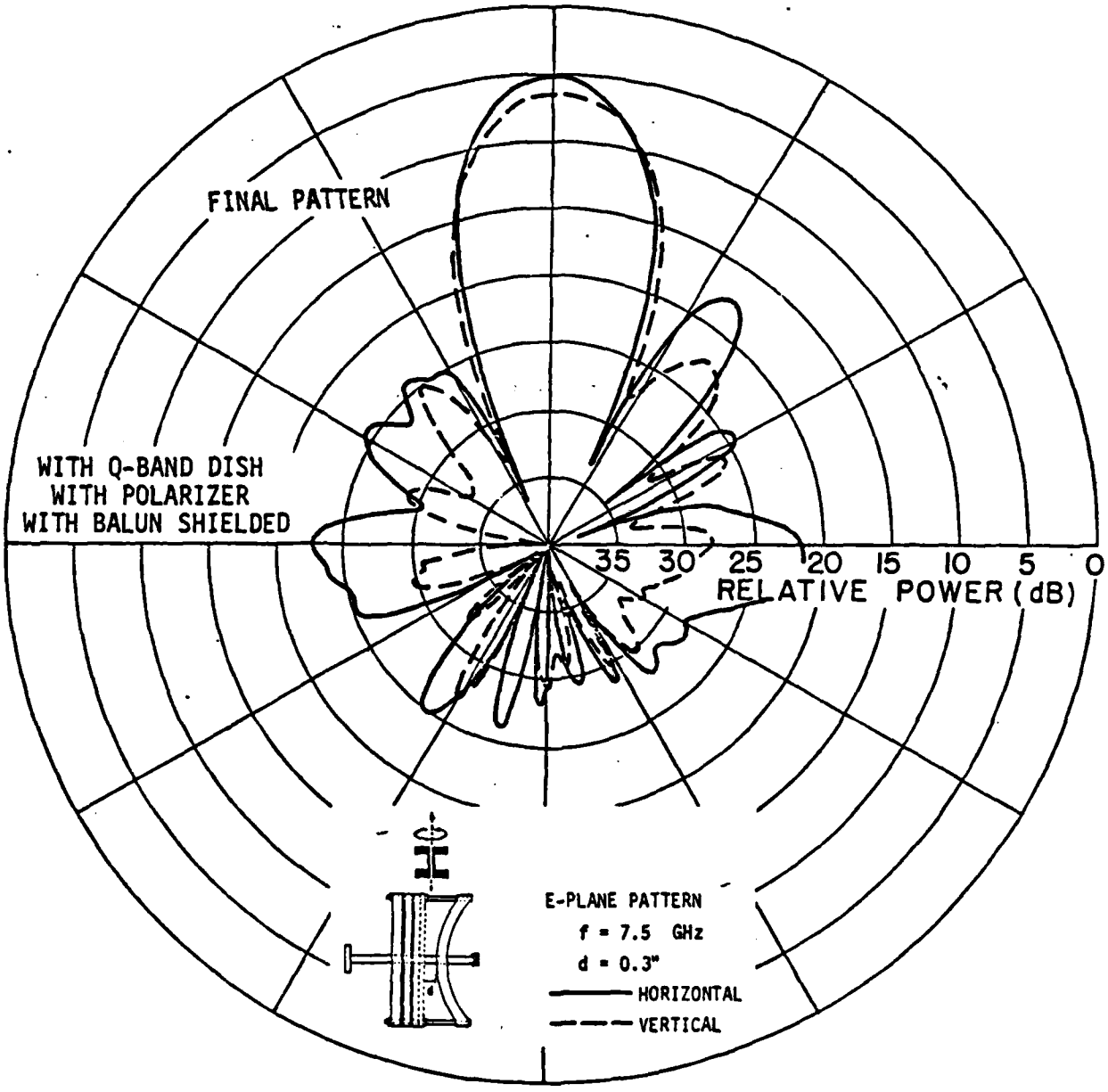

Figure 68. b. Two linear components of circularly polarized radiation pattern in the dipole E-plane, at f = 7.5 GHz, when d = 0.3". (W/ polarizer + parabolic dish + Q-band feed).

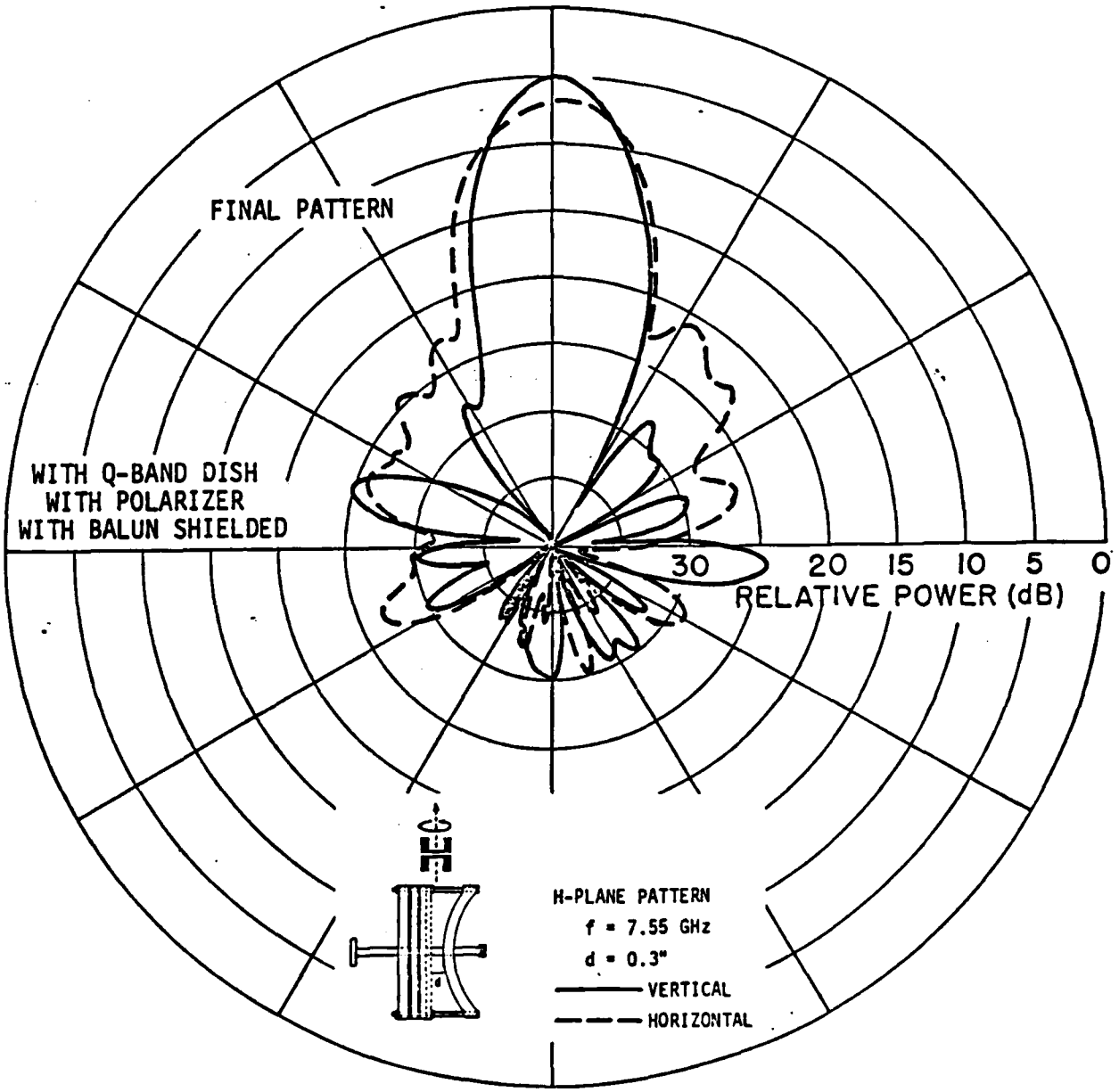

Figure 69. a. Two linear components of circularly polarized radiation pattern in the dipole H-plane, at f = 7.55 GHz, when d = 0.3". (W/ polarizer + parabolic dish + Q-band feed).

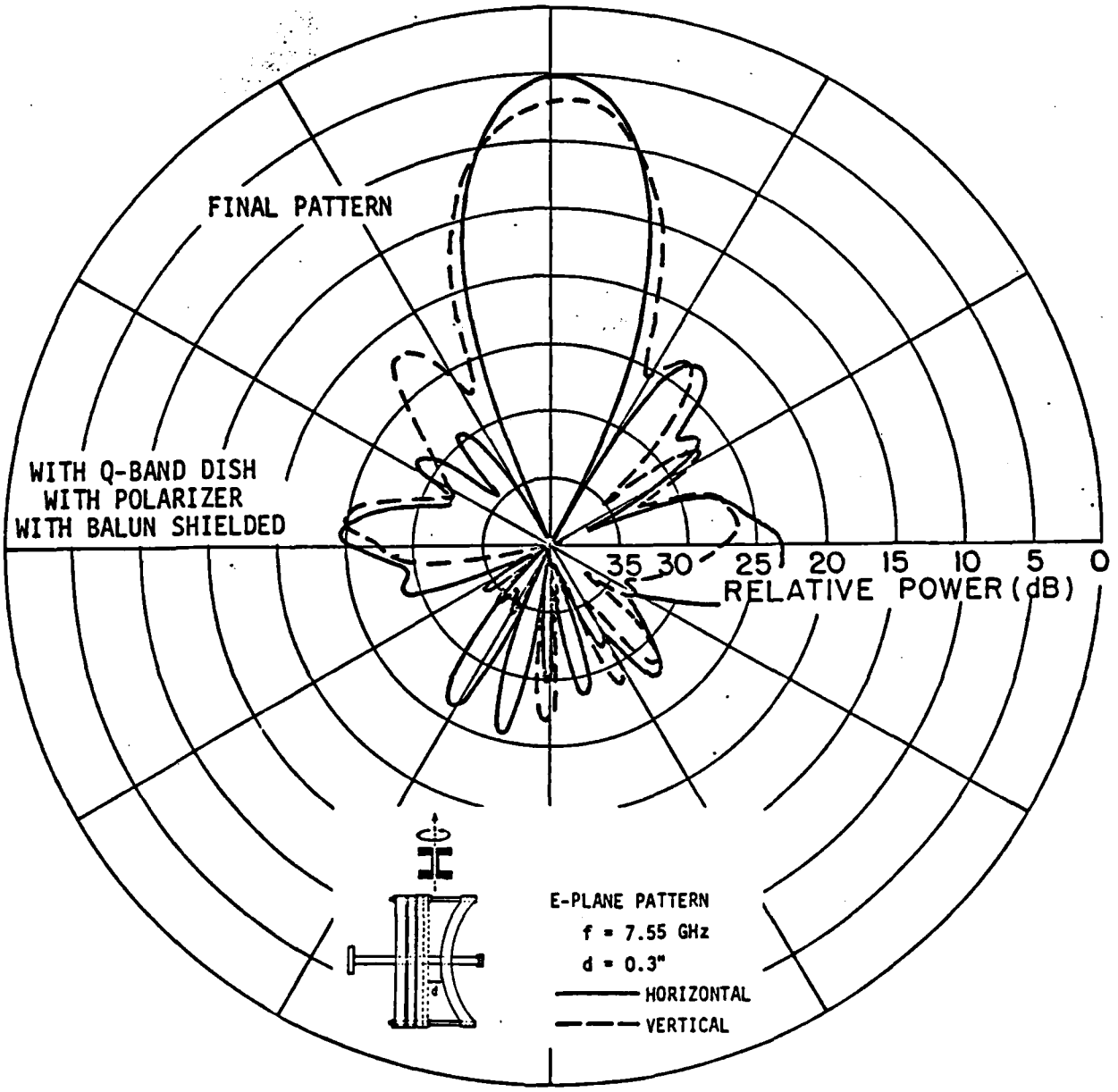

Figure 69. b. Two linear components of circularly polarized radiation pattern in the dipole E-plane, at f = 7.55 GHz, when d = 0.3". (W/ polarizer + parabolic dish + Q-band feed).

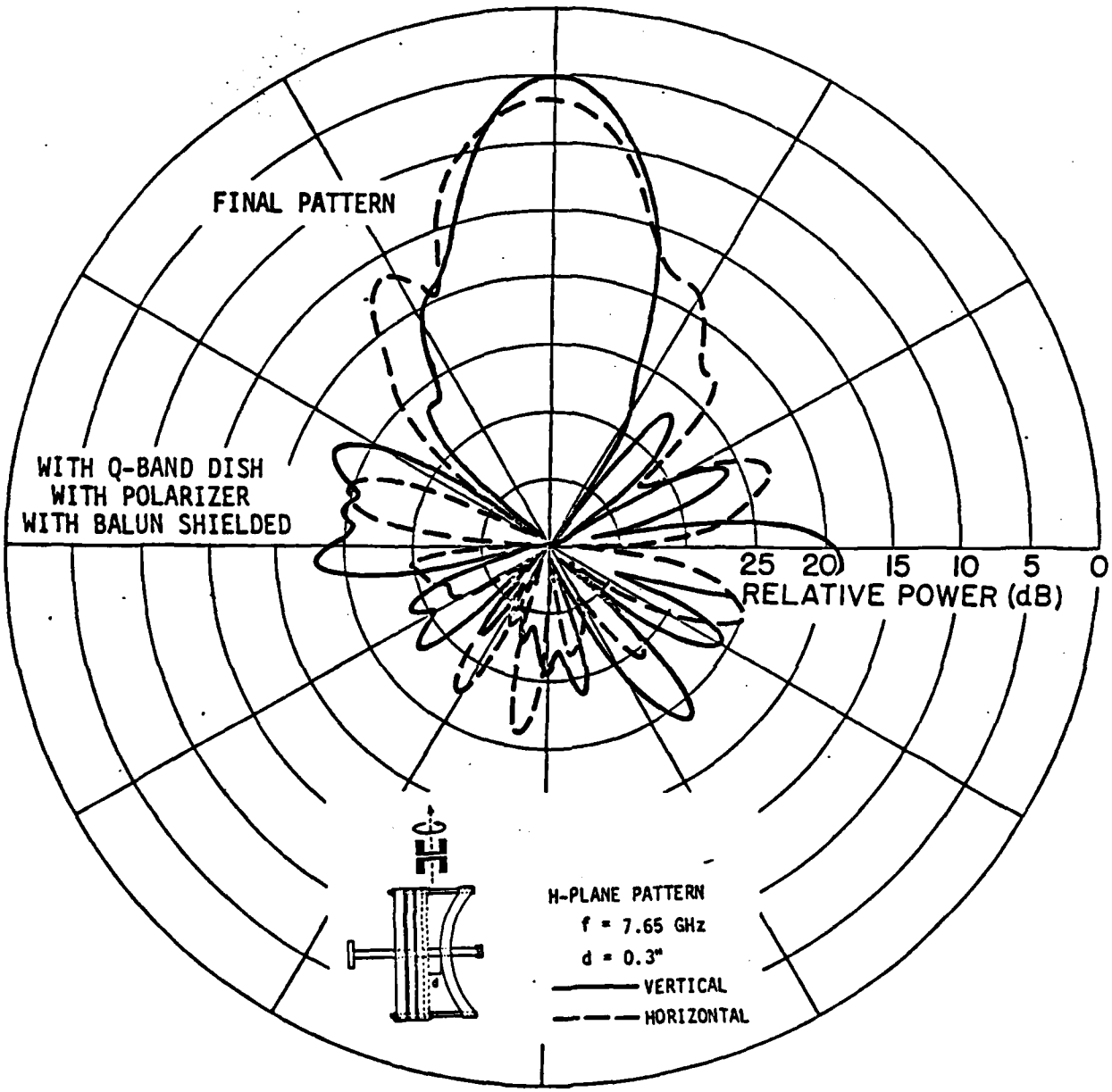

Figure 70. a. Two linear components of circularly polarized radiation pattern in the dipole H-plane, at f = 7.65 GHz, when d = 0.3". (W/ polarizer + parabolic dish + Q-band feed).

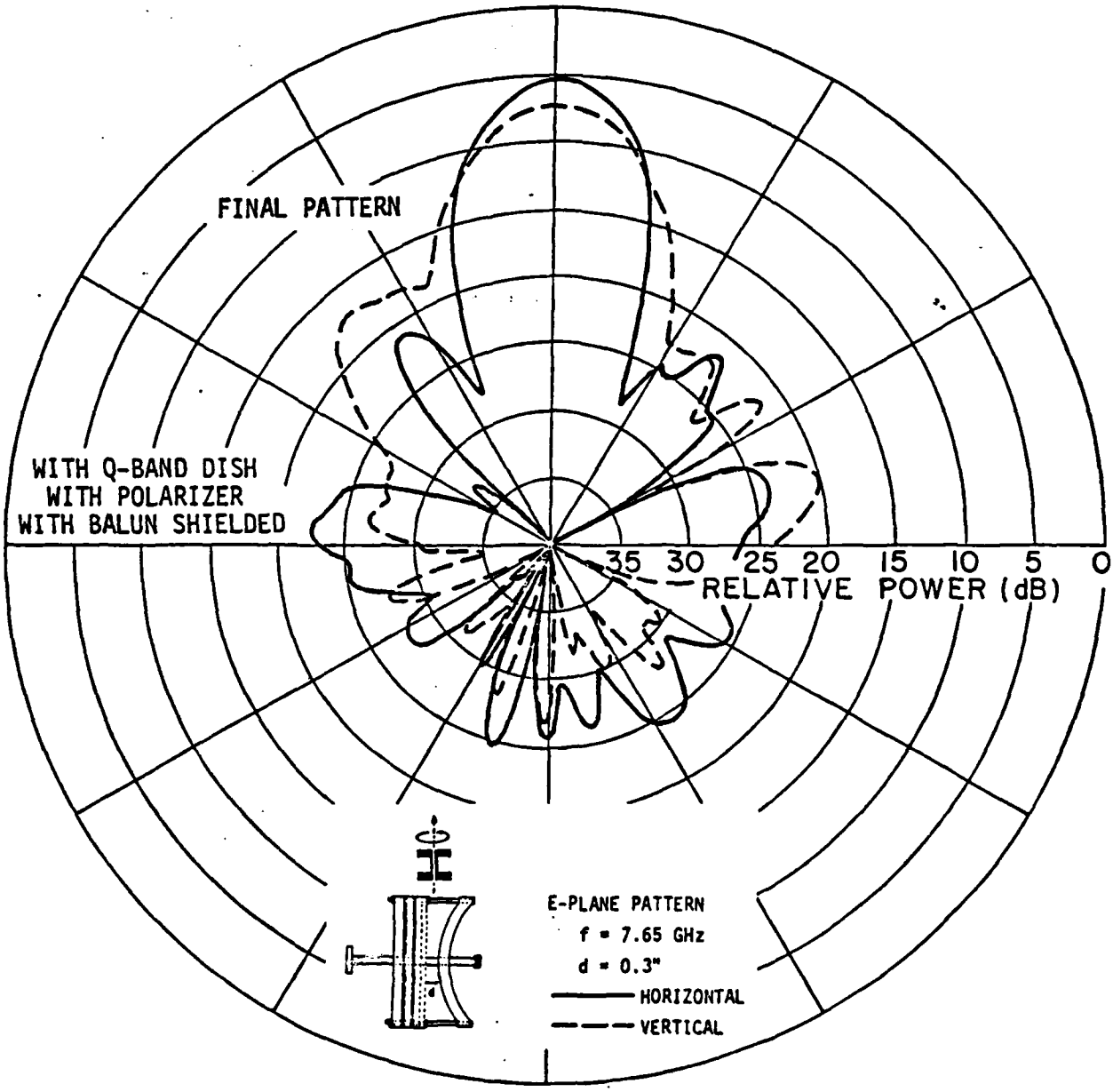

Figure 70. b. Two linear components of circularly polarized radiation pattern in the dipole E-plane, at f = 7.65 GHz, when d = 0.3". (W/ polarizer + parabolic dish + Q-band feed).

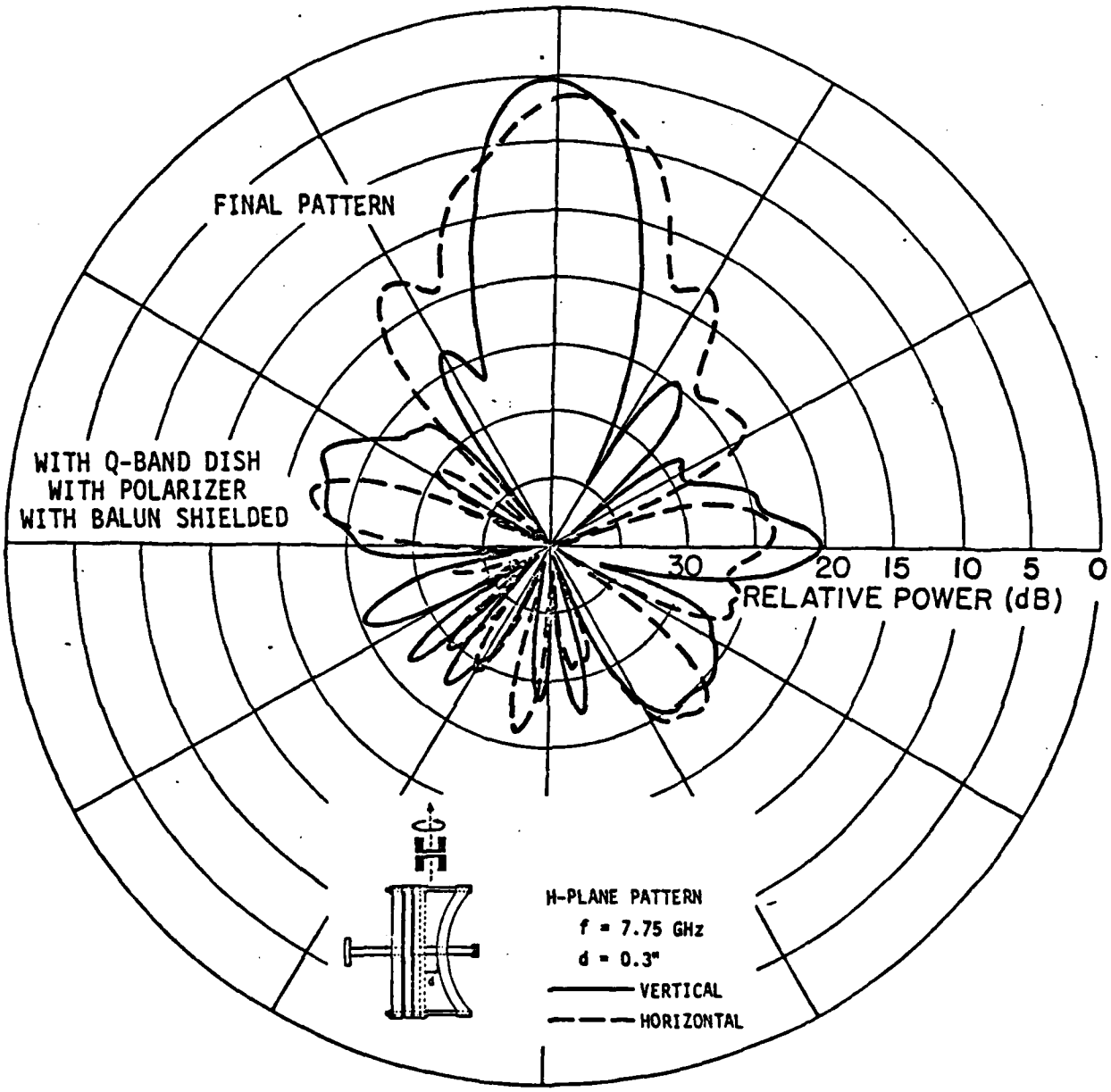

Figure 71. a. Two linear components of circularly polarized radiation pattern in the dipole H-plane, at f = 7.75 GHz, when d = 0.3". (W/ polarizer + parabolic dish + Q-band feed).

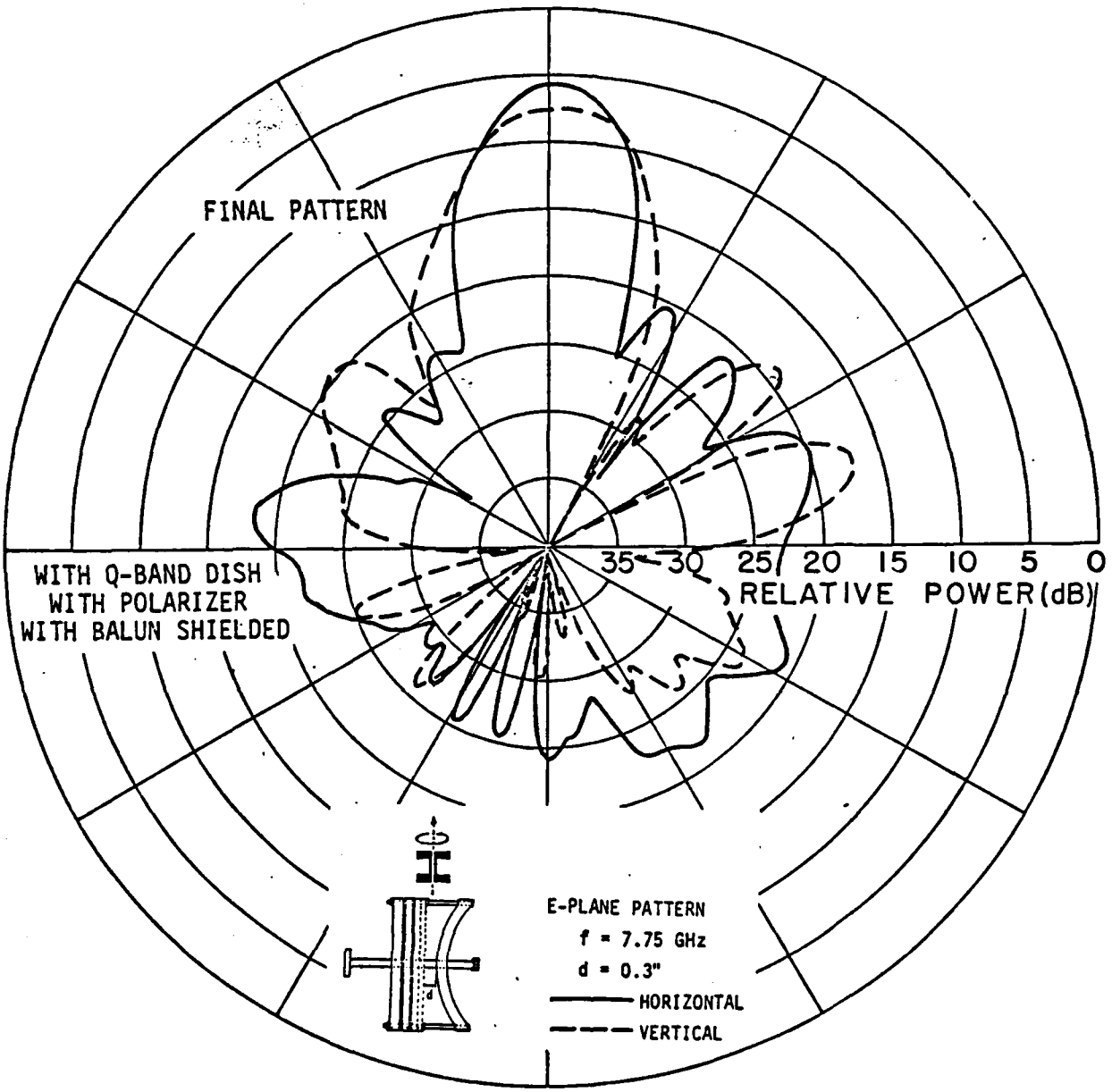

Figure 71. b. Two linear components of circularly polarized radiation pattern in the dipole E-plane, at f = 7.75 GHz, when d = 0.3". (W/ polarizer + parabolic dish + Q-band feed).

Comparing these measured patterns with those shown in Figures 56-62, we can see there is a slight improvement in the X-band pattern in the form of smaller beamwidth and lower sidelobes, which is due to the presence of the dielectric parabolic dish. This indicates that we may possibly experience an effect similar to that of a dielectric rod antenna, or an effect like the image antenna.

8. GAIN OF THE X-BAND ARRAY

The directivity of the X-band array was determined by pattern integration and yielded 18.5 dB at f = 7.50 GHz without counting the cross polarized components. However, when including the cross polarized components, the directivity was reduced to 17.8 dB. This is very much what would be expected from an aperture this size.

SECTION III

CONCLUSIONS

The feasability of a satcom antenna combining the Q-and X-band antennas into the same aperture has been amply demonstrated by actually building a working model to be delivered to the sponsor: NRL. It was found that the dichroic dish behaved almost identically in the Q-band to that of a solid dish both in respect to radiation pattern in the front as well as the back direction. In other words, the dish did not "leak" any signal through but merely exhibited back lobes entirely attributable to edge diffraction like any solid dish. It was further found that the effect of the dichroic dish upon the X-band antenna was not only

negligible but in fact, by proper design, could slightly improve the X-band array performance both in respect to gain and side lobe level.

. . In addition, we also designed, by use of a special new computer program (available separately) a new two layer dichroic surface to be used in a K/Q-band system. A dish for these frequency bands was not constructed. However, based on the promising results obtained at X/Q band, we would suggest this for a future task.

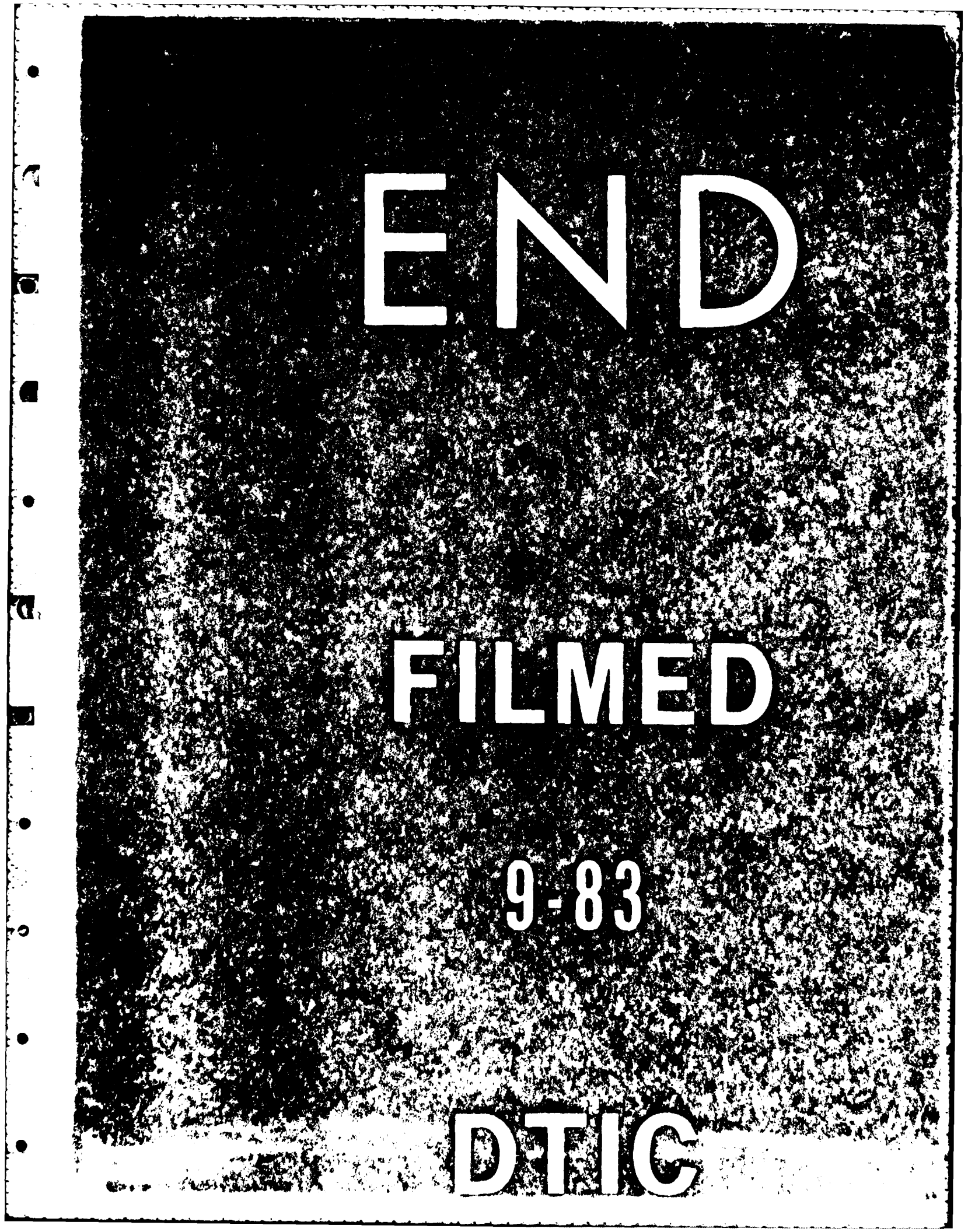
END
FILMED
9-83
DTIC